The Thesis Committee for Silvia Arzate-Gomez
Certifies that this is the approved version of the following Thesis:

High Performance Lightweight Solar Arrays For Electric Vehicle Applications

APPROVED BY

SUPERVISING COMMITTEE:

Gary A Hallock, Supervisor

James Wiley

High Performance Lightweight Solar Arrays For Electric Vehicle Applications

by

Silvia Arzate-Gomez

THESIS

Presented to the Faculty of the Graduate School of

The University of Texas at Austin

in Partial Fulfillment

of the Requirements

for the Degree of

Master of Science in Engineering

THE UNIVERSITY OF TEXAS AT AUSTIN

August 2020

Dedication

Dedicated to the Almighty God, my husband, and my three daughters.

Acknowledgments

I wish to express my most sincere gratitude and appreciation to my supervisor Dr. Gary A. Hallock for his continuous support, invaluable feedback, patience, and always positive guidance throughout this research. Dr. Hallock was always willing to impart his knowledge for the project; without his help and wisdom this project would have not been possible.

I would also like to acknowledge Dr. James C. Wiley. I am grateful for his valuable guidance, support, and comments. For his help with KiCad, his patience in all those meetings while designing the testing boards, and for taking the time to be a second reader of this thesis. A special thanks to Dr. Ahmed Tewfik for his continuous words of encouragement. Thank you to Alfonso Galindo for always willing to contribute in any way he could on this thesis and to all the undergraduate students who contributed with their skills to build the individual modules of the array. I thank you my husband for his devoted support especially when the difficult times came in this journey. To my three daughters who always cheered me up with their excellent school notes and eagerness to go to college. To my almighty Creator for whom I am, for giving me everything I have, and for everything he has done through me.

High Performance Lightweight Solar Arrays For Electric Vehicle Applications

Silvia Arzate-Gomez, MSE
The University of Texas at Austin, 2020

Supervisor: Gary A Hallock

The work reported here describes in detail the design, materials, analysis, and construction of a high quality and lightweight solar array for electric vehicle applications. The solar array consists of two sub-arrays built with Sunpower Corp. Gen III Maxeon solar cells. Each sub-array is optimized with a number of surface-mounted bypass diodes and Resistance Temperature Detectors (RTDs) embedded in the encapsulation. The diodes prevent power interruption during partial shading while the RTDs monitor the temperature of the sub-arrays. The main objective of the array is to power the electric vehicle, while monitoring its performance through the cells' temperature and output power. For optimal performance, the array cells were matched, the equipment and procedures were developed to accurately measure the characteristics of individual solar cells. The materials used in the modules lamination were deliberately lightweight, which is a primary requirement in a solar electric vehicle. The maximum power obtained from the two sub-arrays was 396 W and

406 W, under full sunlight. The total array area is 4 m^2 and its approximate total weight is 4.8 Kg.

Table of Contents

List of Tables

List of Figures

Chapter 1

Introduction

1.1 Objective

Renewable energy systems have been available for many years now. Extensive research has been done to make them more accessible in terms of cost, durability, and efficiency. In the solar power field, solar cells have been manufactured using different combinations of materials in an aim to find the best technology to produce a composite that would absorb sunlight better and to achieve the most output power [1].

Although renewables have come a long way, solar vehicles have not yet become practical. Regardless of the fact that a number of prototypes have been developed, solar vehicles have not yet made it to the market due to energy storage, intermittency of the sunlight, and other factors. Recently, however, mainstream car manufacturers have been investigating integrated solar panels. For example, Toyota recently unveiled the Toyota Prius solar car, a prototype where the solar panels can add 35 miles to the car's range [2]. Most solar vehicles incorporate power storage as in electric vehicles; however, solar vehicles deal with space limitations which dramatically affect the array power available.

Many universities are developing solar vehicles, where the students do the design and construction while learning skills such as working in a team, interdisciplinary collaboration, and others. These are key skills for their future jobs. Although this is not the main focus, breakthrough innovations are always possible, and incremental improvements and cost reductions will allow solar panels to be implemented on future vehicles.

Here at The University of Texas at Austin, the Solar Vehicles Team (UTSVT) has built six solar vehicles in a period of 21 years. It participates in two main races where only universities can compete (The American Solar Challenge and the Formula Sun Grand Prix [3]). UTSVT has manufactured most components of its solar cars, with the exception of the array and the motor. The main goal of this thesis is to describe the process of manufacturing the new car's solar array. Commercial solar array manufacturers are highly proprietary, and it is not very easy to get detailed technical information. The data and procedures described in this thesis represent our own design and development. Future UTSVT teams can use this work to build solar car arrays, or as the basis for additional array improvements.

In addition to the learning process provided to future students, in-house array construction is far less costly than commercial fabrication, and allows a great deal of customization to the specific solar vehicle design. Some of this cost reduction is, of course, due to no-cost student labor.

Once BeVolt (the solar vehicle currently in construction) is completed, UTSVT will have achieved its goal to build another major component of its

cars. At this point, it will be in a position to offer a unique hands-on learning experience to The University of Texas (UT) undergraduate students.

During the process of this array manufacturing, SunPower's monocrystalline silicon cells (MAXEON GEN III Bin Le1) were used. Although all SunPower cells are made out of silicon, there are differences in efficiency, which will be described in more detail in Chapter two.

1.2 In-house vs External Development of an Array

An array developed in-house is not only about customization, but also provides significant cost savings. A commercially developed array is manufactured in external facilities by an independent vendor. In previous years, UTSVT has used outside independent vendors, such as SunCat Solar [4]. The total cost was approximately $18,500 for the cells and lamination assembly. After the modules were completed, UTSVT would receive them and place them on the finalized car body. It is important to note that this cost was effective as of 2013.

During the last few years, we have been doing considerable research to develop an in-house array. UTSVT is now able to manufacture its own array 100%. After the cells have been purchased, the wiring and lamination are done in-house using the materials and lamination method as described in Chapter three of this thesis.

UTSVT spent approximately $6,000 in total for the fabrication of the

array for our next solar car, BeVolt. These costs are current as of 2019. A list of materials and cost is given in Table F.1. As it can be noted, these costs are substantially lower than commercial even though we include some customizations such as the placement of the diodes and the addition of temperature sensors (described in Chapter four). Our design allows the team to acquire more data from the array and avoids unnecessary weight. Additionally, this work gives the opportunity for university students interested in the solar field to have a hands-on opportunity to learn and understand solar array construction. We would also expect future improvements from this process.

1.3 Thesis Organization

This thesis is organized as follows: Chapter 2 describes the specific solar cells we selected for BeVolt. It describes the detailed testing we performed for each individual cell and for each module as well as their respective results. Chapter 3 discusses the arranging of the cells into modules. It also describes the process of module encapsulation and the materials used for the lamination.

The enhancement of diodes, heat sinks, and Resistance Temperature Detectors (RTDs) embedded in the array is detailed addressed in Chapter 4. Finally, Chapter 5 provides the information about the sub-array testing system and the results for each sub-array. Chapter 6 deals with the conclusion and suggestions for future work.

Chapter 2

Cell Performance Testing

Although there are a wide variety of solar cells, the American Solar Challenge regulations only allow three types: Silicon-based, thin-film GaAs, and multi-junction [5]. For BeVolt's array, which is the manufactured array portrayed in this thesis, we used SunPower Maxeon Gen III Bin Le1 silicon monocrystalline solar cells.

2.1 Maxeon Gen III Solar Cell

A monocrystalline solar cell is obtained from a round ingot, which is then sliced into thin wafers that form individual cells. Round solar cells can be assembled into an array. However, this is inefficient in terms of space utilization. Alternatively, a round ingot can be cut into a square or rectangular solar cell. This method would allow almost 100% space efficiency when forming an array. However, it wastes a lot of the original cell area. A compromise is to cut the cell into a square somewhat larger than for full fit. This practice produces a cell that is close to a square but with curved corners. As Fig. 2.1 shows, this is the approach SunPower takes.

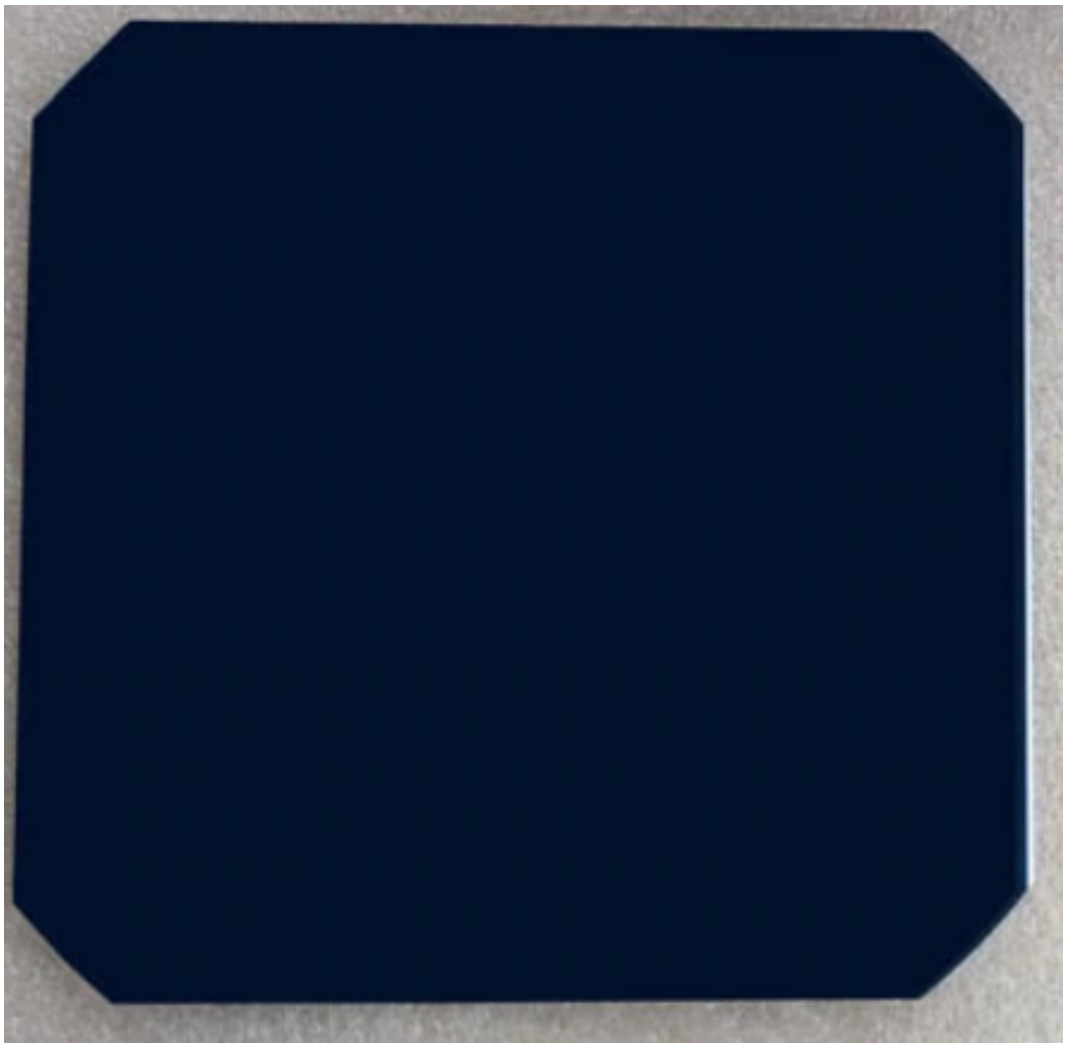

Figure 2.1: **SunPower Maxeon Gen III solar cell.**

The SunPower datasheet indicates an approximate cell area of $153\,\mathrm{cm}^2$ (see Appendix D.1). We desire a more precise cell area. The geometry is shown in Fig. 2.2. The blue circle represents the original round ingot, and the black square the cell cut.

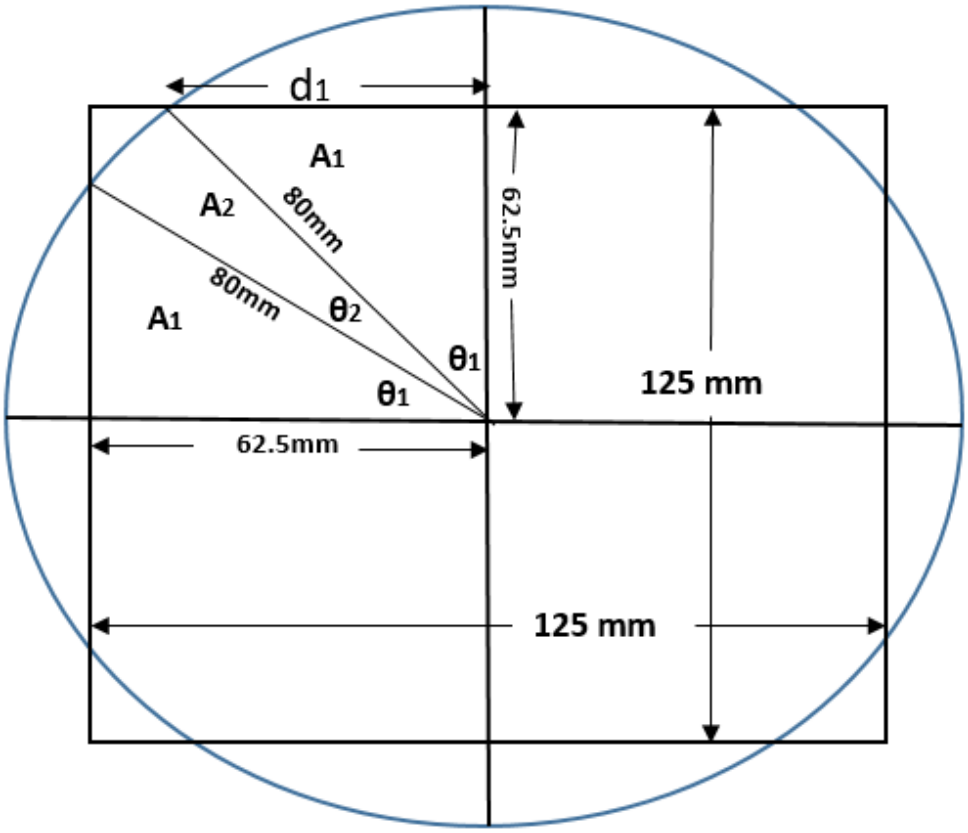

Figure 2.2: **Schematic diagram used to calculate the cell area.**

Taking the curved corners into account and using the given measurements, we calculate the unknown angles as follows:

$$Cos\theta_1 = \frac{62.5}{80} = 0.7813°; \theta_1 = 38.6248°$$

$$Sin\theta_1 = \frac{d_1}{80}^{\circ}; d_1 = 80 Sin\theta_1 = 49.9374\,\text{mm}$$

$$\theta_2 = 90 - 2(38.6248) = 12.7503°.$$

Having calculated the values for both angles, this enables us to compute both A_1 and A_2

$$A_1 = \frac{62.5 d_1}{2} = 1560.5445\,\text{mm}^2$$

$$A_2 = \pi r^2 (\frac{\theta_2}{360}) = \pi (80)^2 (\frac{12.7503}{360}) = 712.111\,\text{mm}^2$$

Now we multiply A_1 by two and add it to A_2 to get the total area of that fourth part of the cell; then we multiply by four which bring us to the total cell area.

$$CellArea = 4(2A_1 + A_2) = 15,332.80\,\text{mm}^2 = 153.328\,\text{cm}^2$$

This information allows us to precisely determine the array area (as required by race regulations) and characterize individual cells accurately.

2.1.1 Solar Cell Cutting Process

SunPower's manufacturing solar cells' strategy with rounded corners optimizes the cost and performance in a typical terrestial array. For a solar car, however, performance and weight reduction are key to a competitive solar car. Therefore, we developed a technique to cut the SunPower cells into actual rectangles.

Our system to cut the cells included a Bausch & Lomb Acu-Rite II digital position readout with a console (Fig. 2.3) and position encoders. The cell cutting machine is a repurposed tabletop mill. The console controls and displays the axes table movement measured by the position encoders [6].

As shown in Fig. 2.4, the precision aluminum plate was indented to hold the cell and bolted to the mill table. A piece of vacuum bag was afixed in

the aluminum indentation where the cell is placed to protect it from any metal roughness that could damage the cell during the cutting process. Additionally, we built the upper aluminum plate holding the dremel head.

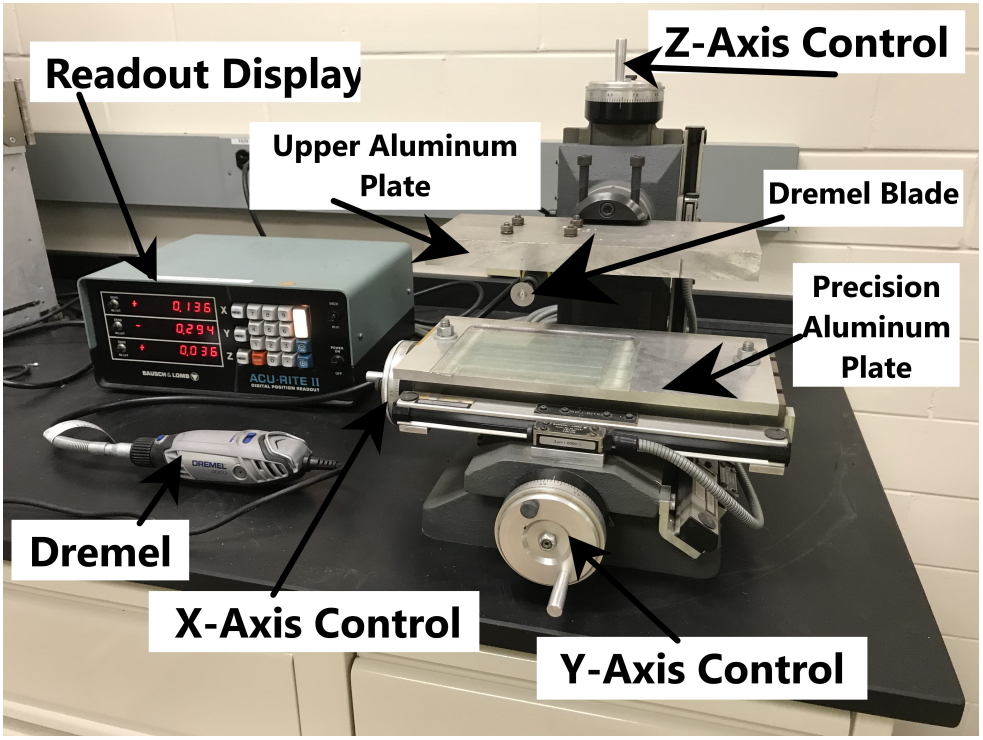

Figure 2.3: **Solar cell cutting system.**

The Dremel 3000 with a thin diamond cutting blade (McMaster 1257A33, 7 mil thick) is secured to the z-axis having the ability to move it up and down using the z-axis position. Then x and y-axis controls allowed the cell to be positioned and cut accurately in between the cell traces without significantly damaging the cell's wiring (located on the back of the cell).

The cutting process consists of mounting the cell in the recessed area

of the aluminum plate against the inside edge. Then, the blade with the z axis knob is lowered until just over the cell. Next, using the y-axis the dremel blade is adjusted and positioned until it is between foil traces. Finally, the x-axis control is used to move the cell to the start point. Once this is completed, the dremel is turned on and cutting process starts. Using one hand to operate the x-axis control and move forward the cut, and with the other hand the cell is held is place until the end of the other side of the cell is reached.

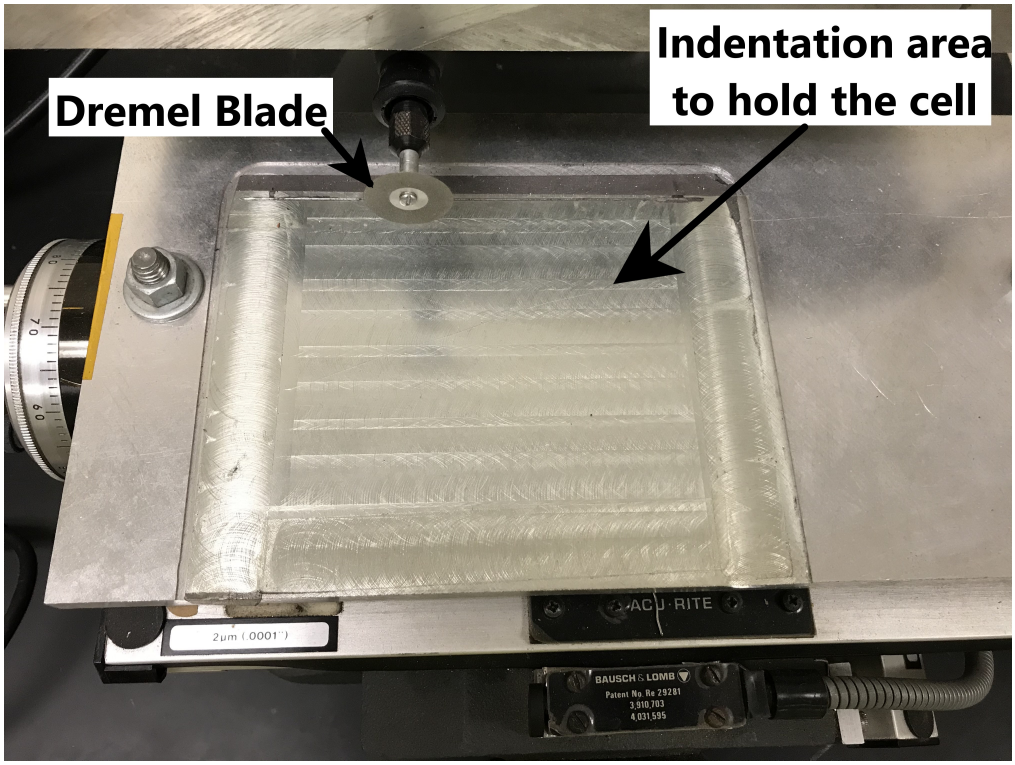

Figure 2.4: **Solar cell cutting table position readout display. This system was used to cut the cells seen in Fig. 2.5 and Fig. 2.6.**

Two cuts are required to form a rectangular cell. Referring to Fig. 2.2,

the cuts are made vertically a distance d_1 from the centerline. This yields a cut cell with dimensions 10 cm x 12.5 cm, or 125 cm^2. Compared to the original cell are of 153 cm^2, approximately 18% has been removed.

An example of a single cut cell is shown in Fig. 2.5, which has been laminated. A full 4x3 array module made with cut cells is given in Fig. 2.6. These and other cut cells were extensively tested, and performed as expected. No degradation from cutting was observed, taking into account the reduced cell area. Fig. 2.5 and 2.6 represent very high-performance modules, which maximize array output for the solar car.

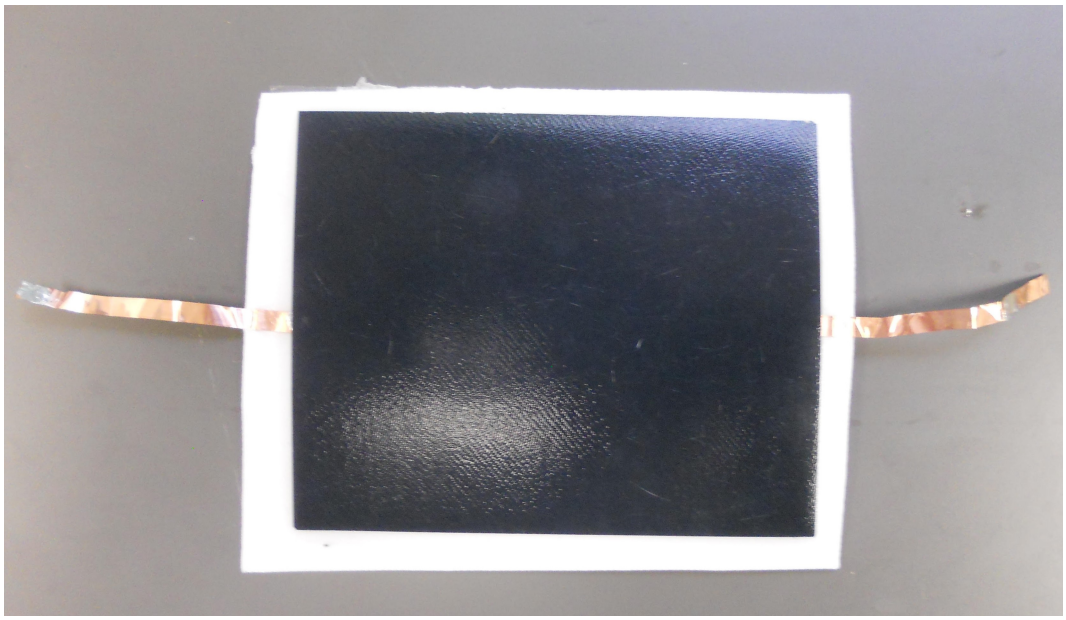

Figure 2.5: **SunPower Maxeon Gen III solar cell which has been cut to a rectangular shape and laminated into a single module.**

Although we successfully developed the technology and the procedure

to cut SunPower cells, the design of BeVolt's body ended up so large that the maximum $4\,m^2$ of allowed solar array fits with uncut cells. Therefore, there was no need to proceed with the extra time and cost to fabricate BeVolt's array with rectangular cut cells. However, this can be considered in a more competitive future solar car.

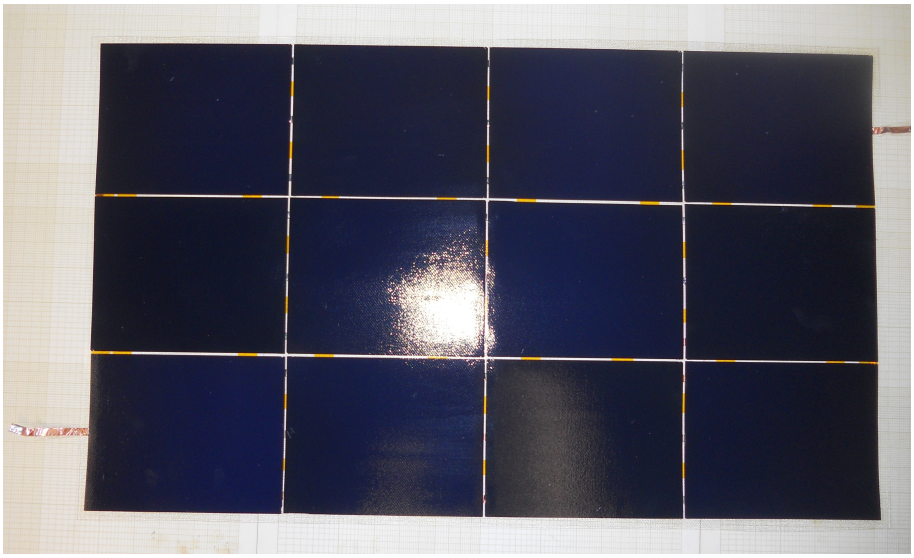

Figure 2.6: **SunPower Maxeon Gen III solar cells which have been cut and made into a 4x3 module.**

2.2 Testing System

Throwing oneself into the solar array manufacturing adventure is to enter into the testing and characterization world. According to the manufacturer data sheet provided in Appendix D for the Maxeon Gen III Bin Le1, the cell's approximate efficiency is the same for all the cells if they are from the same Bin. That said, this is an average, and there will still be cell-to-

cell differences. Knowing that every individual cell can limit the whole array current, we tasked ourselves to test each cell individually to understand the variation between cells. We then select those cells with higher efficiency and avoid limiting the overall array current with low-performance cells. Although there are many methods to characterize solar cells, we relied our testing on scanning the cells from open to short circuit. This approach provides the full I-V performance curve.

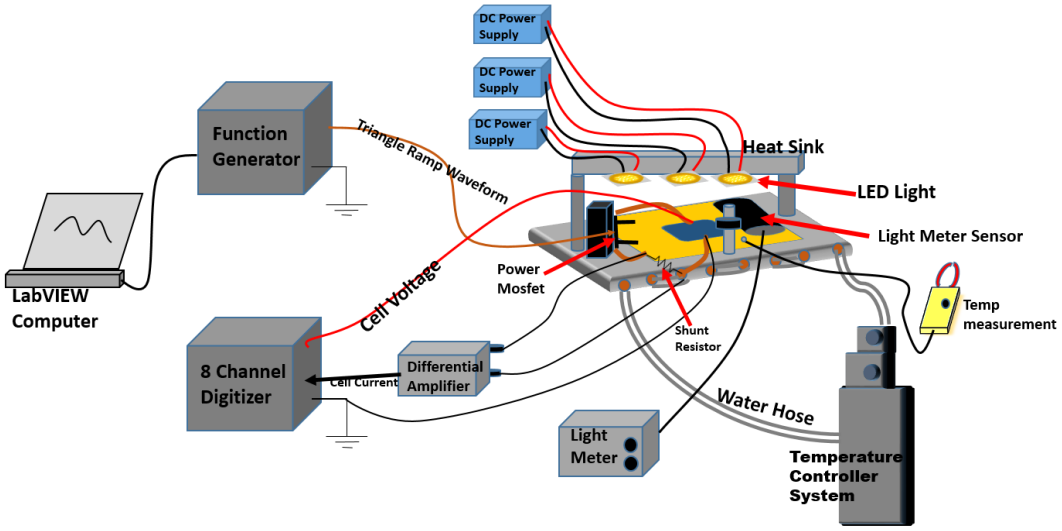

Figure 2.7: **Schematic diagram of the cell measurement configuration showing the complete set up used to test every cell individually.**

A testing system was assembled and used to test the cells presented in this thesis. The system consists of a temperature control system, an aluminum base plate, Kapton tape, an IRFP4368PBF MOSFET (Appendix D.2), two heat sinks, three grow Light-Emitting Diodes (LEDs), three 120V DC power supplies, lightmeters, a Function Generator Model PXI-5406 from National

Instruments (NI), a differential amplifier, an eight-channel digitizer Model PXI-5105 from NI, a 0.5 mΩ shunt resistor, and a laptop computer with LabView software. Fig. 2.7 shows the complete cell measurement configuration set up.

2.2.1 Temperature Controller System

The Thermo Neslab RTE-110 refrigerated circulator consists of an air-cooled refrigeration system, circulation pump, stainless steel bath, a work area cover, and a temperature controller [7].

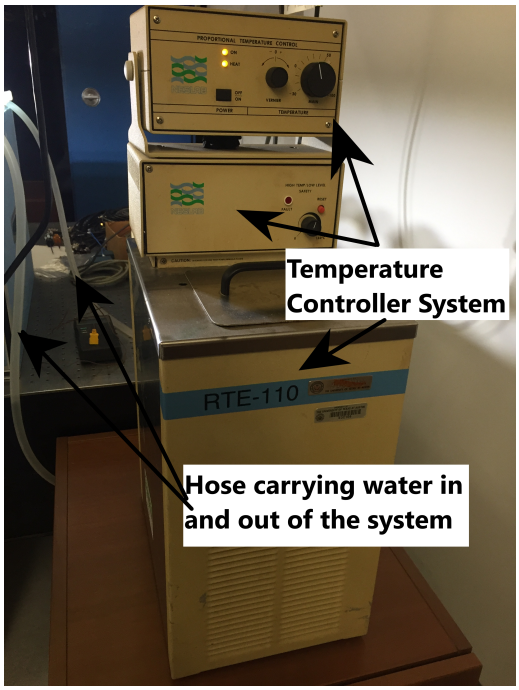

Figure 2.8: **The temperature controller system helps maintain the cell at STC temperature.**

The main functionality of the temperature control system (Fig.2.8) is to

control the temperature of the water circulating under the aluminum base plate of the cell testing system. While the water flowing at the same temperature constantly under the plate maintains its temperature at the desired level, it provides the required STC temperature (25°) to test the cells properly.

2.2.2 Aluminum Cold Plate

The solar cell is tested on the aluminum cold plate, which functions as the base for the testing system (Fig. 2.9).

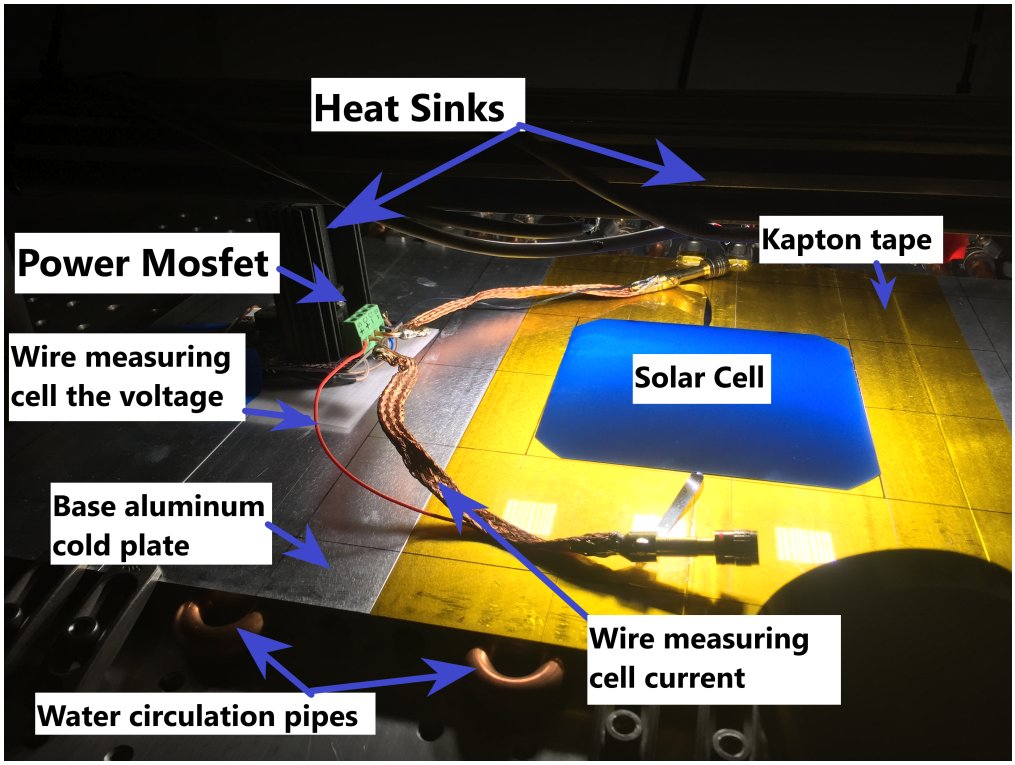

Figure 2.9: **Different components used in the cell testing confuguration.**

The plate has grooves underneath where copper pipes are attached; the

pipes are used to circulate the water coming from and going to the temperature controller system. This water circulation maintains the solar cell at the desired temperature, even under intense illumination.

2.2.3 Kapton Tape

Individual cells were tested before being laminated; hence the cell's copper traces were still exposed, and the base plate is aluminum. Since both materials are conductive, we used Kapton tape in between them as an electrical insulator. The Kapton tape is the yellow material seen in Fig. 2.9, which avoids a short circuit during the test process. The Kapton tape is very thin (5 mils) and does not appreciably insulate the cell from the cold plate.

2.2.4 Power Mosfet

A solar cell is a device that produces low voltage and high current. Fig. 2.9 shows two wires connected from the cell to the power MOSFET. On both sides, a heavy braided wire is used to measure the cell's high current. In parallel to it, there is also a red and a black wire connected to the positive and negative side of the cell, respectively; these are used to measure the cell's low voltage.

The MOSFET serves as a load (similar to a resistor) to the cell. Its gate (input) is scanned and driven by the function generator in a way that the cell is scanned from open-to-closed circuit over a single scan.

2.2.5 Light Meter

The light produced by the grow modules is monitored by a Scientech 361 power meter, as shown in Fig. 2.11. The meter contains an absorption disk in the base of a black tube collimator. It is a calorimeter type device with a broad spectral response. The power meter is used to check for any variations in the grow light output intensity.

2.2.6 LED Grow Modules and Power Supply

Although initially the system had two functioning 50 W grow modules, we managed to include an additional module and provide a total of 150 W of light intensity. The module's spectrum does not match exactly the Sun spectrum. Fig. 2.10 shows that it is a reasonable approximation to it. Comparing Fig. 2.10a and Fig. 2.10b, we can observe that they both have peak output in the visible. However, the grow LED spectra has a dip at 480 nm, which is not present in the Sun. The grow LEDs do provide a consistent, reproducible light source for cell testing, which is very important for determining small differences between cells. Additionally, the grow LEDs are far less expensive than other lamps used for more accurately simulating the Sun's spectra [8]. Although not perfect, grow LEDs provide an excellent low-cost source of light for the relative characterization of cells.

In the system, each grow LED is powered by a 120 V DC power supply to achieve a smooth trace in the measurement waveform. If the grow modules are powered by 120 V AC (as originally intended by the manufacturer), the

light oscillates on and off at the 60 Hz line frequency. This oscillation prevents obtaining a smooth continuous I-V measurement.

We only used three LED modules to illuminate the solar cell due to limited DC power supply availability. Despite that, Fig 2.12 demonstrates that the cell was able to produce approximately half of the expected short circuit current for full Sun, as noted in the datasheet (Appendix D.3).

Another inexpensive way to generate light for indoor solar testing is halogen work lamps. We also implemented this technique, which worked reasonably well. High power is easily obtained; we used two lamps, providing a total of 300 W (power input).

However, these lamps generate a large amount of infrared radiation and make it more difficult to control the cell temperature. We, therefore, used the LED grow modules for all testing reported here.

2.2.7 Heat Sinks

A heat sink is a thermally conductive material that helps to dissipate the heat from an object. The most common material used for heat sinks is aluminum. In our testing system, we use two heat sinks. Fig. 2.9 shows a long heat sink that holds the three 50 W grow modules to minimize the temperature of the modules. Another smaller black heat sink is shown attached to the MOSFET, which cools it off through heat dissipation as with any other electrical device.

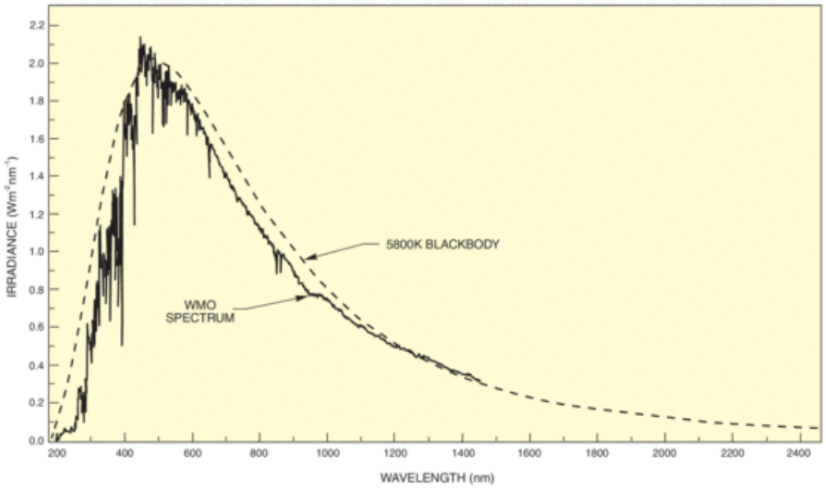

(a) **Spectrum of the radiation outside the earth's atmosphere and spectrum of a 5800 K blackbody [8].**

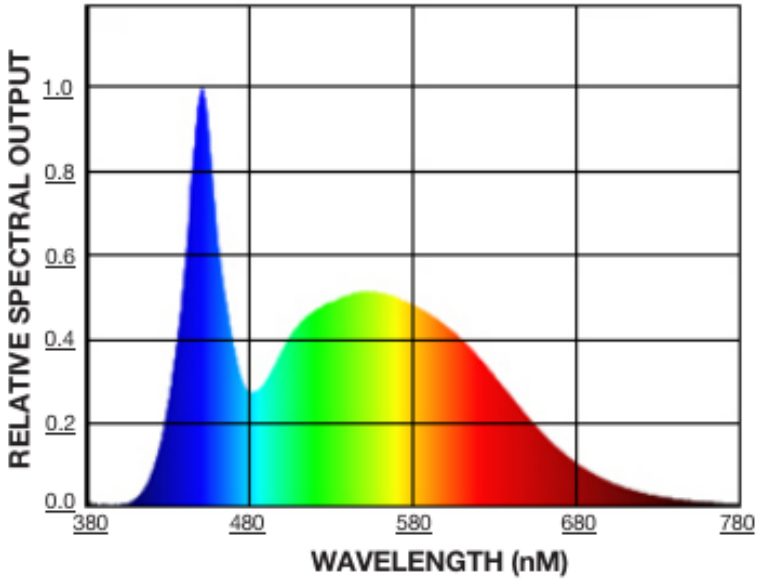

(b) **50W grow LED module spectrum**

Figure 2.10: **Spectrums do not match exactly but there is a reasonable approximation.**

2.2.8 Function Generator

In our configuration, we used a National Instruments (NI) PXI-5406 function generator. The device generates a linear ramp that controls the MOSFET's resistance. We scanned the solar cell at 0.5 Hz.

It is important to understand that a solar cell must be scanned at a very low frequency. This fact is due to the solar cell's own capacitance and other characteristics that would otherwise make the waveform distorted, leading to an inaccurate I-V curve.

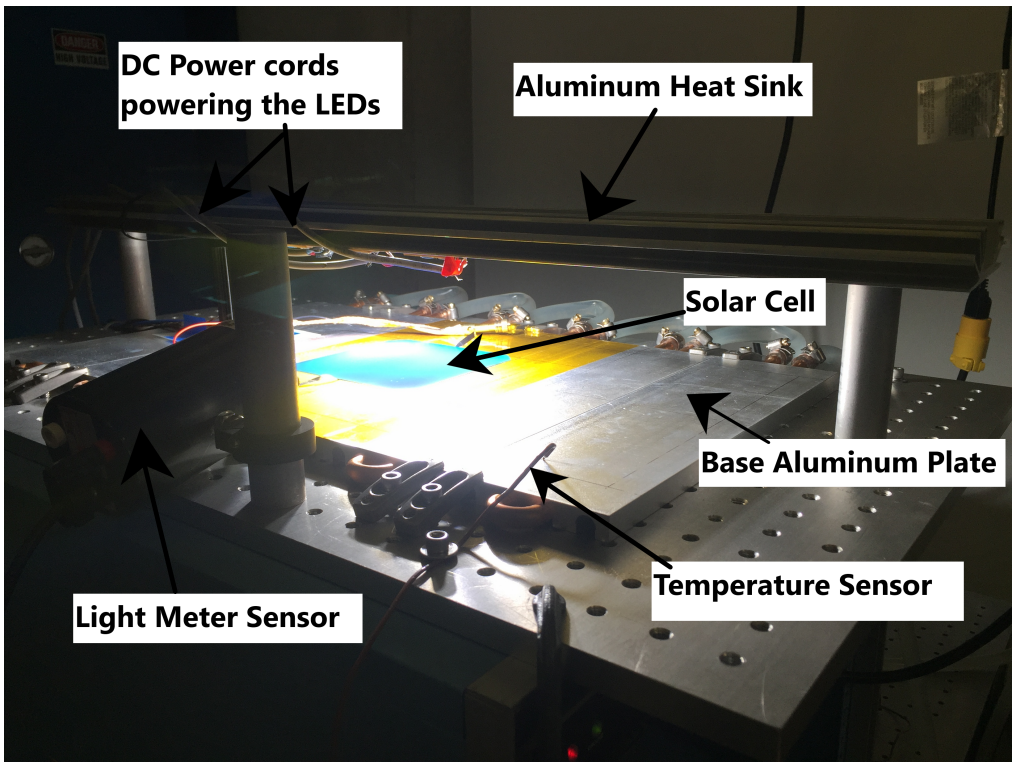

Figure 2.11: **Additional components in the cell testing system.**

2.2.9 Differential Amplifier

A differential amplifier with a voltage gain of ten was connected to the 0.5 mΩ shunt resistor that monitors the cell current, as shown in Fig. 2.7. The amplifier boosts the shunt resistor output sufficiently so that it can be read with adequate signal-to-noise ratio and resolution by the digitizer. A small shunt resistor is used to avoid dropping too much voltage across the shunt resistor; otherwise, it is not possible to fully short the cell.

In our design, the 6 A maximum short circuit current through the 0.5 mΩ shunt resistor develops a voltage of 3 mV. This voltage is the lowest possible across the cell; at full current, the voltage will be slightly higher. Taking into account the resistance of the cables and MOSFET, a short circuit voltage in this range is entirely satisfactory compared to the maximum (open circuit) cell voltage of over 500 mV. Almost all of the I-V curve is obtainable.

2.2.10 Digitizer

We used a NI PXI-5105 8-Channel digitizer in the cell measurement configuration. Although the digitizer has eight channels, we only used two of them: one to receive the voltage data and the other to obtain current data. The digitizer acquires the current and voltage data as a function of time. The LabView software is then used to generate current versus voltage plots and other graphs of interest.

2.2.11 LabView Software

We used a computer with LabView software. The software has three separate VI's, or LabView programs (Virtual Instruments). The first VI generates timing (trigger) signals for the other modules, while the second VI controls the function generator, setting the wave amplitude, scan frequency, etc. The third VI acquires data from the digitizer, processes the data, and produces the output plots.

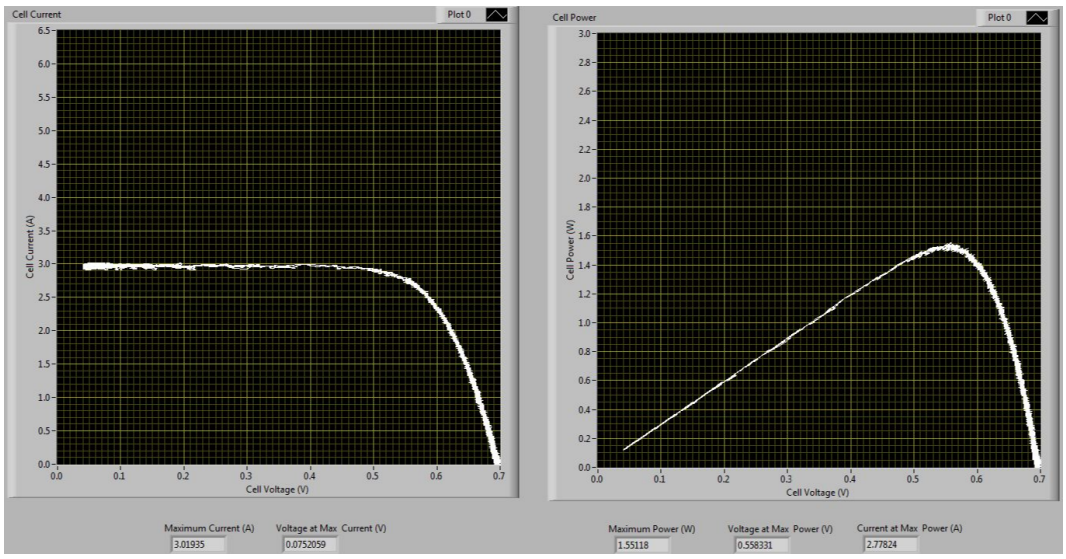

Figure 2.12: **Solar cell output using the measuring configuration shown in Fig. 2.7.**

The left graph in Fig. 2.12 illustrates the I-V curve obtained when testing a typical cell. The short circuit current is about 3 A, and a "knee" is obtained at about 0.55 V, typical of silicon solar cells. The graph on the right is a plot of the cell power produced as a function of the cell voltage. The peak of this curve indicates the maximum power point (mpp) of the cell. Numerical

data below the plots give where the mpp is located, showing the cell's mpp of 1.551 W, and the voltage and current at the mpp of 0.558 V and 2.778 A, respectively. Additionally, the graph contains the cell's short circuit current and the voltage at maximum current; from these two, we consider the short circuit current a key value to determine whether it is a cell with high efficiency or low-performance.

The instrumentation we used in the individual cell tests is top-quality laboratory equipment, which produces highly accurate results. It is an expensive set of equipment that provides more functionality than needed in this system, such as the extra digitizer channels. However, the instrumentation used in this thesis could be replaced with other low-cost devices, such as the NI MyDAQ or other inexpensive data acquisition instruments. A student group could develop low-cost instrumentation tailored to the cell measurement, with only minimal loss of accuracy.

2.3 Cell Testing Procedure

To collect the information from each cell, we followed a structured and organized procedure. First, we examine the cell to check for cracks. Next, a piece of tinned copper ribbon is attached to each polarity of the cell (this is soldered for testing purposes only). Afterward, the cell is identified with a number written with a label maker on a sticky label. Then it is placed on the aluminum cold plate and attached to the wires that connect it to the testing system, as shown in Fig. 2.9.

After the cell has been connected, the LED grow lights are turned on, and we wait for 60 seconds for the cell to reach the aluminum cold plate temperature. Subsequently, we start recording the data such as temperature, light intensity variation, and the cell measurement obtained from LabView (this includes the short-circuit current (I_{sc}), open-circuit voltage (V_{oc}), maximum power (P_{max}), current at maximum power (I_{max}), and voltage at maximum power (V_{max})).

Once the data is recorded, the grow modules are turned off, and the cell is disconnected and removed from the cold aluminum plate. At this point, the tinned copper ribbon pieces are desoldered, and the cell is classified for the highest performance sub-array, next to the best, or excluded depending on its output data.

2.4 Cell Test Results

Although all the cells belong to the same Bin Le1, there were quite a few of them showing significantly higher or lower values than the average. During the testing process, we found that most of the cells stayed within a narrow range, as Sunpower reported. However, now and then, we got high results from some solar cells.

At an early stage of the testing, we had access to two DC power supplies; therefore, we started using two grow modules. We tested from 1-to-103 cells using the two grow modules, which provided a 100 W input power. The ranges along with the corresponding averages and standard deviation values of the

results appear in Table 2.1.

Table 2.1: **Cell test results range using two LEDs applicable to cells from 1 to 103 with their corresponding average and standard deviation.**

	Range	**Average**	**Std Deviation**
P_{mpp}(W)	1.217 to 1.406	1.319	0.039
I_{sc}(A)	2.403 to 2.687	2.570	0.073
I_{mpp}(A)	2.490 to 2.542	2.392	0.071

Later, we added another DC power supply to power an additional grow module; at this point, the total input power grew to 150 W. Table 2.2 presents the range results for the cells (BV104 through BV288) tested after this improvement; additonally, the average and standard deviation can be found in the same table. Table A.1 presents the range of testing results for each cell corroborating the difference of the cells' output power while having illumination of two and three grow lights.

Table 2.2: **Cell test results for the range, average, and standard deviation using three LEDs applicable to cells from 104 to 288.**

	Range	**Average**	**Std Deviation**
P_{mpp}(W)	1.309 to 1.661	1.549	0.046
I_{sc}(A)	2.591 to 3.310	3.090	0.058
I_{mpp}(A)	1.712 to 2.969	2.829	0.106

As discussed previously, the three grow lights provide 150 W input electrical power, which is not enough illumination to achieve a full one Sun

and obtain the cell maximum electrical characteristics as given in the datasheet (Appendix D.3). They provide approximately 0.5 Sun, or about 500 $\frac{W}{m^2}$ at the cell surface.

After we tested each cell, we were able to "bin" them into three groups for our array construction. We decided to base our cell selection in the highest I_{sc} outputs. In an array where the cells are connected in series, the current flowing through it is the same, therefore, having a more dramatic effect in the array output power compared to the impact of the V_{oc} [9]. Therefore we first considered those with the highest I_{sc} outputs. Then we included the cells with amperage range given in Table 2.3 to form the highest-performing sub-array. Each range, average and standard deviation corresponds to the specific illumination of either two or three LEDs as indicated in the table.

Table 2.3: **Range in I_{sc} selected to assemble the best performance sub-array.**

	I_{sc} Range (A)	**Average (A)**	**Std Deviation (A)**
Two LEDs	2.571 to 2.687	2.618	0.070
Three LEDs	3.102 to 3.310	3.134	0.031

The second sub-array was assembled with the next to best cells, having I_{sc} values varying in range, average, and standard deviation as given in Table 2.4. As in the first sub-array, each range is specific to two or three LEDs, respectively. Finally, we excluded the lowest-performing cells to avoid degrading the output of either sub-array.

Table 2.4: **Range in I_{sc} selected to assemble the next to best performance sub-array.**

	I_{sc} Range (A)	Average (A)	Std Deviation (A)
Two LEDs	2.500 to 2.570	2.536	0.027
Three LEDs	3.050 to 3.101	3.072	0.021

The light intensity average and standard deviation for the different illumination is given in Table 2.4. As it can be noted, the values for the cells illuminated by two LEDs differs fromthose illuminated with three LEDs.

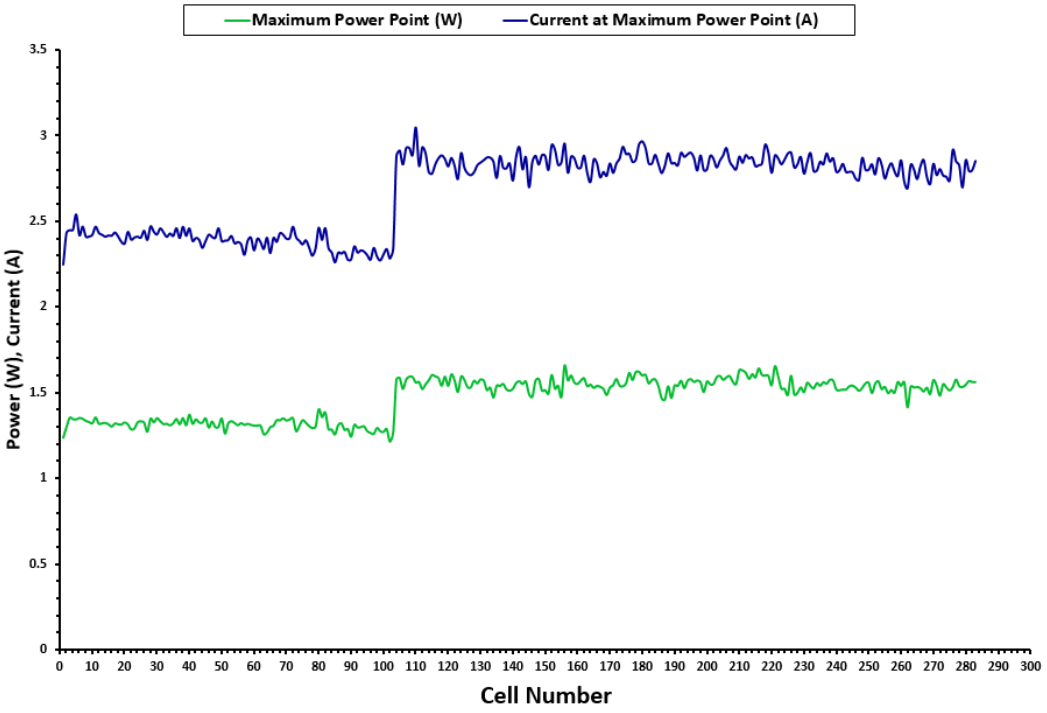

Figure 2.13: **Performance of each individual cell.**

Using the data presented in Table A.1 we plot P_{max} and I_{max} in Fig. 2.13

to show the cell-to-cell variation. Note that the graph like the table shows the output increase with the illumination from two to three grow lights; however, the graph does not include the cracked cells listed in Table A.1. Additionally, it shows the highest performance cells (in particular cells # BV5, BV80, BV82, and BV110, to name a few).

The results shown in the graph prompt four different values for the average and four for the standard variation corresponding to two and three LEDs in each sub-array shown in Tables 2.3 and 2.4 respectively. Considering all values, the standard variation of the cells illuminated with two LEDs in the best sub-array represent the largest of all with a 70 mA variation. Although this number seem small, it represent a $\pm 5.21\%$ of I_{max} in the cells when considering the difference from the mean to the maximum or minimum standard deviation. Though, we try to match the cells, the variation between them still exists and therefore makes a difference in the performance of each sub-array.

The graph does not represent any of the damaged cells; however, Table A.1 indicates the low I_{max} measured in cells BV175, BV211, BV235, BV262, and BV270 due to discontinuous traces after being cracked.

2.5 Module Test Results

The testing approach for the modules was entirely different compared to the process done for testing each individual cell. The cells were tested in the lab to facilitate the suitable STC; due to the lack of enough illumination for the area of a module, the modules were tested outside in sunlight.

The modules were tested for short-circuit current (I_{sc}) and open-circuit voltage (V_{oc}). The positive and negative output wires were soldered to a braided wire shorting them to measure I_{sc} using a Fluke 325 clamp-on ammeter. Then we removed the braided wire and connected the test leads to the common and voltage input jacks to measure V_{oc}. These tests were performed with clear skies only (no clouds); while taking the measurements, we tilted the modules in an aim to align the module perpendicular to the Sun to get the maximum values for both measurements.

After the cells were matched, interconnected, and soldered into a module, they were tested outside before being laminated. This process was primarily to check for any soldering failure interrupting the power output. Next, the module was encapsulated using the technique described in this thesis, by implementing the checklist given in Appendix B.1. Then, when the lamination was completed, the modules were tested again outside.

Fig. 2.14 demonstrates two examples of the modules' manufacturing results. In Fig. 2.14a it can be seen a Type 1 module, which is one of the most popular layouts; meanwhile, Fig. 2.14b shows a Type 5 which is a more complex electrical configuration.

Measured results for all the encapsulated modules are shown in Table 2.5; as expected, these values are closer to those claimed in the datasheet for individual cells as a result of the modules being exposed to a full Sun illumination.

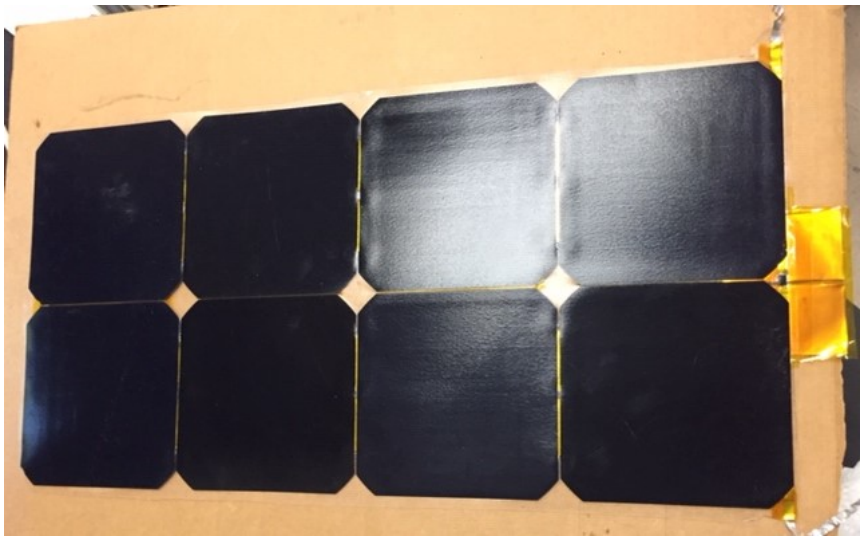

(a) **Module encapsulated Type 1, which is one of the most popular types.**

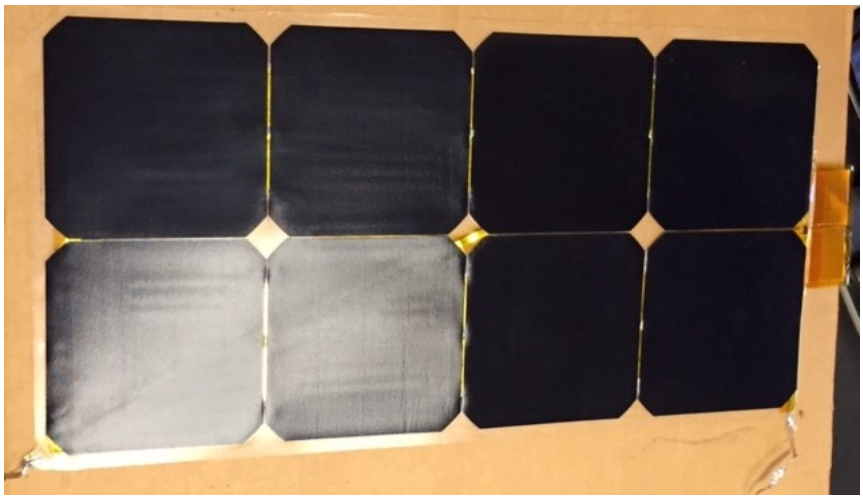

(b) **Module encapsulated Type 5 with a diagonal wire to adapt the needs of module interconnect wiring.**

Figure 2.14: **Two examples of the modules encapsulated that will be part of BeVolt's solar array.**

Note that these values are open-circuit voltage V_{oc} and short-circuit current I_{sc} measurements, not the voltage and current at the maximum power

point (mpp). Table 2.5 indicates that some modules' output is relatively low (below 6.5 A), but they are still above the mpp values, which are considered a good performance.

Although most of the modules provide a performance according to the datasheet specifications, modules 0, 1, and 4 have a low I_{sc} compared to the others. These low measurements are a consequence of cracks due to module mishandling after lamination. There is no fix at this point, such as replacing cracked cells to increase the current; the only fix possible is to make a new module and exchange it for the cracked one.

Table 2.5: **Modules test results**

Module #	**Mod Type**	**I_{sc} (A)**	**V_{oc} (V)**
-	$T12$	6.77	2.60
*0	$T10$	6.09	2.70
*1	$T10$	5.94	2.80
2	$T10$	6.38	2.80
*4	$T11$	6.20	1.70
5	$T11$	6.77	2.70
6	$T12$	6.70	2.70
8	$T1$	6.86	5.40
10	$T1$	6.75	5.50
13	$T1$	6.62	5.40
14	$T1$	6.27	5.40
15	$T1$	6.77	5.50
17	$T2$	6.60	5.40
18	$T2$	6.50	5.60
19	$T2$	6.50	5.60
20	$T2$	6.48	5.60
21	$T2$	6.50	5.50
22	$T2$	6.45	5.60

Continued on next page

Table 2.5 – *Continued from previous page*

Module #	**Mod Type**	**I_{sc} (A)**	**V_{oc} (V)**
23	$T2$	6.95	5.30
24	$T2$	6.34	5.50
25	$T1$	6.30	5.40
26	$T1$	6.41	5.50
28	$T1$	6.96	5.40
29	$T1$	6.82	5.60
30	$T1$	7.40	5.60
31	$T2$	6.66	5.60
32	$T3$	6.56	5.60
33	$T4$	6.62	5.50
34	$T5$	6.58	5.50
35	$T6$	6.57	5.60
36	$T6$	6.47	5.40
37	$T2$	6.63	5.50
38	$T2$	7.14	5.50
39	$T2$	6.30	5.30
40	$T8$	6.54	5.60
41	$T9$	6.49	5.50
42	$T9$	6.37	4.80

* Damaged Module

We calculated the mean and standard deviation for the types of modules with two or more of the same type. The results are in Table 2.6. Note that the largest standard deviation of 0.40 reported is between modules of type T11.

Damaged modules or those with a single module for that specific type were not considered in these calculations. Overall, the individual cell measurement and module manufacturing are the two most time-consuming array fabrication tasks and require sensitive handling and accurate execution to achieve good results.

Table 2.6: **Mean and standard deviation of the short circuit current (I_{sc}) for the modules.**

Module Type	Number of Modules	Mean (A)	SD (A)
T1	10	6.72	0.32
T2	12	6.59	0.24
T6	2	6.52	0.07
T9	2	6.43	0.08
T11	2	6.45	0.40
T12	2	6.73	0.05

Chapter 3

Module Encapsulation

3.1 Module Design

The encapsulation and electrical design of each module embedded the novel ideas presented in this thesis. The traditional way to encapsulate a solar panel is to use the following layers in the given order: front cover, encapsulant, cell, encapsulant, back cover. However, in our design, double-sided Kapton tape was substituted for the encapsulant at the bottom of the cell. This is because the encapsulant (EVA) represents one of the heaviest construction materials. The Kapton tape acts as an adhesive reducing the weight of the module and consequently of the array overall. Other innovations found in the design of BeVolt's array is that bypass diodes are embedded in the modules' encapsulation; additionally, some RTDs are integrated and placed in strategic points to measure the array's temperature. Finally, the detailed procedures and techniques for module fabrication are considered proprietary by the commercial module vendors. Through extensive research and experimentation we developed a fabrication process with results as good as the best modules available commercially.

3.1.1 Module Weight

The modules constructed according to the method and techniques described in this thesis are weight comparable to several other professional manufactured modules. Table 3.1 provides the weight for three of the modules encapsulated according to these method and using the materials detailed in this chapter. These three modules contain the bypass diodes and wiring, but do not have the diode heat sink attached.

Table 3.1: **Weight for modules without heat sink manufactured according to the method and techniques described in this thesis.**

Module #	Weight (g)	Cells/Module	Weigh/Cell (g)
BU7	138.80	8	17.35
BU27	137.20	8	17.15
27	131.85	8	16.48

We weighed some of the modules manufactured by SunCat Solar, which is a company that specializes in the manufacturing of solar modules for solar vehicles. Results are shown in Table 3.2. These modules were encapsulated and bought in 2013, and are spares for our previous solar car, TexSun.

Table 3.2: **Weight for three modules manufactured by SunCat Solar purchased for TexSun in 2013.**

Module #	Weight (g)	Cells/Module	Weigh/Cell (g)
45	161.80	12	13.48
46	162.80	12	13.57
31	43.35	3	14.45

Due to the modules not being the same size, we used the average weight per cell to compare them, this was done as follows:

$$\frac{17.35 + 17.15 + 16.48}{3} = 16.99 \, \frac{g}{cell}$$

for the modules we made and

$$\frac{13.48 + 13.57 + 14.45}{3} = 13.83 \, \frac{g}{cell}$$

for those manufactured by SunCat Solar. Then, we divided the results to find the percentage difference $\frac{16.99}{13.45} = 1.2284$; therefore, giving a 22.84% weight difference. A main factor that makes the difference between the weighed modules is the EVA thickness. Table 3.3 shows the results of the thickness and weight per area of each module tested.

Table 3.3: **Thickness, weigh per area of three laminated modules.**

Manufacturer	**EVA Layers**	**Thickness (mils)**	**Weight/area ($\frac{g}{cm^2}$)**
SunCat	2	16	0.0888
In-House	2	41	0.1528
In-House	1	25	0.1150

Comparing both modules that we manufactured with everything the same except for an EVA layer added, we discovered that the module with two EVA layers was 64% thicker and 33% heavier than the module with a single EVA layer. Then we measured SunCat's module weight and thickness and found that our module with a single layer of EVA was 56% ticker and 30% heavier. This comparisons demonstrate that the thicker the EVA, the heavier

the cell.

Additionally, it is important to note that the modules we made have already included the bus electrical wiring and the diodes, which are not found in the SunCat Solar modules. SunCat Solar modules still need the bus wiring and the heat sinks for the diodes to be soldered. Therefore, if we would have been able to obtain and use the same EVA thickness as that used in SunCat's modules, our modules would be lighter than SunCat's modules considering all the factors combined.

Another weight factor that makes a difference is the number of cells in each module due to the material weight distribution at the edge of each module. More cells in a module uses the edge weight distribution more efficiently. For example, the modules we manufactured which contain 8 cells show a weight (Table 3.1) that lies between the SunCat's modules with 3 and 12 cells (Table 3.2). If we take the weight average of all three modules from each table there is a 10.84% of weight difference. Thus, we believe that if we make larger modules, the materials' weight distribution will improve in the modules and, consequently, the array.

We also weighted some modules manufactured by SunWize in 2008. SunWize is another company that has made modules for solar vehicles. The weight results obtained are given in Table 3.4. The modules came from spares that we have had since 2008. SunWize modules were purchased for Solorean, the UTSVT solar car before TexSun.

Figure 3.1: **SunWize lamination drawing showing the materials and the encapsulation stack.**

Table 3.4: **Weight for five modules manufactured by SunWize, which were spares for Solorian in 2008.**

Module #	Weight (g)	Cells/Module	Weight/Cell (g)
1	343.20	12	28.60
2	351.60	12	29.30
3	335.20	12	27.93
4	336.20	12	28.02
5	75.10	3	25.03

Fig. 3.1 shows that Tedlar is the back cover of the lamination, which is a very sturdy but heavy material. We used the same method to compare as before, we found that SunWize's modules average weight per cell is

$$\frac{28.60 + 29.30 + 27.93 + 27.93 + 28.02 + 25.03}{5} = 27.78 \, \frac{g}{cell}.$$

Then comparing SunWize's modules with ours, $\frac{27.78}{16.99} = 1.6351$ shows that our modules weight is only a fraction of the SunWize's modules. We believe that the additional 63.51% weight on SunWize's modules comes from the thick heavy materials used in their lamination.

Table 3.5: **Weight for each module including the embedded diode and heat sink manufactured for BeVolt.**

Module #	Weight (g)	Cells/Module	Weight/Cell (g)
-	82.00	4	20.50
0	78.90	4	19.73
1	79.10	4	19.78
2	77.30	4	19.33
3	79.30	4	19.83
4	81.30	4	20.33

Continued on next page

Table 3.5 – *Continued from previous page*

Module #	**Weight (g)**	**Cells/Module**	**Weight/Cell (g)**
5	78.85	4	19.71
6	78.81	4	19.70
8	139.20	8	17.40
10	139.50	8	17.44
13	138.70	8	17.34
14	139.30	8	17.41
15	143.10	8	17.89
17	141.00	8	17.63
18	141.85	8	17.73
19	137.50	8	17.19
20	139.00	8	17.38
21	139.70	8	17.46
22	138.00	8	17.25
23	141.50	8	17.69
24	142.50	8	17.81
25	140.40	8	17.55
26	138.70	8	17.34
28	141.65	8	17.71
29	140.70	8	17.59
30	136.75	8	17.09
31	142.40	8	17.80
32	140.20	8	17.53
33	142.70	8	17.84
34	142.60	8	17.83
35	142.20	8	17.78
36	145.50	8	18.19
37	138.50	8	17.31
38	141.20	8	17.65
39	143.20	8	17.90
40	143.00	8	17.88
41	144.50	8	18.06
42	145.30	8	18.16

Weight measurements for each module to be placed on BeVolt are given in Table 3.5. The weight given in this table includes the diode, heat sink, electrical bus connections, and in some of them, the RTD embedded in the encapsulation. Consequently, there is no need to add anything else to these modules, whereby all the weight is already included.

3.2 Encapsulation

Regardless of its material, manufacturer, or efficiency rating, PV modules endure various and different environmental conditions: wind, thermal cycles, and of course, extreme heat here in Texas. Encapsulation is a process that all modules undergo to have some protection against these conditions. Encapsulation is a delicate process and must be done precisely to lessen the stress that the heat applied to the cells and the effect that the materials add to the module as a whole. Additionally, the materials used contribute to the overall end efficiency results and output of the solar array.

A number of stages must be executed with high precision during each solar module's lamination process to achieve a successful encapsulation. Appendix B.1 provides each phase with a list of steps to accomplish an encapsulation using the tools and materials specified in this thesis.

3.2.1 Soldering Cells Together

We used Maxeon Gen III Le1 solar cells to manufacture BeVolt's solar array.

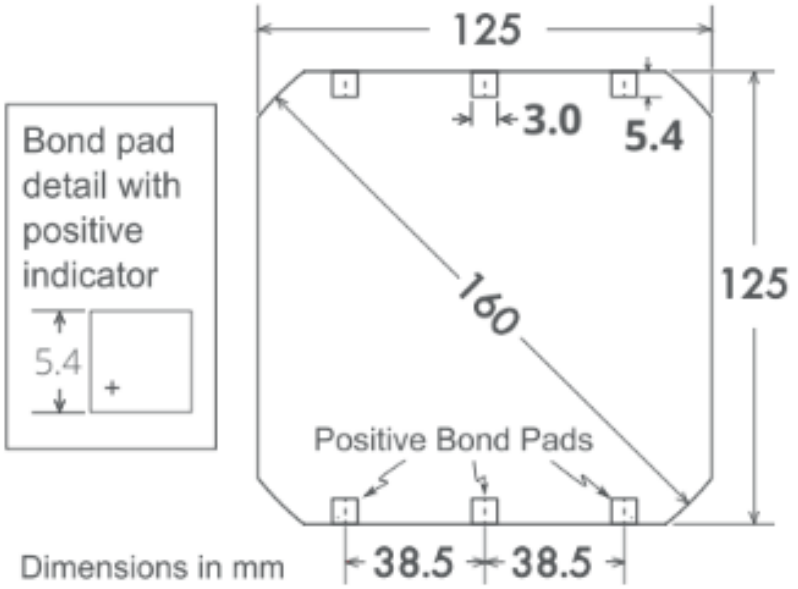

(a) **Individual cell dimentions**

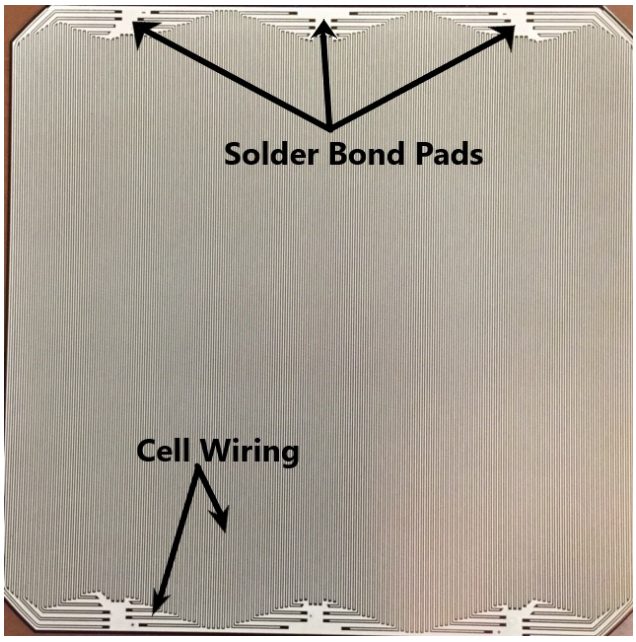

(b) **Bond pads and wiring**

Figure 3.2: **Individual cell dimentions and wiring for SunPower Maxeon solar cells.**

Soldering Sunpower Maxeon solar cells is challenging and requires precision due to the cell's fragility. These cells have a thickness of approximately 150 µm, and its soldering bond pads are 5.4 mm^2 (Fig. 3.2a). The limited space makes the soldering challenging due to the cell being a good heat conductor.

It is important to note that the cells are back-contacted, and the solder bond pads are at the back of the cell as well as the wiring (Fig. 3.2b). If melted solder extends outside of the area provided in the bond pad, the cell becomes short-circuited due to the extremely narrow separation of the traces.

Bond pads are designed for wiring the cells together. Sunpower recommends special interconnect tabs that they manufacture to make the soldering easier. These tabs have the correct gap between each bond pad and the separation between cells; however, the distance between cells must be carefully manipulated to prevent the connection from becoming tilted. For this purpose, we used a mold with fixed-width spacers to have a uniform separation (Fig. 3.7 on page 57).

3.2.2 Monitoring Time and Temperature

Most of the materials used for encapsulation include a temperature range in their datasheet as one of the most critical elements. Usually, the Ethylene-Vinyl Acetate (EVA) will define the curing time and temperature range for the process; the rest of the material's temperature is adjusted accordingly. It is noteworthy that curing times and temperature must be closely observed to avoid undesirable results, i.e., having a non-bonded encapsulation

if the temperature is too low or highly stressed module, which breaks with a minimal mishandling.

3.3 Materials

One of the essential characteristics that the selected materials for the lamination of cells for a solar vehicle must have is weight requirements (as is every component in the car). There are two types of materials used to laminate modules: the elements that become permanently part of the lamination and those that are used temporarily to facilitate the lamination without losing a great deal of the cell efficiency.

The materials that become part of the module are single-sided Teflon, Ethylene-Vinyl Acetate (EVA), cell module, Kapton tape, tinned copper ribbon, and double-sided Teflon. These materials proved to have suitable properties to allow the module to produce a competitive output power, as demonstrated with the results in Table 2.5. Temporarily used materials are a frame, vacuum bag, two pieces of Teflon fabric, yellow sealant tape, and a small piece of breather fabric.

3.3.1 Materials That Permanently Become Part of the Module

Everything that permanently becomes part of the array has to meet the weight and high-temperature requirements. Fundamentally, the array will be exposed to the radiation of the Sun to produce power. In summer in Texas, temperatures go above 100°F; consequently, after the module has been

laminated, its components are required to be stable while being exposed to up to 200°F to prevent the lamination from coming apart.

3.3.1.1 Single-Sided Teflon

As is widely known, virtually nothing sticks to Teflon. For example, Polytetrafluoroethylene (PTFE) is used in cookware to avoid food sticking to a pan. A Teflon film is similar. The term single-sided Teflon is defined by the chemical treatment given to one side only of the film to allow its adherence on that particular side. In our research, we found that this type of film is useful as the primary material protecting the module overall from environmental exposure, i.e., water, dust, wind. Using a piece of single-sided Teflon on the top of the encapsulation facing the treated side to the module ensures its adherence to the rest of the stack in the lamination process. In contrast, the untreated outer side expels anything that becomes in contact with it. Additionally, Teflon film is available in a wide range of thickness, allowing us to have an array with the necessary characteristics and reducing the mass added by this material to meet the weight requirement for the lamination.

3.3.1.2 Double-Sided Teflon

Double-sided Teflon film has the same characteristics as the single-sided Teflon film, except it is treated on both sides. We use this piece of film at the bottom of the module. One side of it bonds to the module while the other side will affix to the vehicle's surface; thus, having it treated on both sides is

required.

3.3.1.3 Ethylene-Vinyl Acetate

Ethylene-Vinyl Acetate copolymer is better known in the encapsulation world as EVA. The EVA softness and flexibility is a rubber-like material. In the lamination process, we use it as an adhesive by melting it at a temperature of 300°F. The standard thickness used to be 0.5mm; lately, thinner EVA has emerged in the market. Although it is still not easy to get this new EVA locally, we managed to acquire a thinner (0.3mm) material. In our research, we discovered that EVA added substantial weight due to its thickness. We compared the weight of two laminated cells where everything was the same except for the EVA thickness; we observed that the lamination with 0.3mm (thinner) EVA weighted approximately $\frac{1}{3}$ less than the cell with 0.45mm (thicker) EVA. Consequently, using thinner EVA is the best solution for meeting the weight requirement in BeVolt's solar array.

3.3.1.4 Cell Module

The technique to assemble each cell module is nearly repetitive when soldering them; however, the arrangement designed for each type of module varies according to its position in the solar array as a whole. In Appendix B.1 there is a list describing the process step by step to assemble a module. There are twelve different module configurations in the solar array. Appendix C has the design for each module layout.

3.3.1.5 Kapton Tape

Kapton is a polyimide film developed by DuPoint in the late 1960's. It is an excellent electrical insulator and is stable over a wide temperature range. According to kaptontape.com, Kapton tape is "made from Kapton polyimide film with silicone adhesive making it compatible with range temperatures of -269°C to +260°C." We use double-sided Kapton tape as the layer between the cell and the bottom protecting film in the module encapsulation. It acts as an adhesive, protector, and electrical isolator. Thanks to its thickness of 5 mils, its weight is practically negligible, decreasing the weight of the array overall.

3.3.1.6 Tinned Copper Ribbon

In contrast to most other electrical components, solar cells require a thin, flat, highly conductive wire for the interconnections to avoid the problem of cells cracking. Today, the tinned copper ribbon has become a well known and commonly used interconnect in the module encapsulation. A tinned coating makes it easier to solder to the cells. We used this material extensively in the manufacturing of BeVolt's solar array.

3.3.2 Materials Used Temporarily

Although these materials do not become a permanent part of the array, they play a critical role in the encapsulation. Furthermore, except for the frame, they must be high-temperature resistant due to their exposure during

the lamination process.

3.3.2.1 Vacuum Bag

The main functionality of the vacuum bag is to compress all the stack materials together making the bonding between them easier. Now since we do not use a top hot plate in our lamination, the Vacuum Bag has three aditional roles: being the last top layer in the lamination stack, it automatically works as a top plate in the system. Additionally, it prevents the air from escaping the encapsulation. Finally, it helps maintain the whole system's temperature at the desired level during the curing time enclosing the stack within.

3.3.2.2 Yellow Sealant Tape

Around the hot plate, a double row of yellow sealant tape (sometimes known as tacky tape) is used to hold the vacuum bag in place without letting any air get into the lamination stack for the time that the lamination process lasts. This sealant is strong enough to stay in place regardless of the vacuum pressure.

3.3.2.3 Frame

We straighten the vacuum bag before sticking it on the yellow sealant tape placed on the hot plate, using a frame made out of aluminum window screen frames and plastic corners. Placing the vacuum bag to the frame first, makes it easier to attach it to the yellow sealant tape afterward while avoiding

having significant air bubbles or wrinkles in the enclosed stack.

3.3.2.4 Teflon Fabric

To help the air within the enclosed area of the encapsulation travel towards the base of the thru-bag vacuum connector to be pumped out, we use two pieces of Teflon fabric; one on the top of the stack and one at the bottom. This dynamic is essential to avoid rough surfaces on the module.

3.3.2.5 Breather Fabric

The thru-bag vacuum connector that goes inside the vacuum bag evacuates the air within the encapsulation. A small piece of breather fabric is placed under the connector to keep the air traveling towards it and allow pumping the air out of the lamination stack. This procedure is critical to have a smooth top surface on the module. If an adequate vacuum is not obtained, the module could show bubbles, dents, or ripples on the surface, which in turn will add friction and drag when the car is running.

3.4 Lamination Tools

Some of the tools used in the encapsulation process described here are not absolutely required but facilitate the task, ex., the soldering mold and fans. However, others are essential; these could only be replaced by a different tool that provides the same function, for example, the hot plate and infrared camera.

3.4.1 Hot Plate

Designing a hot plate to laminate solar cells could be a highly sophisticated or impressively simple system; we chose the second option. Some of its fundamental characteristics are to avoid damaging the cells, to have a smooth, even surface without marked lumps or indentations, and to be sufficiently large for the modules being constructed. The hot plate we designed to laminate the modules is composed of three pancake griddles, a thick aluminum plate, and thermal conductive grease, as shown in Fig. 3.3.

The thickness for the aluminum plate ($\frac{1}{4}$ in) is optimized (not too thick or too thin) to produce uniformly distributed heat and reach the desired temperature at the same time. To help the griddles transfer the heat efficiently, we spread Tracit-1100 thermal conductive grease (manufactured by Chemax Corporation and available from McMaster) in between the aluminum plate and the griddles.

We cut off the plastic edges of the griddles to expose the metal heating surface and allow them to come close together and essentially create a single large metal plate. Once they were close together, we placed the aluminum plate to form a single surface (Fig. 3.3). The thermal grease minimizes the gaps between the aluminum plate and the griddle heating surface, efficiently transferring heat to the aluminum plate.

A thermal camera (FLIR One Pro) was used to monitor the system temperature.

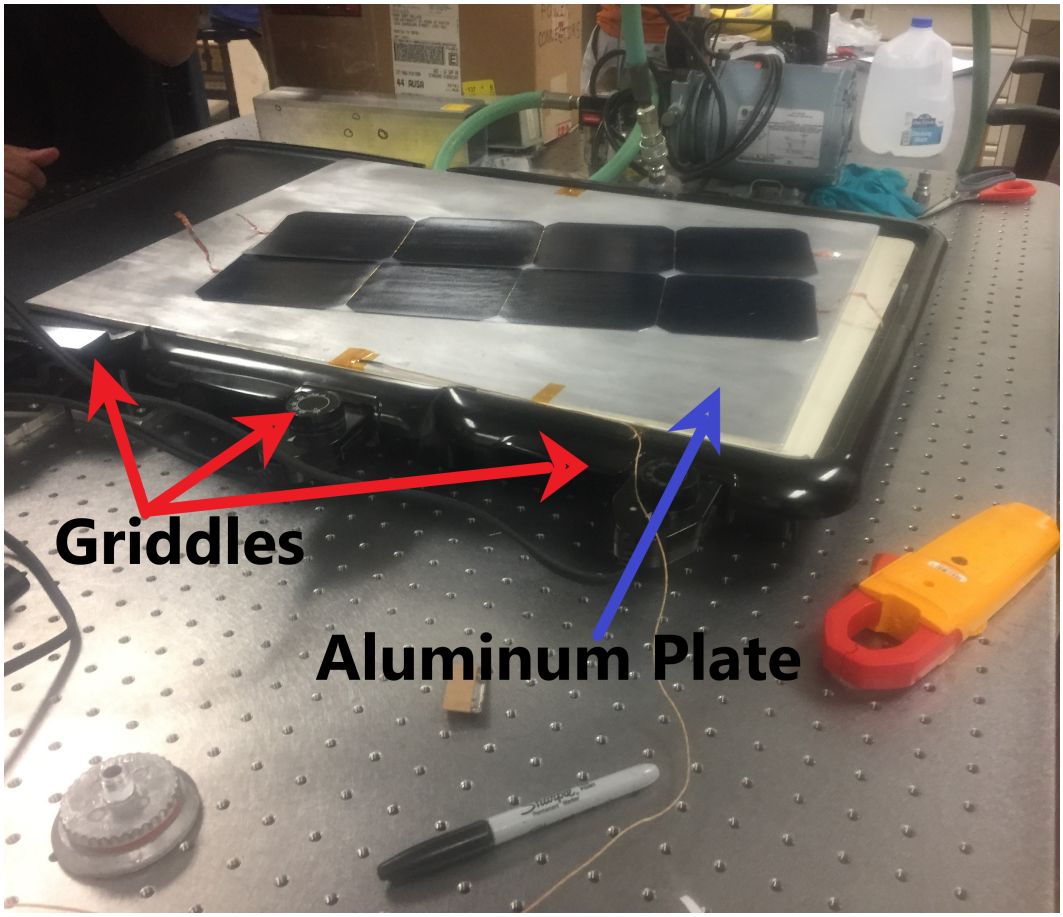

Figure 3.3: **Griddles and an aluminum plate make the hot plate configuration.**

When the griddles were heated without adding anything, the infrared camera would show that the temperature of the coils underneath the plate to be approximately 90°F hotter than the rest of the griddle (Fig. 3.4a). After adding the aluminum plate with the thermally conductive grease in between, the heat distribution is considerably improved. The improvement is seen not only on the plate but also in the enclosed area of the encapsulation (Fig. 3.4b).

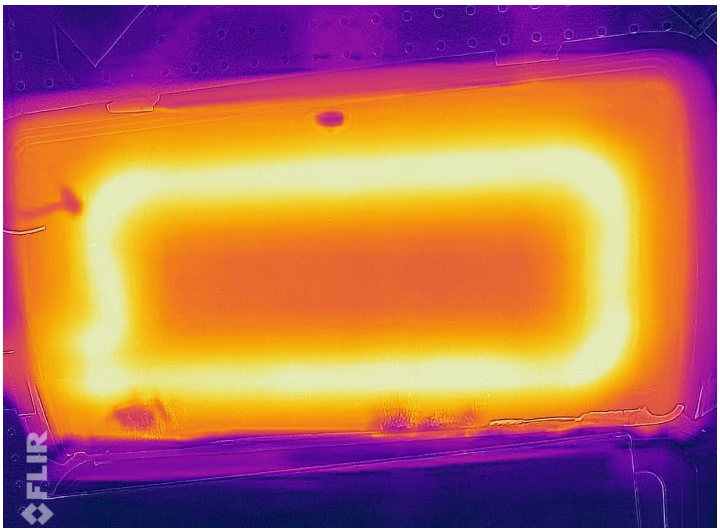

(a) **Griddle Without Aluminum Plate**

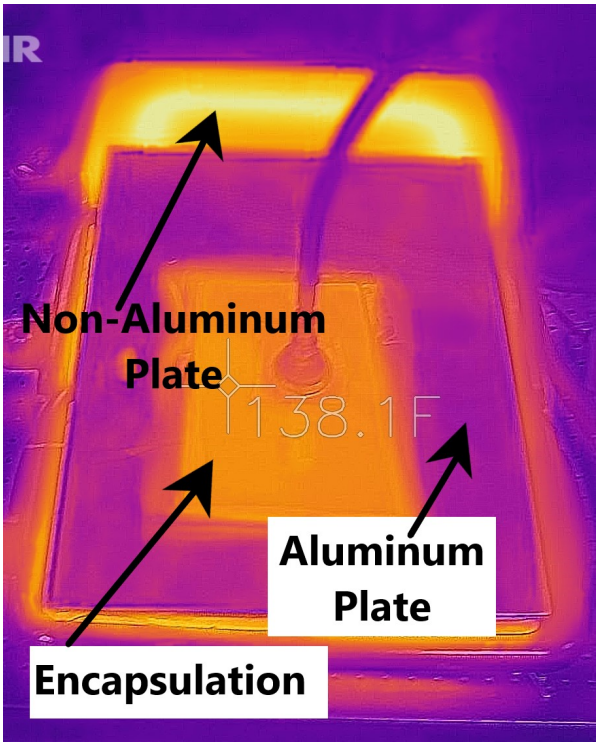

(b) **Griddles with Aluminum Plate**

Figure 3.4: **Effect of the aluminum plate on the heat distribution.**

Due to the high-temperature used during the lamination, the yellow sealant tape firmly sticks to the plate, making it difficult to remove after the curing time (during the cleaning procedure). Therefore, the hot plate system was attached to the table to avoid movement when cleaning.

3.4.2 Vacuum System

The solar cell encapsulation we chose is a baked vacuum-based technique, where controlling the vacuum is one of the critical aspects of the system. Earlier in the development of the lamination technique, we started the process using the vacuum pump after the hot plate had reached 150°F temperature. However, we experienced some vacuum problems while using this method. One of the issues we found was that if the vacuum bag was not completely sealed and the heat was turned on, the EVA would start getting soft. By the time the vacuum system was turned on, it was too late to avoid the development of ripples on the top surface as it is shown in Fig. 3.5. Curing EVA outgasses volatile monomers, and allowing those gasses to form air bubbles inside the lamination risks the correct bonding between the EVA and the Teflon film, and the ripples would stay and still appear at the end-product. Turning on the vacuum after those gasses have started to move around the enclosed module is very risky. We learned that it is best to turn on the pump from the beginning to make sure that there are no air leaks, and when that is confirmed, to keep it on to the end of the curing phase. Due to this problem, we modified our approach and resolved the first problem by turning on the vacuum much

earlier (Appendix B.5).

Figure 3.5: **Cell showing loss of vacuum due to the vacuum system being turned on after the EVA volatile gasses have started to move around forming bubbles inside the lamination.**

Another challenge was the loss of vacuum during the heating process, where the yellow sealing tape would come off the hot alumninum plate allowing air to go into the lamination stack causing ripples. These would also show at the module ultimate result. We overcame that outcome by adding another strip of yellow "tacky" tape around the lamination stack, providing a much better vacuum seal. This prevents air from leaking into the stack and therefore the air bubbles from forming on the module. Having these ripples and air bubles on the modules is not just a cosmetic matter but also an aerodynomic matter. If many modules have the same issue, the surface of the array becomes

rough putting friction on the car which in turn will result in the use of more power. Therefore, we need to prevent these cases if at all possible.

3.4.3 Infrared Camera

With the availability of technology becoming more sophisticated on a daily basis, devices to monitor temperature have become more available and less costly. We opted to use the FLIR One Pro thermal camera.

This camera allows us to continuously monitor the temperature without installing sensors (RTDs, thermocouple, etc.) inside the lamination stack. It avoids the risk of air infiltration through the small opening required where the temperature sensor wires exit the vacuum bag. The camera method minimizes the risk of bubbles produced by air coming into the encapsulation and also gives an accurate temperature measurement in two dimensions. It is expected that the temperature will be lower outside of the encapsulation compared to the enclosed area. We temporarily placed a thermocouple inside the vacuum bag then applied vacuum (Fig. 3.6) to compare the sensor measurement with the infrared camera.

While these two did not match exactly the same, the difference shown between both devices was of 10°F. This way, we ensured to apply the enclosed temperature accurately without the need of introducing temperature sensors within the encapsulation stack.

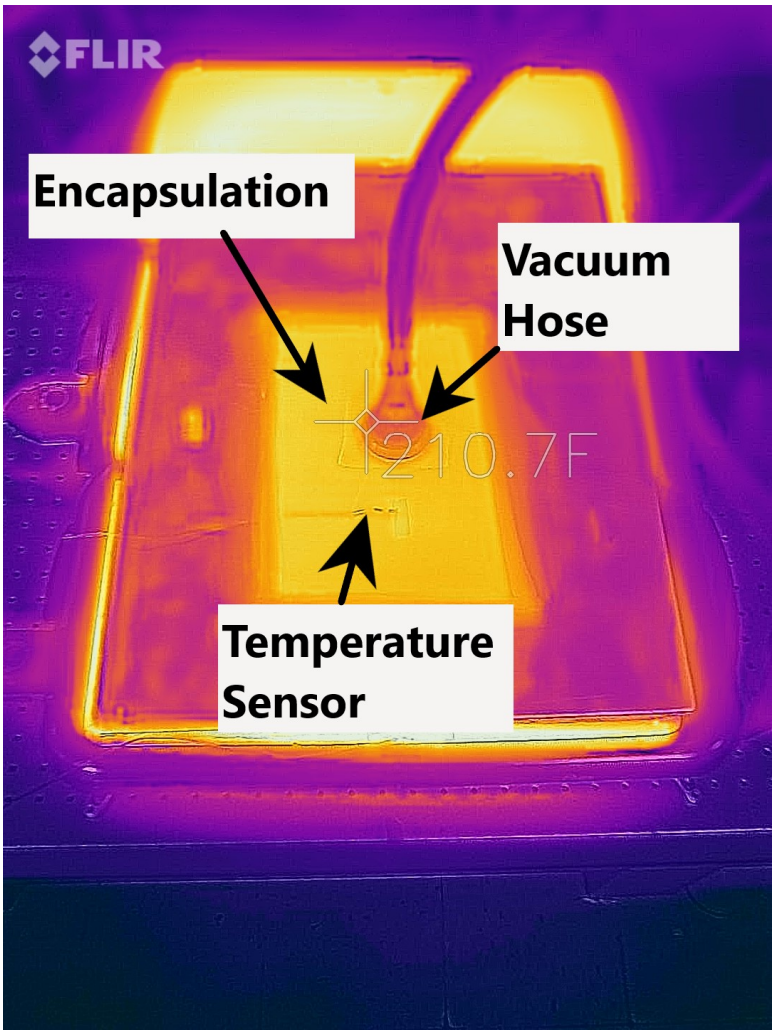

Figure 3.6: **Wired Sensor and Camera Temperature Comparison.**

3.4.4 Soldering Mold

A mold was fabricated with wood to accurately position the solar cells and form a module. On top of the wood, we placed a layer of G10 Fiberglass to reduce the wood contaminants from reaching the cells when soldering them.

The fiberglass has small slits of 1mm width to hold Teflon pieces that are placed in between cells. The Teflon has a dual purpose: first, to prevent the cells from moving around at the time of soldering them together. Second, to have a precise and uniform separation between cells.

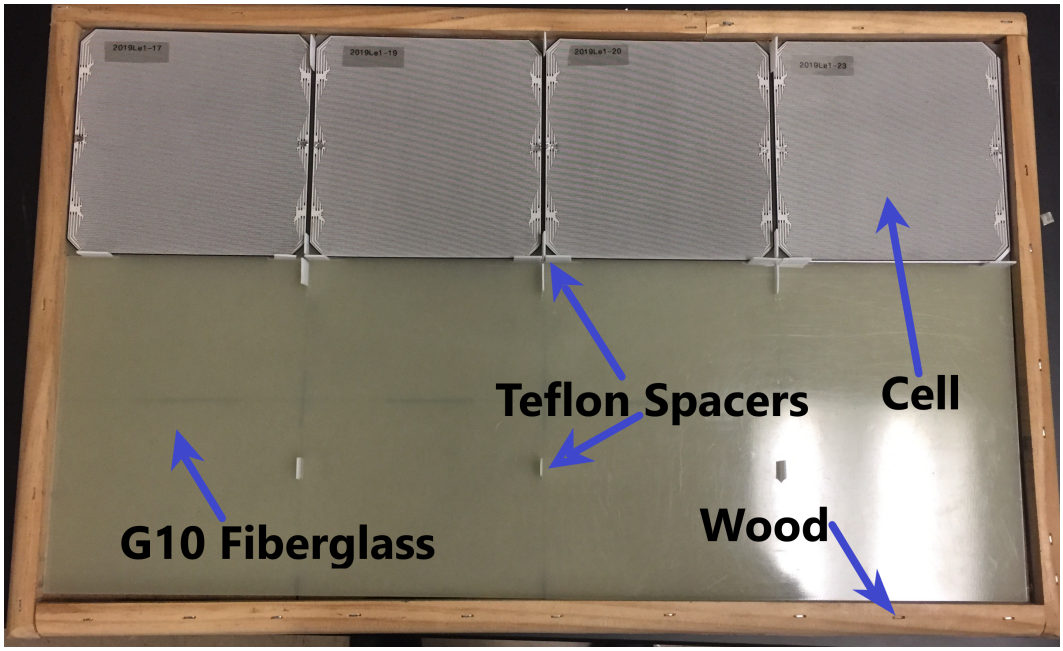

Figure 3.7: **Soldering Mold.**

3.4.5 Fans

We use fans to minimize the cool-down time. After the encapsulation process is complete and the heat is turned off, the hot plate is at approximately 300°F. Allowing the hot plate to cool down by itself to room temperature takes 1.5-2 hrs. A single fan blowing directly at the hot plate lowers the time to 50-60 minutes while adding a second fan reduces time to 30 minutes to reach

the 100°F required to start disassembling the lamination stack.

As described in this chapter, our technique and tools implemented in this process lead to a successful module encapsulation. The permanent materials used for the module's encapsulation have substantially improved the overall weight of the array compared to others using the widely standard materials. On the other hand, the temporarily used materials effectively facilitated the process of the lamination.

3.5 Lamination Stack

The arrangement of the stack is assembled using each of the materials described in this thesis. Each part has its role in the lamination; therefore, the placement of each is critical to accomplish the desired purpose in the encapsulation (Fig. 3.8).

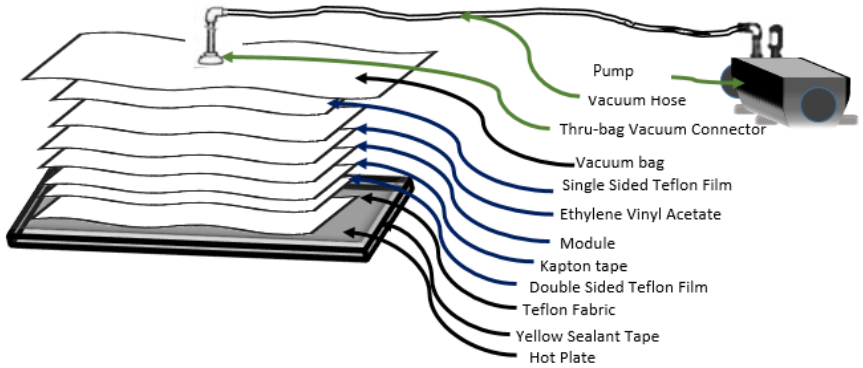

Figure 3.8: **Stack for vacuum bagging setup. The black arrows show temporary materials while the blue ones distinguish those which become permanently part of the module after the encapsulation.**

Chapter 4

Embedded Bypass Diodes and Temperature Sensors

4.1 Bypass Diodes

Most solar arrays incorporate bypass diodes. Typically, these diodes are external to the array, requiring considerable high current wiring for the connections. This practice adds size and weight to the array system, both undesirable in a high-performance vehicle application. We have developed a method to incorporate bypass diodes directly within an array module. This technique required the use of miniature diodes (TO-277B package), solving the heat dissipation issue, and developing interconnect wiring compatible with module construction.

Bypass diodes are wired in parallel with a cell or group of cells, which are electrically removed from the array when shading occurs. Ideally, each cell should have its own bypass diode to avoid dropping the voltage too far down; however, due to costs and practical considerations, most manufacturers have three or more cells per diode, depending on the size of the panel. Solar cells connected in series increase the voltage, which is generally preferred compared to parallel connections. Nonetheless, series connections pose some risks, i.e.,

if a cell stops working, the path for the current is interrupted, which causes the whole circuit to fail. Likewise, if a panel is shaded partially or totally due to clouds, snow, or other reasons, the shaded area produces little or no power. This fact will actively reduce the array output, all the way to zero power produced if the current is fully interrupted. Bypass diodes prevent this situation, allowing the non-shaded part of the array to continue to deliver full output power.

During normal conditions, when there is no shading disruption, the current will flow through the modules adding each cell's voltage and keeping the current at the same level, as Fig. 4.1a shows. Although the bypass diodes are always present, under these circumstances, they are not activated (reverse bias); therefore, they do not add any counterproductive electrical effects such as resistance except for a small leakage current. However, if a shading disturbance occurs, bypass diodes get activated (forward bias) to provide a low resistance path for the current to keep flowing, preventing major interruption or high resistance in the circuit. During this case, the current flows, as seen in Fig. 4.1b.

In our design for BeVolt's array, shading does not occur only due to clouds or snow; for example, the car's canopy can shade a cell, a whole module, or multiple modules depending on the orientation of the vehicle and the Sun. If the motion is around a circuit and the shading is repetitive, the interruption will be likewise. With a single bypass diode per module, the BeVolt modules range from four to eight cells. Having the diode makes a significant difference

in the performance of the array. Although the diode itself is quite small, we did not use multiple diodes per module, primarily due to the complexity and size of the required heat sink.

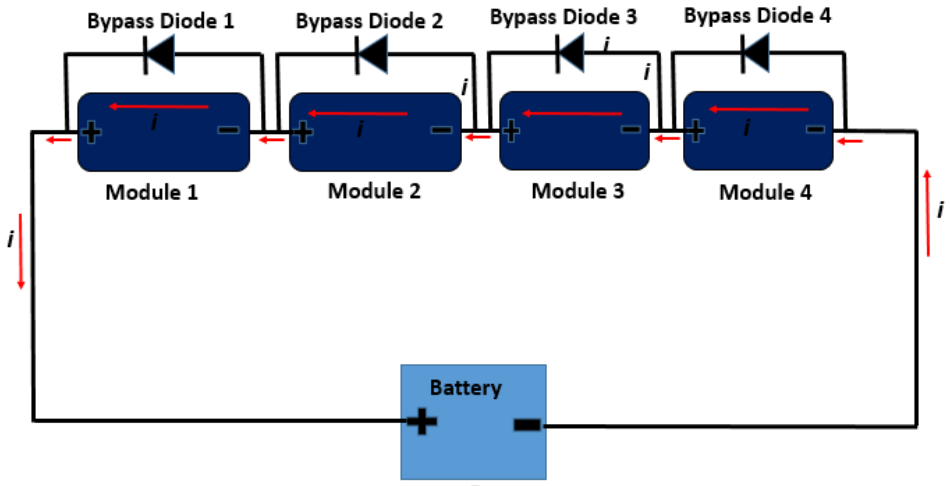

(a) Non-activated bypass diode, no shaded modules

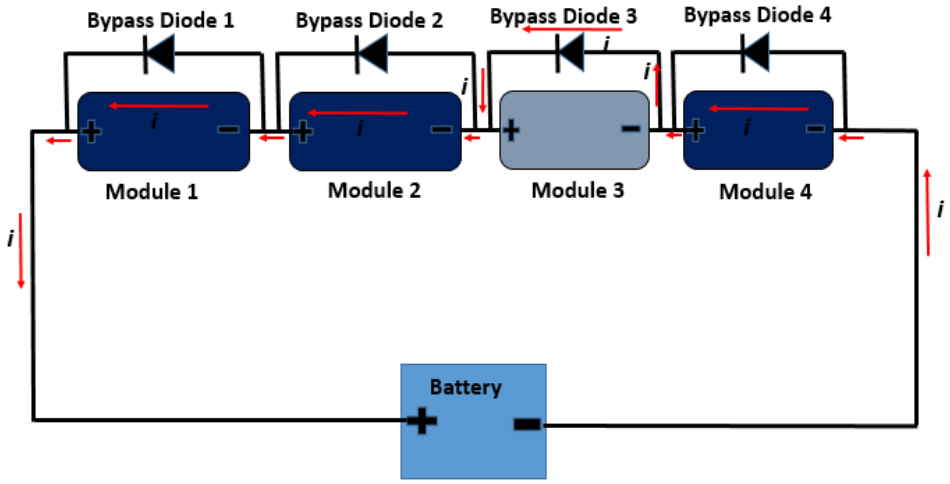

(b) Activated bypass diode due to a shaded module (shown in a lighter shade)

Figure 4.1: **Non-activated versus activated bypass diode to effectively keep the current flow.**

4.1.1 Wiring and Placement

Smaller arrays experience a higher impact with any module disruption; consequently, due to the constant motion of the car, the diode arrangement has to be strategic.

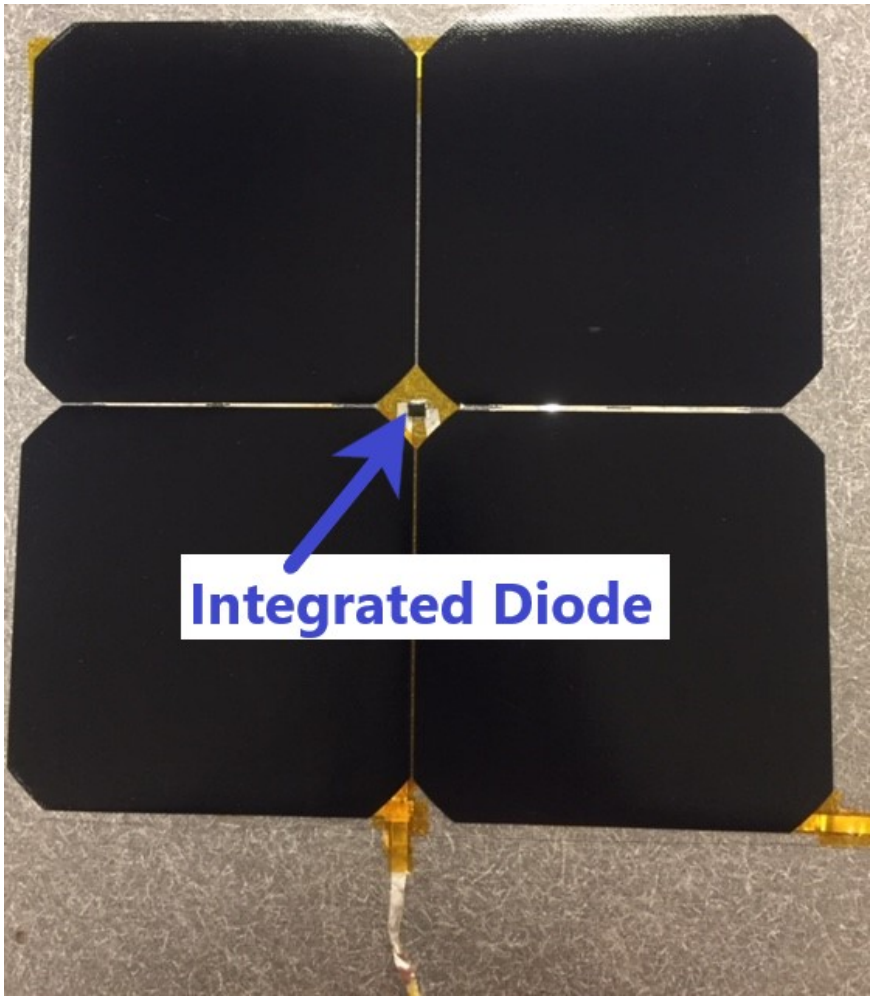

Figure 4.2: **Laminated array module with integrated diode in one of the most complex electrical layout (T12).**

Solar vehicles competing in the ASC races usually carry bypass diodes underneath the array to avoid shading by the wiring and the diodes themselves, as well as aerodynamic considerations. It is critical to ensure that the full short circuit array current can safely flow through the diodes without causing any damage. The array design described in this thesis applies a newly developed configuration compared to the traditional design. This new design uses surface mounted diodes embedded during the encapsulation process.

We selected the Littelfuse Schottky diode and rectifier (DST10100-A), which has a thickness of 1.10mm, a width of 3.05mm, and a 6.5mm length. As Fig. 4.2 shows, this diode is small enough to fit in between the cells without module shading from the diodes or external wires. We integrated a diode in parallel with every module, which forward current rating of 10A gives a good safety factor with the 6A array short circuit current. Its peak inverse voltage rating of 100V minimum is well above the output voltage of all individual modules. This diode offers minimal loss with a forward voltage drop of 0.65V at 10A and a reverse current of 36mA at junction temperature (T_j) of 125°(Appendix D).

4.1.2 Heat Sinks

Most electronic components have a limited temperature range to work correctly and prevent them from getting damaged; diodes are not an exception. The DST10100S-A diodes have a maximum operating temperature of 125°C. Normally, solar racing cars will race during the summer when temperatures

can rise well beyond 100°F. However, that is not the highest temperature the diodes embedded in the array will experience. Inside the encapsulation, the temperature will be significantly hotter due to the constant exposure to the sun and the thermal insulation of the encapsulation layers. Furthermore, when the diodes get activated, they become even hotter due to diode power dissipation that occurs when the modules are shaded and the array current flows through the diode.

To ensure the diode temperature remains within specifications, we added heat sinks in the encapsulation. First, we performed experimental tests without heat sinks. During summertime, the diodes experienced up to 150°C without a heat sink, being exposed to the Sun heat. This caused some of the diodes to fail. Since diodes fail shorted, the module is effectively removed permanently from the array. Therefore, bypass diode failure represents major array degradation and must be avoided.

Developing the heat sinks required considerable time and experimentation. We considered several different materials, including aluminum and copper in a range of size and thickness. Different tests were performed, such as biasing the diodes with a power supply and full module tests in sunlight in various ambient temperatures.

4.1.2.1 Indoor Testing

First, we started our tests indoors with a diode attached to a 12V DC adjustable power supply, and varied the current from 0 A to 6.5 A. In Table

4.1 are shown the results for two types of heat sink, tape and shim. Tape is a 2 inches wide copper material that comes in roll form with conductive adhesive backing. Shim is flat copper shim stock (copper plate) of thickness as specified in the table. The temperature results in Table 4.1 are given for 6.5A diode current (which is the highest current used in all array tests). It also indicates the copper or tape size and the placement of the diode on the heat sink.

Table 4.1: **Diode tests done inside biased by a power supply, set to 6.5 A using copper tape and shim. Results show varying temperature with the different conditions.**

Tape/Shim	Thickness	Placement	Size	Temp (C)
Tape	2 mils	2" Mid	4"x6"	150
Tape	2 mils	3" Mid	4"x6"	130
Shim	7 mils	2" Mid	4"x6"	101
Shim	7 mils	3" Mid	4"x6"	81

The 7 mils copper shim with its high conductivity proved to be a better heat sink than the copper tape in the indoor tests, showing a temperature of 81°C as reported in the last row of Table 4.1. Next, we performed additional tests outdoors.

4.1.2.2 Outdoor Testing

For the outdoor experiments, all the tests were done with the seven mils thick copper shim heat sink with the diode placed in the middle of the 3" (longest) sides. Our first trial was with the diode biased by the DC power supply (DC PS). We followed the same procedure as inside, varying the current

from 0 to 6.5A. The recorded data of this current variation and the diode temperature is provided in the first seven rows of Table 4.2.

Table 4.2: **Diode tests done outdoors biased by the DC power supply and then with two 1x4 module using a 2"x3" copper shim**

Module/DC P S	Current (A)	Placement	Size	Temp (C)
DC PS	1.0	3" Mid	4"x6"	52
DC PS	2.0	3" Mid	4"x6"	62
DC PS	3.0	3" Mid	4"x6"	70
DC PS	4.0	3" Mid	4"x6"	79
DC PS	5.0	3" Mid	4"x6"	92
DC PS	6.0	3" Mid	4"x6"	102
DC PS	6.5	3" Mid	4"x6"	112
*Modules	6.7	3" Mid	4"x6"	110

* Tested with two other 1x4 encapsulated modules

Although the temperature results were higher this time, the highest value of 112°C was within the diode's rating temperature (150°C). Next, we experimented with single bare cells, which stayed approximately at the same temperature as the DC biased diode. Then, with actual sunlight conditions, we place the diode on the middle of the heat sink's 3" edge side and connected in parallel to a 1x4 encapsulated module. Next, we connected this module in series with two other encapsulated modules and proceeded to cover one of the cells of the module with the diode. After three minutes, we started to monitor the diode's temperature for a few minutes. Here, the highest diode temperature we obtained was 110°C as given in the last row of Table 4.2. The

rest of the tests we performed with encapsulated modules were in the same range with a ± 2°C variation. Therefore, we conclude with these findings that the size and placement of the newly designed heat sink is suitable for the array needs.

The heat sink we designed consists of two 3"x2" pieces of copper shim, as shown in Fig. 4.3, giving a total of 4"x6" conductive surface to dissipate the diode's heat. Fig. 4.3 shows each piece's measurements (3" x 2") making up the heat sink and the diode placement in the middle of the 3" (longest) side. Fig. 4.4 displays how the diode looks from the top view.

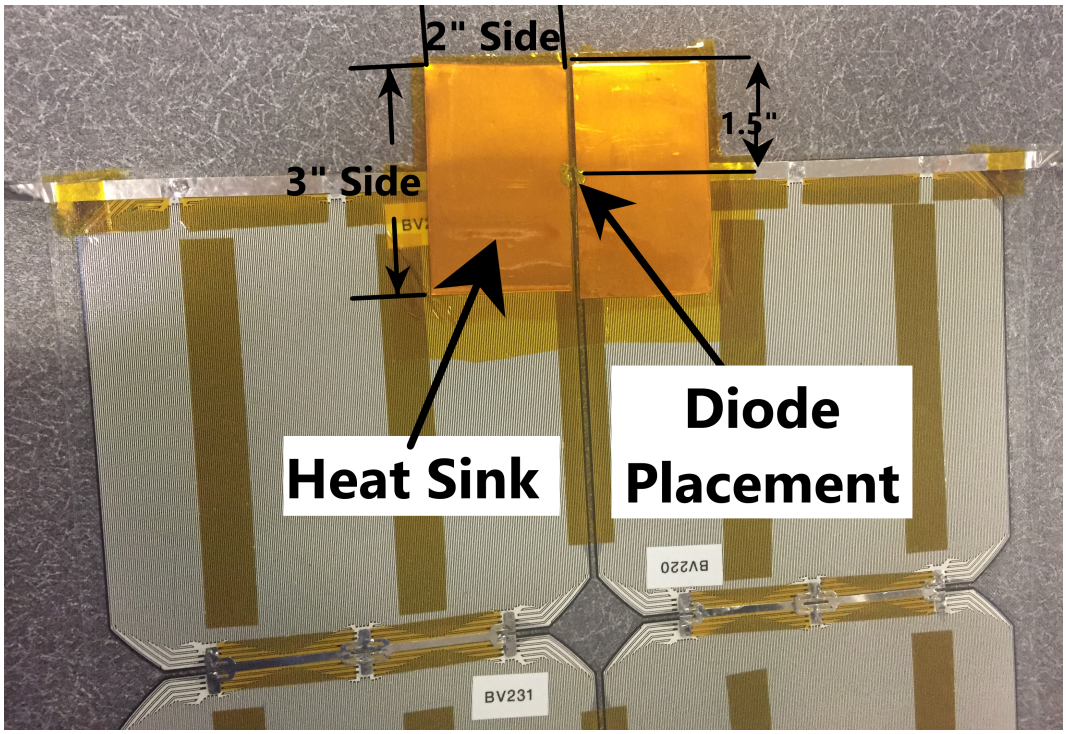

Figure 4.3: **Heat sink bottom view showing the size measurements and the placement of the heat sink.**

Subsequently, after connecting a diode in each panel, we proceeded to connect all the panels as a single sub-array to be tested, which process and results are presented in Chapter 5. No diode failure ocurred during any of the sub-array testing.

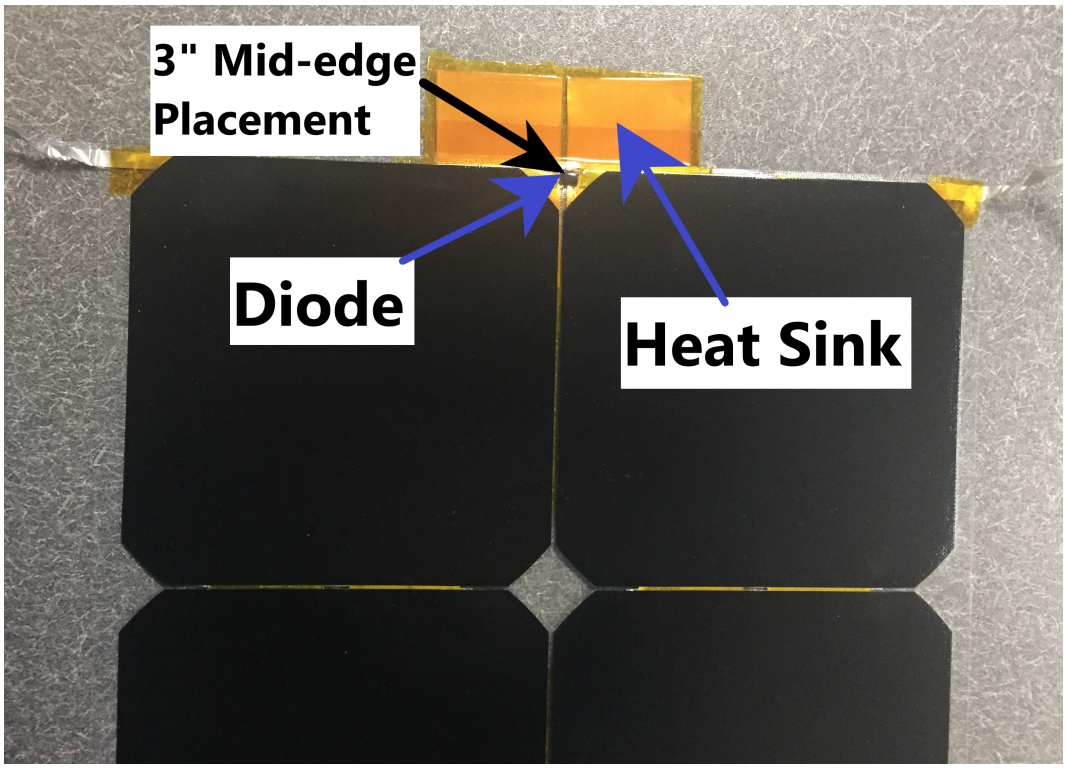

Figure 4.4: **Heat sink top view integrated in the encapsulation.**

4.2 Temperature Sensors

A solar array needs sunlight to function; therefore, the modules are constantly exposed to the heat of the Sun. Unfortunately, as the cells get hot due to solar radiation, their efficiency is reduced, and the output power

decreases. To monitor the array temperature, we have integrated Resistance Temperature Detectors (RTDs) in the array. RTDs are embedded in the modules' encapsulation on the cells, as shown in Fig. 4.5.

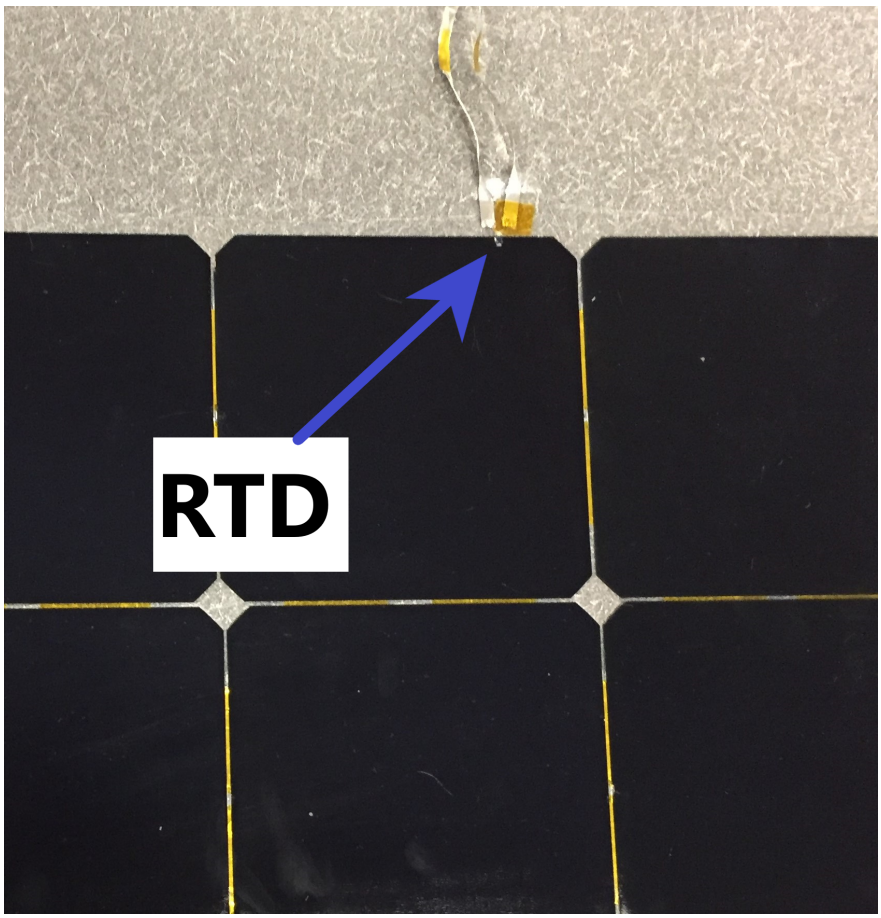

Figure 4.5: **RTD Embedded in the encapsulation.**

The passivated thin-film platinum element deposited on a ceramic substrate has excellent stability ranging from -50°C to +500°C, as stated and shown on the RTD datasheet found in Appendix D. Additionally, it notes

the high accuracy through resistance and temperature deviation, which can be controlled to within ±0.06% and ±0.15°C.

The RTDs are placed right on top of the solar cell making direct contact with cell's surface; however, its tiny size of 0.079" (±0.007") width, 0.118" (±0.008") length, and a 0.049" thickness blocks a negligible amount of light of 0.0392% of the 153.3cm^2 total cell area. With this placement, they measure the actual cell temperature inside the lamination.

Fig. 4.6 gives the analog circuit used with the RTDs. The RTDs are connected to an operational amplifier (op-amp), which coverts the RTD's resistance to a voltage proportional to temperature. Then, the voltage is digitized by an ST microsystem NUCLEO-L432KC embedded microprocessor.

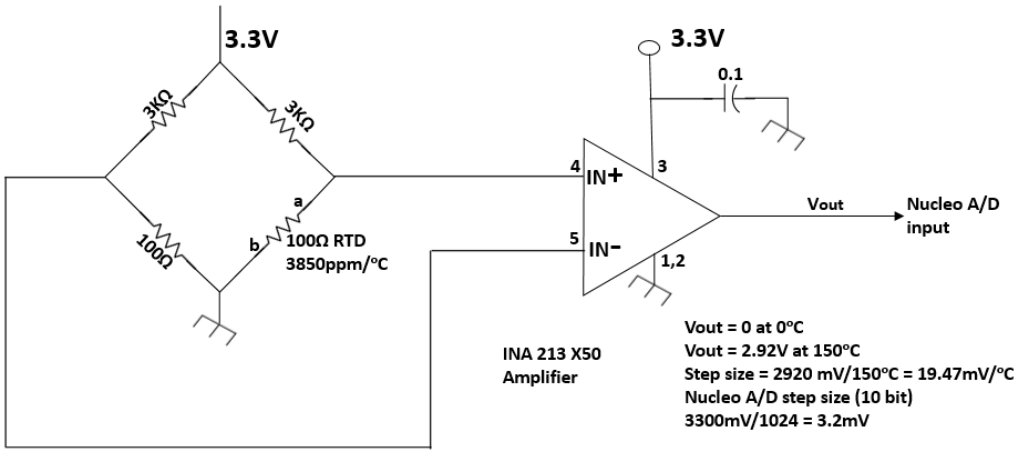

Figure 4.6: **Diagram of the temperature sensor circuit used to measure the cells' temperature on the array.**

Typically data is recorded and stored at approximately one-second in-

tervals.

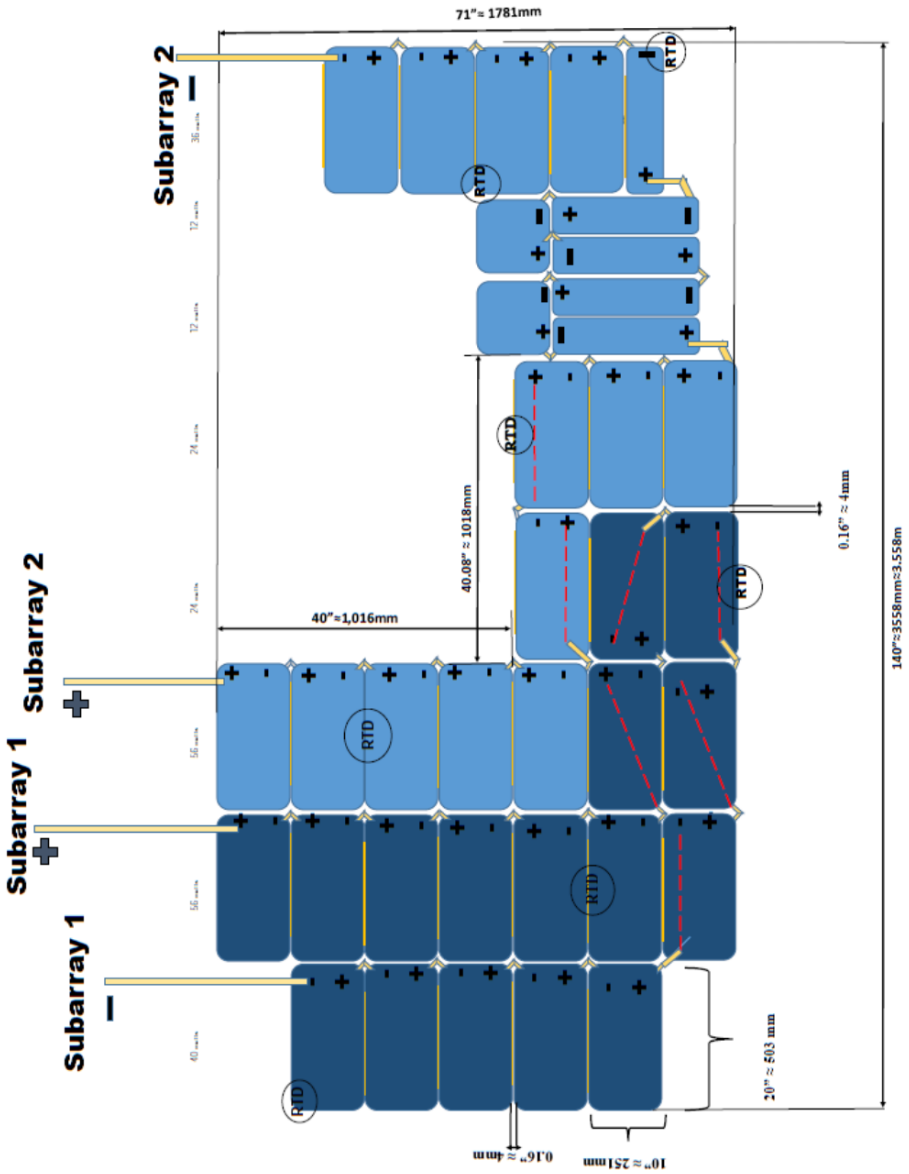

Figure 4.7: **Plan view of the BeVolt array showing the location of the seven RTD temperature sensors.**

Knowing the cell's temperature enables the user to correct the expected

array output with temperature variations. During a race, one strategy is to stop the vehicle temporarily to spray water on a hot array to cool it down.

Another use of the temperature sensors is simply to monitor if the sub-arrays are putting out the expected power.

4.2.1 RTD Locations in the Array

There are seven RTDs distributed in the $4.0\,\mathrm{m}^2$ area of the array. Strategic points were selected to collect representative data for the entire array. Fig. 4.7 gives the location of the RTDs on BeVolt's array.

In our design, the RTD wiring is done through holes made on the surface of the car body. The hole is made immediately under the module that contains the RTD running the wire in the car's interior. Their placement is determined according to two main constraints: the design of the car's top shell, which has metal supports underneath, and the measurement points of interest according to the arrangement of the array itself.

Chapter 5

Array

Following the American Solar Challenge (ASC) size regulations, the maximum array size permitted for BeVolt is 4.0 m^2 [5]. Considering the $153cm^2$ cell area that the datasheet provides and using $(\#ofcells)(cellarea) = 4.0m^2$ substituting would give $(260)(153cm^2) = 3,9780cm^2 = 3.978m^2$ which is very close to the 4.0 m^2 allowed by the ASC regulations. Therefore, it was determined that BeVolt's solar array should consist of 260 cells configured as two subarrays with the cells in each subarray connected in series. The full array consists of 36 modules.

There are several ways to encapsulate solar panels to assemble a solar array; however, the novelty of this array is its lightweight, which significantly impacts the performance of a solar vehicle. Less weight translates into less power used and higher performance. The lightweight construction materials have been described in Chapter 3, which gives a total array weight of approximately 4.8 Kg. Aniket reported that the average weight found in a typical rooftop solar panel varies between 40 to 50 Kg [10]; therefore, our whole array is just a small fraction of the average weight found in a typical rooftop solar panel. An additional distinction of this array is its low cost compared

to commercial fabrication, as noted in the introduction. Although this array was specially designed for BeVolt, the technique and optimizations can be applied to any solar vehicle; thereby, the manufacturing process is standard but unique.

5.1 Layout

Each module layout differs depending on its position in the subarray, which in turn make up the array as a whole. The array has a total of 12 layout variations for the various modules. Although some of them are very similar, some differences are necessary to adapt to the shape and size of the car's body. Two types of modules cover the majority of the array, type one (T1) and type two (T2), the rest of the different types are used only for one or two modules. Some panels are similar to the two main types, with a few differences such as polarity in reverse or an extra-long wire going to the other side of the module.

In Fig. C.1 is shown one of the most numerous layout types, T1; all others can be seen in Appendix B. The layout for T1, with its eight cells, is one of the largest modules in the array. While there are some modules with more complex interconnections, T1 is one of the simplest forms. Each module is soldered together (Appendix C), and then each is carefully tested before it becomes part of a subarray. There are two subarrays in BeVolt's array. Each subarray contains approximately half of the total cells.

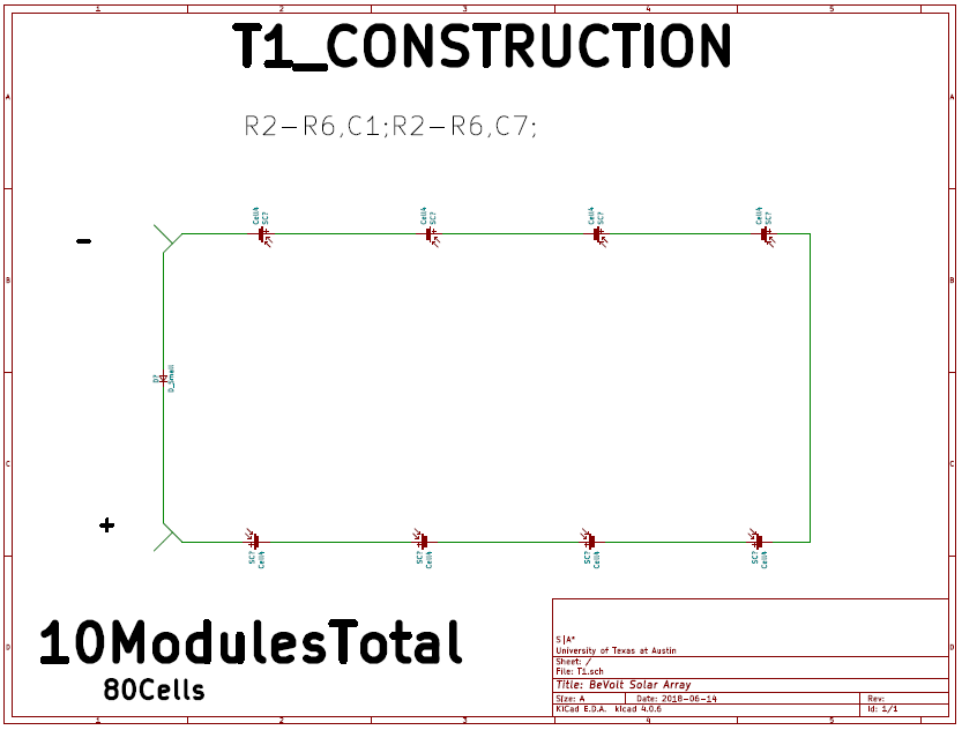

Figure 5.1: **T1 Module configuration displays the electrical connections for the solar cells and a bypass diode in parallel.**

The T1 module is known as a "4 by 2" module, meaning that it contains two rows of four cells. as shown in Fig. C.1. In the figure, the interconnect wiring and the location of the positive and negative outputs are also shown. The output locations are designed to minimize the external wiring; essentially, the output of one module is adjacent to the input of the next module in the subarray position. This arrangement saves significant weight and complexity when connecting the modules. This figure also shows the location and wiring of the bypass diode. Every module contains a bypass diode.

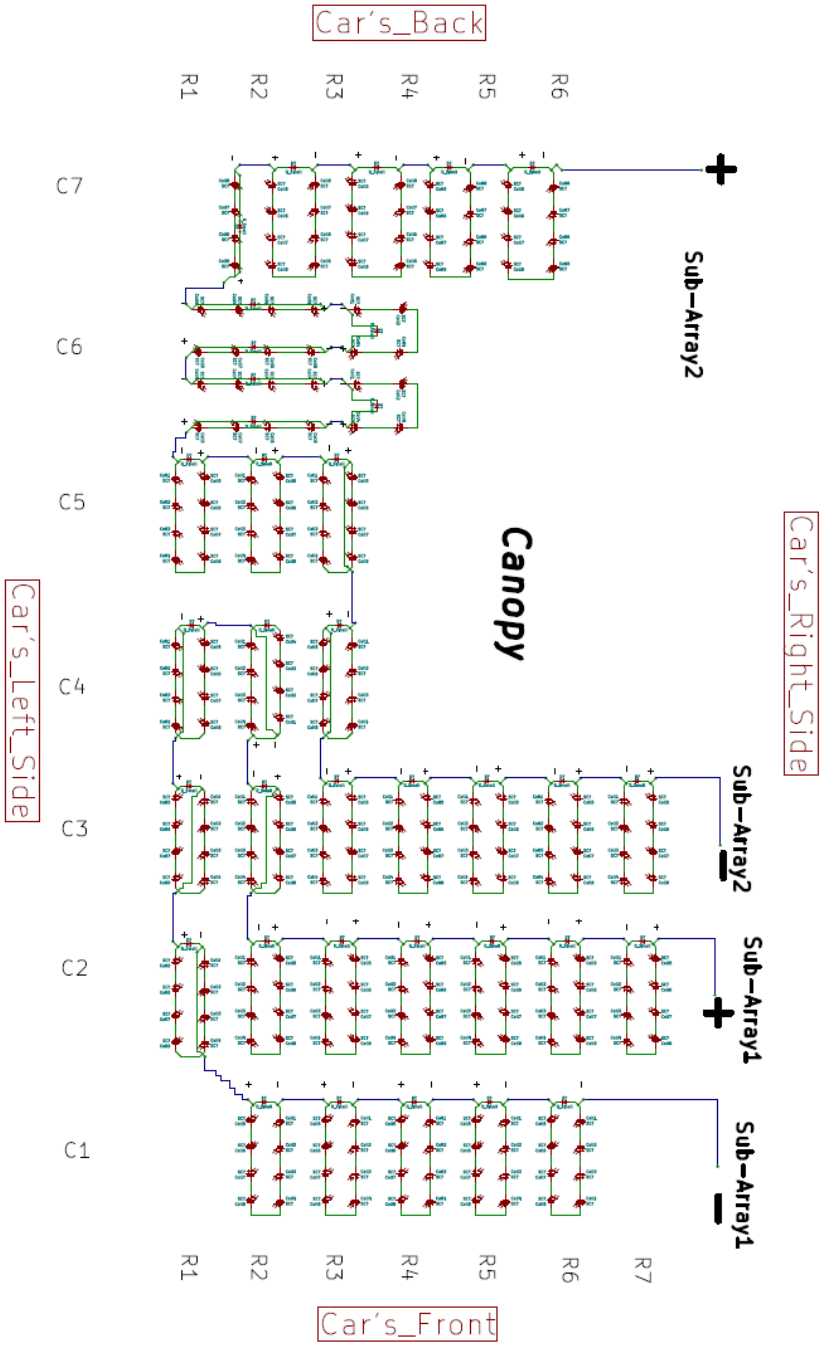

Figure 5.2: **Plan view of the array layout on BeVolt.**

The location and interconnection of all of the modules that make up BeVolt's array are shown in Fig. 5.2. Module placement must account for the body, shape, and area available, body structure, and the canopy. The module design and layout have been optimized for minimum distance module interconnections, and to have the sub-array outputs on one side of the car only (right side) due to the canopy hinge being on the other side. Shading of the canopy was also considered in the design. Some modules also have embedded temperature sensors, which are spaced out over the body.

5.2 Testing

Testing is a crucial step to determine the array performance. The two main goals of this testing are to test the array's hardware as complete subarrays and to measure the array's output power under actual operating conditions. It is essential to understand that in a design consisting of series connections, as shown in Fig. 5.2, each module has the same current flow, and an underperforming module can affect the entire sub-array.

5.2.1 Sub-array Testing System

The sub-array testing was quite different compared to single cells and modules. Although we tested the sub-arrays outdoors as we did with the modules, for the sub-arrays, we measured the actual power produced at the maximum power point rather than just the short and open-circuit values. To obtain the sub-arrays power measurements, we connected the sub-array to

commercial Drivetek Maximum Power Point Trackers (MPPTs), which detect the maximum power point. The communication between the MPPTs and the Microcontroller is a CAN transceiver. The input PV voltage, current, and power data from the MPPTs is sent over the CAN bus. The MPPT input voltage and input current is recorded by the ST embedded processor and gets written to a text file by a laptop computer (an example of the output data is given in Appendix E). A data point is obtained approximately every 0.84 seconds. A diagram of the system is given in Fig. 5.3.

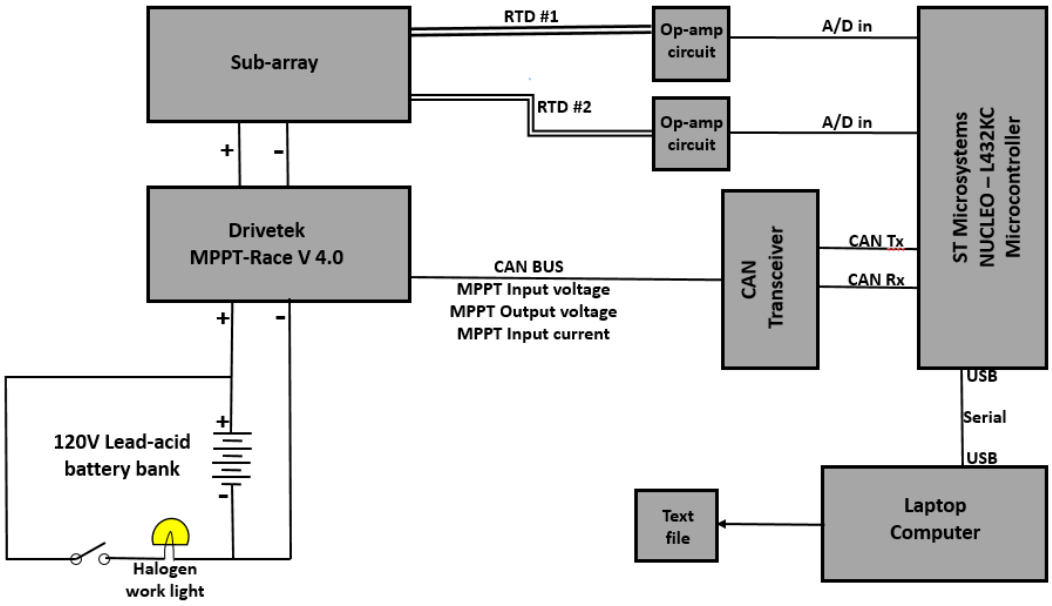

Figure 5.3: **Diagram of the sub-array testing system.**

Two of the RTDs embedded in the sub-array are connected to the ST Microcontroller, so their data gets recorded, processed into the text file, and output by the laptop computer. This temperature data is also included in the

example of the output data given in Appendix E for both sub-arrays.

The battery is configured as a bank of ten acid batteries, as seen in Fig. 5.4 and is charged by the sub-array being tested. The maximum voltage is set by the MPPT.

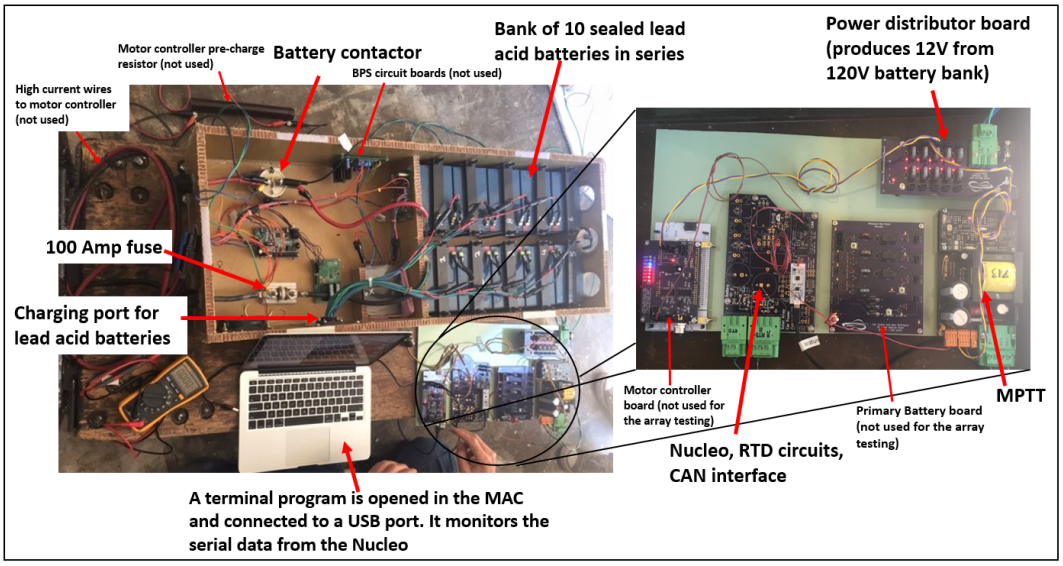

Figure 5.4: **Sub-array testing system with acid batteries in series.**

The battery voltage is the same as the MPPT output voltage and is sent to the nucleo over the CAN bus (as shown in Fig. 5.3). We use a light bulb to keep the battery at approximately 120V. If the battery voltage rises to 125 V the MPPT fully charged setpoint is reached, and the MPPT turns off. Therefore, it is necessary to keep the battery below this value. Note that Fig. 5.4 shows the testing set up system for both sub-arrays.

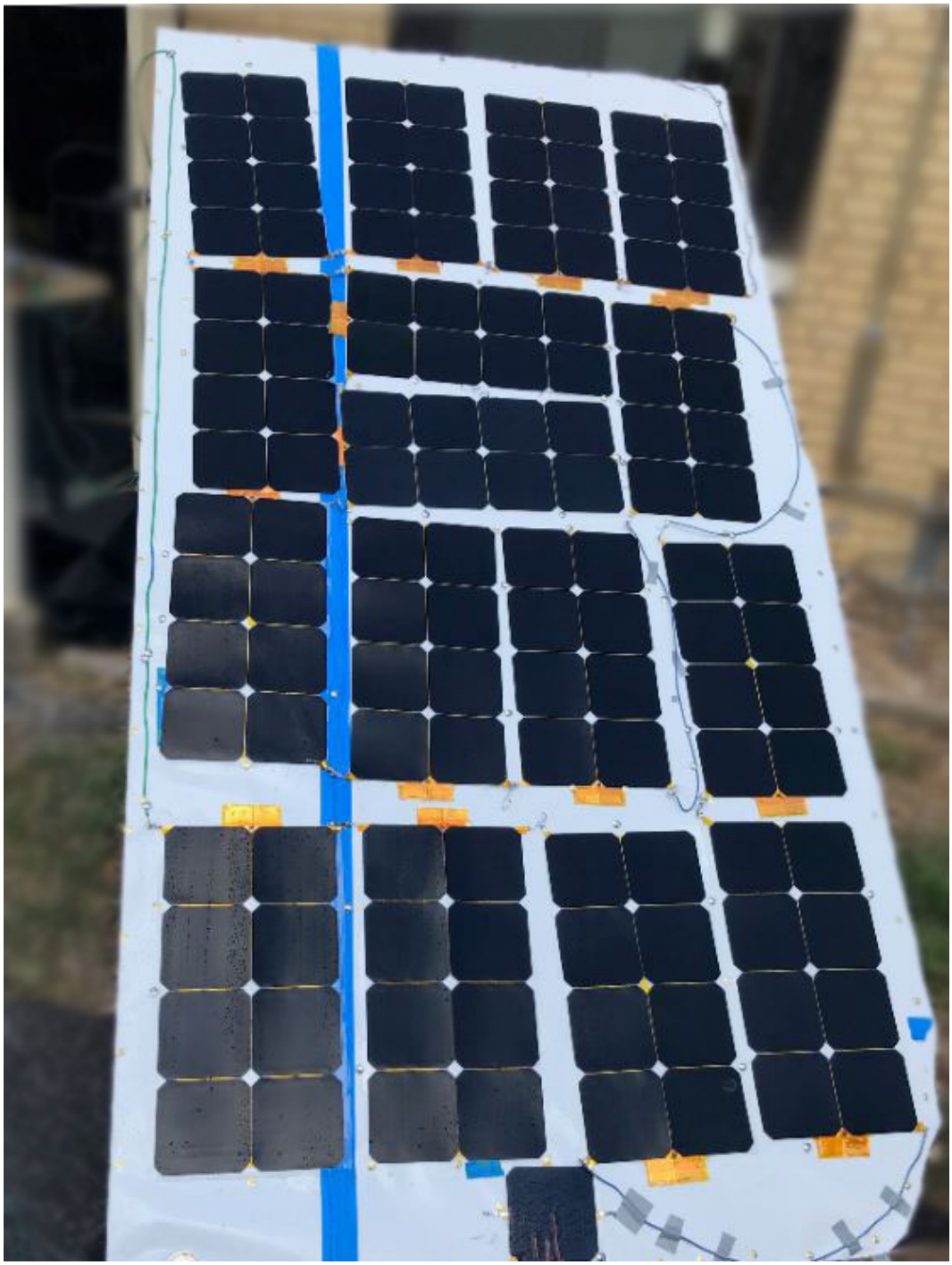

Figure 5.5: **Temporary assembly of sub-array one for testing.**

This set up was also used to test BeVolt's motor and other components before using it with the sub-arrays; therefore, some components are not used while testing the sub-arrays.

Due to BeVolt's body not being available yet, the sub-arrays were temporarily assembled on a flat board, as shown in Fig. 5.5 for sub-array 1. This assemblage was somewhat challenging due to the temporary electrical connections and the temporary mechanical attachments of the modules.

Fig. 5.5 shows the bypass diode heat sinks, which are the orange rectangles. Some modules were temporarily covered to disable them and cause the bypass diodes to conduct and determine their performance. No diodes or modules overheated or failed while running for several hours continuously.

5.2.2 Results for Sub-array One

As for the output power produced by the array, the two sub-arrays were tested separately. This section contains results for the sub-array one. Sub-array one was assembled temporarily, as seen in Fig. 5.5. To obtain accurate results, we carefully adjusted the sub-array, so it was perpendicular to the sunlight. To accomplish this, we attached a long bolt on the board of the sub-array temporary set up, leaving the shaft of the bolt exposed to project its own shadow.

The sub-array was manually adjusted until the bolt would stand over its own shadow (no visible shadow around the bolt); consequently, resulting in a right angle between the Sun and the board, as illustrated in Fig. 5.6.

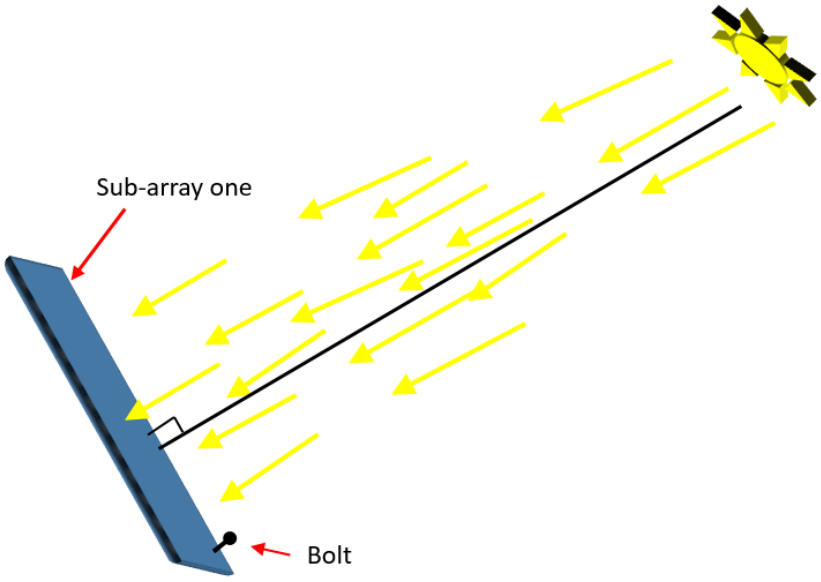

Figure 5.6: **A bolt was attached on the sub-array board to adjust it towards the sunlight until there was no shadow.**

The graph in Fig. 5.7 shows sub-array one expected output power at 1000 $\frac{W}{m^2}$ (red curve) and the actual output power (black curve). The expected power is calculated from the cell data sheet (Appendix D.1), using the actual measured cell temperature. As clearly shown, there are a number of variations in the graph. Low values of measured power are due to random clouds covering the Sun either partially or entirely. Some were for short periods of time, and a couple were longer. High peaks can be attributed to the array being sprayed with distilled water to lower the temperature of the cells.

The expected output power without any losses at Standard Test Conditions (STC) is

$$P_{STC} = (\#ofCells)(STCPmpp) = (128)(3.62) = 463.36W$$

where the # of Cells is the number of cells in the sub-array being tested and the STCPmpp is the power at the maximum power point of a typical cell Gen III Bin Le1 at STC.

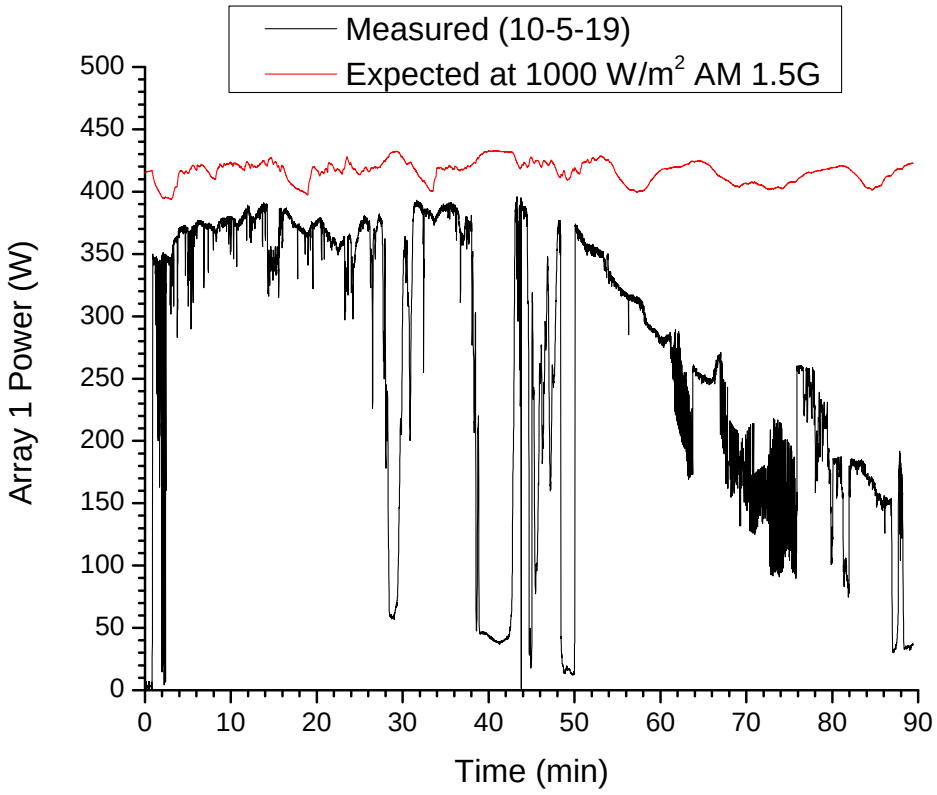

Figure 5.7: **Measured and expected sub-array 1 output power. Data was collected over an 89 minute time interval on Oct. 5, 2019, from 12:50pm to 2:19pm.**

The cell output at STC is given in the electrical characteristics of the

cell's datasheet (Appendix D), which is specified for a cell illumination of $1000\frac{W}{m^2}$ AM 1.5 G at 25°C cell temperature. The measurements shown in this figure were taken on October 5th, 2019, from 12:50 pm to 2:19 pm. The solar altitude angle corresponding to this date and time of the year affects the array output power.

Therefore, the power loss due to atmospheric attenuation of approximately 6.5% was obtained after computing the Sun Latitude Location (SLL), the solar noon angle (ϕ_N), and the Sun zenith angle (ϕ) using the following equations:

$$SLL = (ESVDA)\sin(\frac{180(D-82)}{182.5})^\circ \tag{5.1}$$

$$SLL = 23.5\sin(\frac{180(278-82)}{182.5}) = -5.41^\circ$$

$$\phi = 90 - (90-\phi_N)\sin(\frac{180(ST-SR)}{DL})^\circ \tag{5.2}$$

$$\phi_N = AL - SLL = 30.25^\circ + 5.41^\circ = 35.66^\circ$$

$$\phi_{ST} = 90 - (90-35.66)\sin(\frac{180(12.83-7.43)}{11.75})^\circ = 36.10^\circ$$

$$\phi_{ET} = 90 - (90-35.66)\sin(\frac{180(14.32-7.43)}{11.75})^\circ = 37.69^\circ$$

where SLL = Sun Latitude Location

ESVDA = Earth Seasonal Variation of the Declination of the Angle

D = Day of the year when the data was recorded =278th day of 2019

T = Time of the Day (Military Digital)

ST = Starting Time of the Day = 12:50 pm = 12.83hrs (Military Digital)

ET = Ending Time of the Day = 2:19 pm = 14.32hrs (Military Digital)

SR = Sunrise time = 7:26 am = 7.43 (Military Digital)

DL = Day length = 11:45 = 11.75 (Military Digital)

AL = Austin Latitude = 35°15' = 30.25°

Then considering the solar altitude angle, the array could produce up to:

$$P_{array} = P_{STC}(\cos\phi)^{0.3}W \tag{5.3}$$

substituting values we get

$$P_{arrayST} = P_{STC}(\cos 36.10)^{0.3} = (463.36)(0.938) = 434.65\,W and$$

$$P_{arrayET} = P_{STC}(\cos 37.69)^{0.3} = (463.36)(0.932) = 431.94\,W.$$

P_{array} is being calculated twice, to account for the starting test time $P_{arrayST}$ and for the ending testing time $P_{arrayET}$. Averaging these two values we get

$$\frac{434.65 + 431.94}{2} = 433.30\,W.$$

Therefore, producing an average result of approximately 6.49% lower than P_{STC} due to atmospheric attenuation. Although this is an approximation, the change in the output from the starting to the end testing time is small.

Atmospheric attenuation affects the amount of light that reaches the array, and therefore its power output. Additionally, as discussed in Chapter 4,

the temperature is another element that affects the performance of each cell and, therefore, the whole array.

During testing, we used three different types of temperature sensors: two RTDs, a Fluke temperature probe, and an IR camera. The IR camera was used to monitor any hot spots on the array. In Fig. 5.8, the IR camera indicates the sub-array temperature at three different locations.

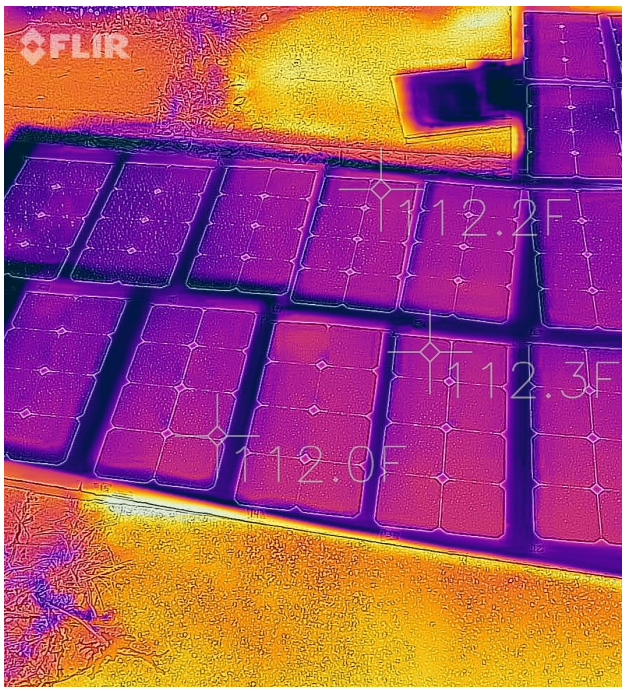

Figure 5.8: **Infrared camera showing the sub-array temperature while this latter is tested under sunlight illumination.**

The IR camera also gives temperature information according to the color observed in the image, which enabled us to detect if any module was significantly hotter than the rest. Note that the color temperature scale is

adjustable, and therefore there is not a fixed color scale. In Fig. 5.8 the yellow color (on the concrete) is much hotter than the purple color on the sub-array. Therefore, if a module becomes too hot, we can quickly identify it through the color change difference.

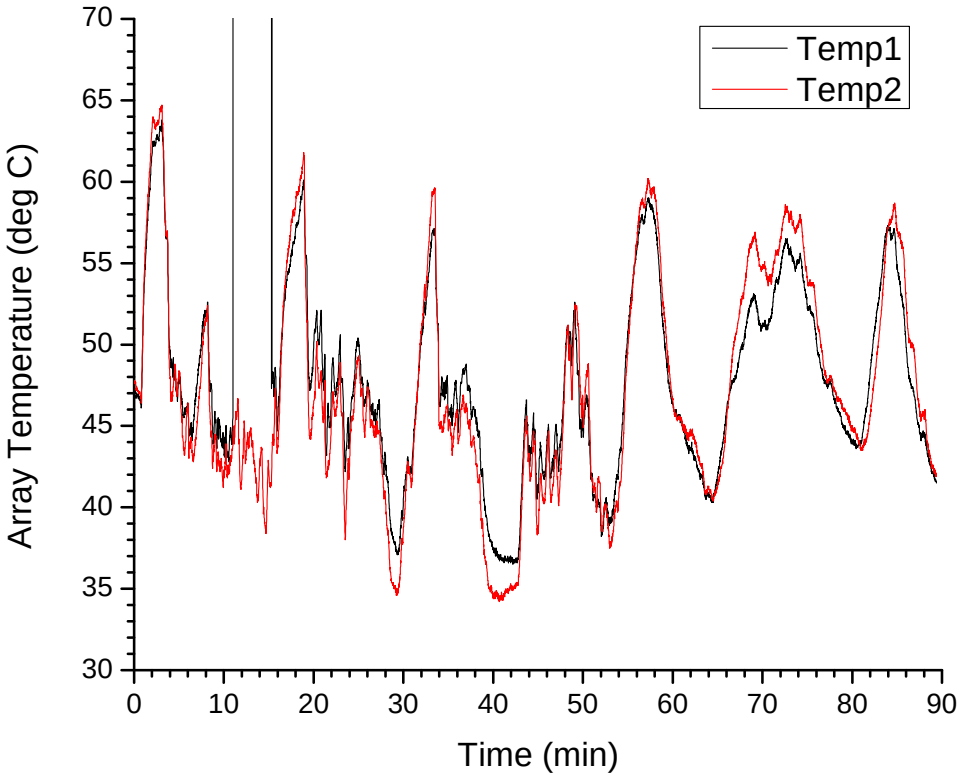

Figure 5.9: **Sub-array 1 measured temperature during the 10-5-2019. Temp 1 data is missing from about 10-15 minutes, due to a disconnected temperature sensor cable.**

We also implemented two RTD sensors embedded in the array modules and described in Section 4.2. The graph in Fig. 5.9 shows the data recorded

for those RTDs.

As can be noted, both sensors show approximately the same temperature most of the time. The different locations of the sensors are responsible for the temperature difference of approximately 5°C at some points.

Fig. 5.10 shows the results for sub-array one, which shows a 10 minute interval. The expected power is given as the red curve, which is highest in the graph. The expected power was computed, accounting for temperature and lamination corrections as follows:

$$P_{exp} = P_{STC}[1 - (T_{emp2} - T_{STC})(P_{TempCoeff})](L_{Correct})W \tag{5.4}$$

where P_{STC} is the power at standard conditions. T_{emp2} is the measured temperature by the sensor 2. Temperature sensor 1 was not used in this calculation due to an accidental disconnection during the test. T_{STC} is the standard temperature conditon. $P_{TempCoeff}$ is the power temperature coefficient affecting the output power by $\frac{-0.29\%}{^\circ C}$ given in the solar cell data sheet (Appendix D.1). $L_{Correct}$ is the lamination losses correction. In this thesis we used a 3.93% losses value due to lamination, resistance of ribbon, and mismatch of solar cells taking as a reference the results of a research report [11] where "the total Cell To Module (CTM) is 3.93% for solar module composed of 72 cells (125mm 125mm) connected in series".

Then after substituting values for two points of temperature data at time 33.4 min and 34.4 min in the graph shown Fig. 5.10 (the highest and one

of the lowest points respectively for temp 1) would result in

$$P_{exp1} = 463.36[1 - (57 - 25)(0.0029)](0.9607) = 403.84\,W and$$

$$P_{exp2} = 463.36[1 - (48 - 25)(0.0029)](0.9607) = 415.46\,W$$

which correspond to the values for the power expected value in Fig. 5.10. Consequently, as noted, the temperature peaks coincide with the power expected valleys and vice-versa for the rest of the data.

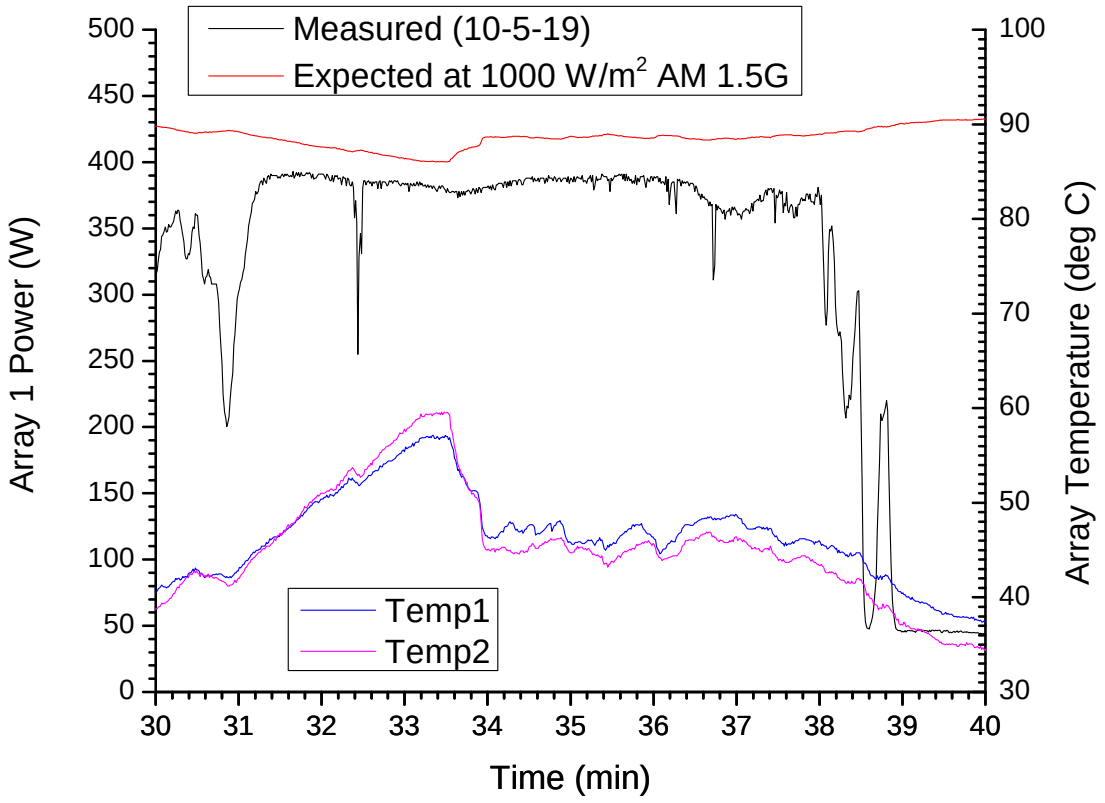

Figure 5.10: **Sub-array one expected and actual output power and temperature variation.**

In addition, Fig. 5.10 shows the actual measured output power and temperature variations. In this graph, there are a few intervals of low measured power due to clouds. Regardless, the output power is mostly maintained approximately constant. Comparing the two P_{exp} data points calculated previously, we find that there is a 2.8% of output power difference from one point to the other due to temperature variance ($\frac{P_{exp2}}{P_{exp1}} = 1.0279$).

The highest output power measured ($P_{measured}$) for this sub-array was 396.35 W at 13:33:06 pm. Using the same temperature to calculate P_{exp}, we get:

$$P_{exp} = 463.36[1 - (42.8 - 25)(0.0029)](0.9607) = 422.17\,W$$

leading to $\frac{422.17}{396.35} = 1.0651$ where the sub-array P_{exp} comes out to be approximately 6.51% higher than $P_{measured}$. This value matches almost exactly the difference we know from Eq. 5.3 which losses from the solar attenuation effects are 6.49%.

We decided to estimate what percentage of the 3.93% CTM corresponds to the wiring losses. We used the following equation to find the wire resistance

$$R = \frac{l\rho}{A} \tag{5.5}$$

where ρ_{copper} is the copper resistivity at 20°C ($1.7 * 10^{-8}\Omega m$). The temperature calculation was adjusted using +0.393% per degree C higher than 20°.
The total length of the ribbon cable used to interconnect the modules is

$$l = 20.344\,\mathrm{m}$$

The ribbon cable area has been calculated with two different widths w_1 and w_2. w_1 is the width of the ribbon cable used throughout the array except for the tabs where the cells are connected side to side. w_2 is the width for the tabs used connecting the side to side cells which is 2 times wider than w_1. Below is the corresponding area for each width.

$$A_1 = (w_1)(thickness) = (0.00475)(7.62 * 10^{-5}) = 3.62 * 10^{-7}\,\mathrm{m}^2 and$$

$$A_2 = (w_2)(thickness) = (0.0095)(7.62 * 10^{-5}) = 7.24 * 10^{-7}\,\mathrm{m}^2$$

Since the highest array output power ocurred at temperature 42.8°C then we adjusted the resistivity by 20.8°C corresponding to the measured temperature as follows:

$$\rho_{corrected} = (20.8)(0.393) = 8.17\,\%$$

and added to ρ_{copper}

$$\rho = \rho_{copper} + \rho_{corrected} = 1.84 * 10^{-8}\,\Omega m.$$

Using Equation 5.5 we found the resistance added to the system due to the wiring

$$R = \frac{(20.344m)(1.84 * 10^{-8}\Omega m)}{3.26 * 10^{-6}m^2} = 0.3446\,\Omega.$$

Now, the current flowing through the system at $P_{measured}$ for this sub-array was 5.6 A, then we calculate the lost power due to wiring resistance as follows:

$$P = I^2 * R = 5.6^2 * 0.3446 = 10.81\,W$$

which is approximately a 2.65% out of the 3.93% CTM losses.

5.2.3 Results for Sub-array Two

Sub-array two has four additional cells compared to sub-array one, its standard testing conditions power is:

$$P_{STC} = (132)(3.62) = 477.84\,W$$

with cell illumination of $1000\frac{W}{m^2}$ AM 1.5 G at 25°C cell temperature. As expected, its P_{STC} is higher compared to sub-array one.

Figure 5.11 illustrates the expected power at $1000\frac{W}{m^2}$ results for the testing of sub-array two. The figure exhibits a very unstable measured output power due to the cloudy skies. The test on sub-array two was performed on September 14th, 2019, which is a month before the testing for sub-array one. Hence, due to the different solar altitude angle and the four additional cells, the results of this sub-array compared to the sub-array one are expected to be different.

We followed the same process to compute the solar altitude angle using Equations 5.2.3, 5.2, and 5.3

$$SLL = 23.5\sin(\frac{180(257-82)}{182.5}) = 3.026^\circ$$

$$\phi_N = AL - SLL = 30.25^\circ - 3.026^\circ = 27.22^\circ$$

$$\phi_{ST} = 90 - (90 - 27.22)\sin(\frac{180(12.47-7.23)}{12.37})^\circ = 29.02^\circ$$

$$\phi_{ET} = 90 - (90 - 27.22)\sin(\frac{180(13.55-7.23)}{12.37})^\circ = 27.26^\circ$$

subsistuting values we obtain

$$P_{arrayST} = P_{STC}(\cos 29.02)^{0.3}\,\mathrm{W} = (477.84)(0.9610) = 459.0\,\mathrm{W} and$$

$$P_{arrayET} = P_{STC}(\cos 27.26)^{0.3}\,\mathrm{W} = (477.84)(0.9653) = 461.26\,\mathrm{W}.$$

Again, we calculated P_{array} twice to account for the starting and the ending testing time. Averaging these two values we get

$$\frac{459.0 + 461.26}{2} = 460.13$$

resulting in an average where P_{STC} is approximately 3.85% higher than P_{array} due to the atmospheric attenuation effects on the sub-array. This approximation is about half of the percentage compared to sub-array one for the change in the output from the starting to the end testing time. This is expected since this test was done closer to summer (September vs. October), when the Sun is higher in the sky, and travels through less atmosphere. This test was done also slightly earlier in the afternoon, again leading to a higher elevation of the Sun.

As for temperature, sub-array two also had the three types of temperature sensors (RTD, Fluke meter, and IR camera) similar to the test performed on sub-array one. The IR camera was again used to detect any hot modules during the test with fast time response.

Fig. 5.12 shows the recorded temperature for the two RTDs embedded in the sub-array.

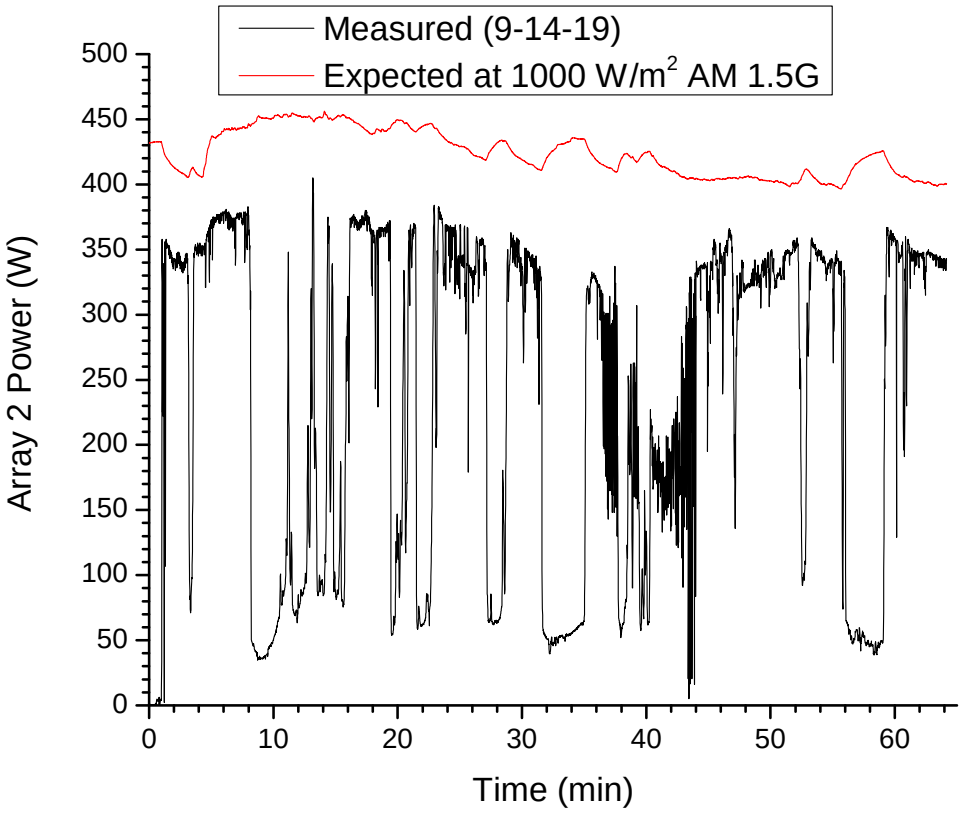

Figure 5.11: **Sub-array 2 expected and actual output power. Data was captured for an interval of 65 minutes on Sept. 14, 2019, from 12:28pm to 1:33pm.**

The temperature variation for the RTDs is due to the distilled water being sprayed on the array, effectively lowering the temperature of the modules. While the temperature highly varied, likewise did the measured output power, which surpassed 400 W momentarily. This is shown in Fig. 5.13 at about 13.2 minutes.

In Fig. 5.13 the RTDs' temperature discrepancy is a result of sensor

placement separation, and the water sprayed on each at different times and rates.

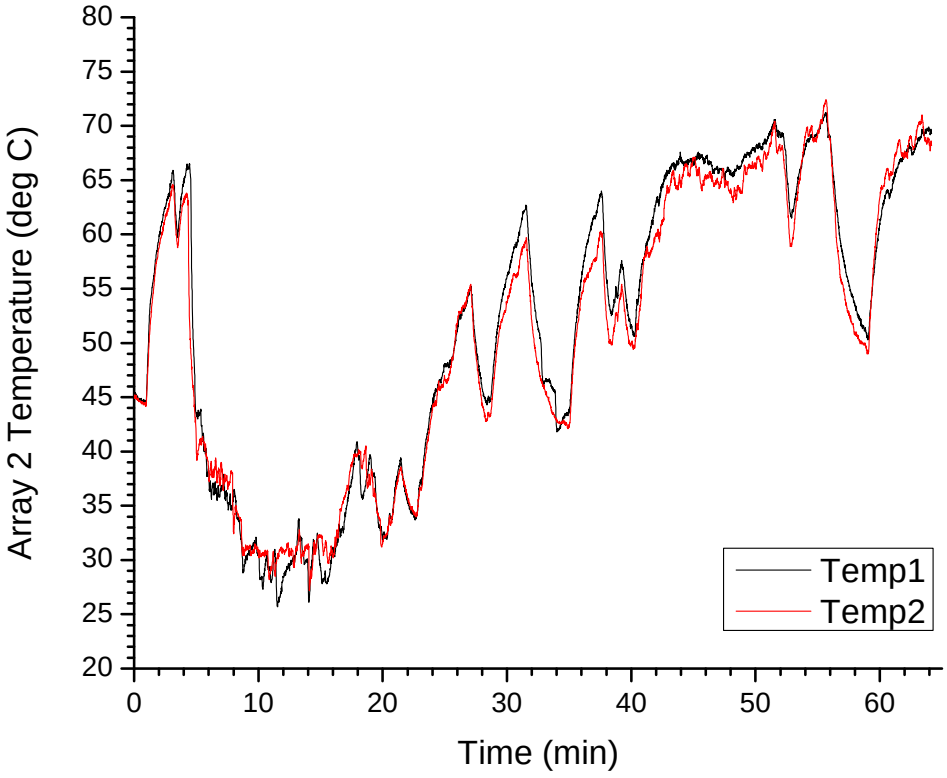

Figure 5.12: **Sub-array 2 temperature variation.**

Regardless, the highest $P_{measured} = 405.79\,\text{W}$ shown in Fig. 5.13. When it comes to P_{exp}, we used Equation 5.6 to compute its value instead of 5.4 to account for both RTDs. Note that in this case the temperature of both sensors is averaged and for the lamination correction $L_{Correct}$, the 3.93% value

was taken again from Equation 5.4

$$P_{exp} = P_{STC}[1 - (\frac{T_{emp1} + T_{emp2}}{2} - T_{STC})(P_{TempCoeff})](L_{Correct})\,\mathrm{W} \qquad (5.6)$$

$$P_{exp} = 477.84[1 - (\frac{33 + 31.8}{2} - 25)(0.0029)](0.9607) = 449.21\,\mathrm{W}$$

Then,

$$\frac{P_{measured}}{P_{exp}} = \frac{405.79}{449.21} = 0.9033\,\mathrm{W}$$

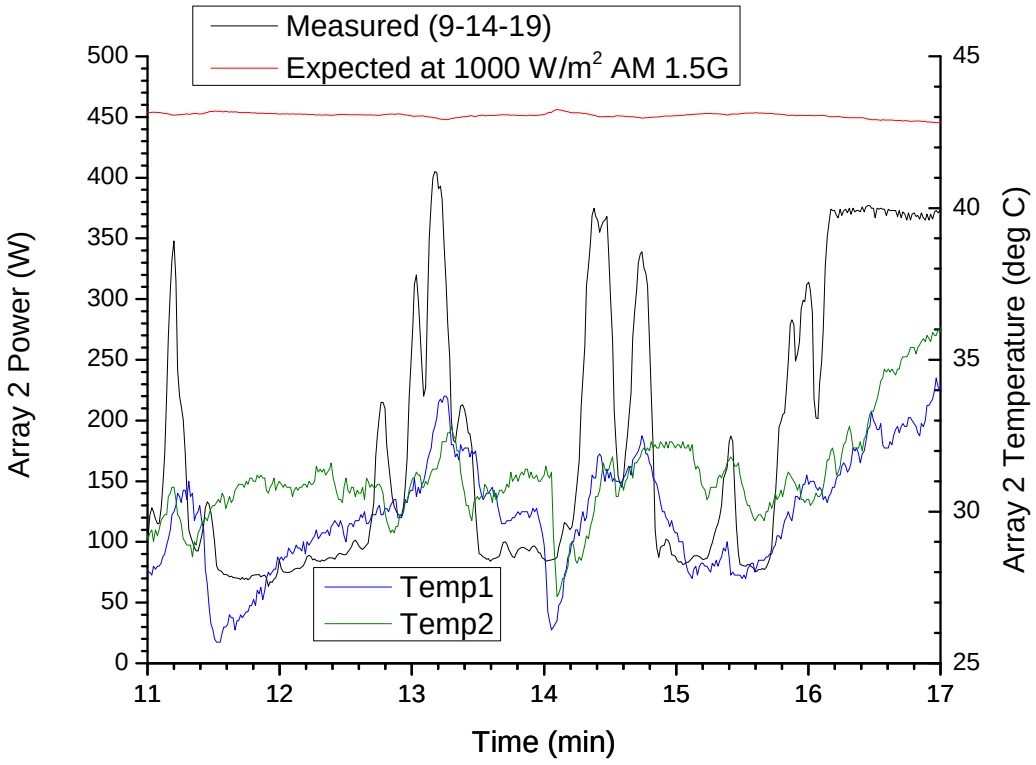

Figure 5.13: **Sub-array 2 actual output power and temperature variation.**

This calculation shows that there is 9.67% less output power than the

expected power. Of this percentage, 3.85% comes from the attenuation effects we calculated earlier. The remaining 5.96% is attributed to the extra wiring resistance and other possible errors such as MPPT tracking accuracy. Though this sub-array only has four additional cells, it also has four additional modules. The design required a clear space with an oval shape to fit the car's canopy. To accommodate all the cells required longer connections with smaller modules, therefore, leading to higher wiring resistance.

As before, we wanted to know the approximate wire resistance of this sub-array. We proceed to calculated using the same equation from sub-array one (5.5).

$$\rho_{corrected} = 4.76\,\%$$

added to ρ_{copper} then,

$$\rho = \rho_{copper} + \rho_{corrected} = 1.78 * 10^{-8}\,\Omega m$$

$$l = 26.474\,\mathrm{m}$$

and

$$A = 3.26 * 10^{-6}\,\mathrm{m}^2$$

leading to

$$R = \frac{(26.474m)(1.78 * 10^{-8}\,\Omega m)}{3.26 * 10^{-6}\,\mathrm{m}^2} = 0.4342\,\Omega$$

The current flowing at $P_{measured}$ for this sub-array was 5.7A, then we calculate the lost power due to wiring resistance as follows:

$$P = I^2 * R = 5.7^2 * 0.4342 = 14.11\,\mathrm{W}$$

which is approximately a 3.48% out of the 5.96% CTM losses. Although, this values do not match as accurate as those in sub-array one, the difference is still reasonable.

Sub-array one performs well within expectations after taking into account the different losses and factors that affect the sub-array performance. Sub-array two had a power and design trade-off producing approximately 2.48% less power than the output expected power after considering the losses, its size, and testing conditions. However, since the difference is small and the absence of power is due to design effects rather than cell performance, it was concluded that the array generated the power correctly.

Thus, it was concluded that both sub-arrays delivered satisfactory output power according to their design, size, and testing conditions. Additionally, we concluded that the hardware performs correctly, and this design is robust and appropriate for its purpose.

Chapter 6

Conclusion and Future Work

6.1 Conclusion

This thesis describes the construction of an optimized, high-quality, lightweight solar array at a lower cost than available from commercial vendors. This work also presents the system and process to test single solar cells. We used these results to match and bin them according to their short-circuit output to achieve a higher performance array.

Upon completion of the cell testing, cells were arranged and laminated into modules that have embedded bypass diodes and temperature sensors. The diodes prevent total current interruption due to partial shading. The temperature sensors provide real-time data that enables the user to determine what is the best approach to maintain the highest output power. Additionally, the method to test modules is discussed in this thesis.

The encapsulation materials were carefully selected according to the needs of the sub-array in terms of weight and power generation. Thus, the modules were designed in a novel way so that the weight of the total sub-array was a fraction of a conventional roof solar panel.

There were different procedures to test each stage of the array con-

struction. Single solar cells were tested indoors at a set temperature and with artificial illumination. The modules were tested outdoors on open and short-circuit output only, to check that there were no soldering failures or bad connections. Finally, the two complete sub-arrays were tested outdoors at their maximum power point (MPP). The two sub-arrays were tested at different times of the year and consequently slightly different conditions. The testing of the sub-arrays was complex and lengthy due to the fact that in these tests, every component of the array had to be temporarily connected. Each sub-array layout was precisely designed to have the positive connection of a module right next to the negative polarity of the next module to avoid wiring bulk.

Both sub-arrays produced excellent results according to their specific design and testing conditions, showing that the array was resilient and ready for its purpose to power a solar car.

6.2 Future Work

There are multiple future projects relevant to this work. The first would be to construct a larger hot plate. The current hot plate has space limitations and risks for the lamination process. Having a larger hot plate would enable a faster placement of the encapsulation stack and speed the procedure, decreasing the lamination time. Additionally, it would allow us to build larger modules which would distribute the materials weight better as explained in Section 3.1.1. Thus, constructing larger modules would be

beneficial weight wise.

The second would be to build a module testing system that can scan them from open to short-circuit (similar to the single-cell testing). The short and open-circuit test we performed was good enough to ensure that the modules were functioning as expected. However, it would be ideal to have a system at STC conditions and without needing solar angle estimates to test them before and after lamination. This improvement would provide data that would enable the calculation of lamination losses accurately. Therefore, having an indoor testing system at a set temperature would improve the accuracy of data which might even lead to finding materials with better light-transmittance.

Another research focus project would be to incorporate an auto cooling system to the solar array. Ironically, solar cells need Sun irradiance to generate energy; however, their output production drops dramatically upon reaching higher temperatures. Therefore, integrating an auto cooling system would benefit the array to stay at the desired temperature and maintain the power generation nearly constant.

Appendices

Appendix A

Individual Testing Results

Table A.1: **Testing results for each cell showing maximum power point and the short circuit results. Note that under the "Use" column, 1 indicates the cell was used in subarray 1, 2 indicates subarray 2 and N indicates the cell was not used.**

Cell #	Use	I_{sc} (A)	V at I_{sc} (V)	P_{max}(W)	V at P_{max} (V)	I at P_{max} (A)
BV1	N	2.403	0.055	1.240	0.552	2.249
BV2	N	2.536	0.053	1.301	0.534	2.434
BV3	2	2.614	0.079	1.356	0.553	2.450
BV4	2	2.615	0.048	1.348	0.550	2.452
BV5	2	2.687	0.061	1.346	0.529	2.542
BV6	2	2.612	0.043	1.355	0.560	2.420
BV7	2	2.657	0.070	1.350	0.546	2.471
BV8	2	2.537	0.073	1.338	0.555	2.412
BV9	1	2.600	0.051	1.331	0.552	2.413
BV10	2	2.596	0.041	1.324	0.546	2.423
BV11	1	2.609	0.046	1.358	0.550	2.470
BV12	2	2.577	0.041	1.321	0.543	2.434
BV13	2	2.610	0.051	1.324	0.546	2.423
BV14	1	2.584	0.041	1.326	0.550	2.412
BV15	2	2.560	0.116	1.318	0.545	2.419
BV16	2	2.576	0.043	1.305	0.540	2.418
BV17	2	2.592	0.043	1.323	0.543	2.436
BV18	2	2.580	0.044	1.318	0.546	2.412
BV19	N	2.541	0.043	1.317	0.553	2.381
BV20	N	2.564	0.055	1.329	0.560	2.372
BV21	N	2.553	0.184	1.317	0.540	2.440
BV22	2	2.578	0.051	1.288	0.538	2.395

Continued on next page

Table A.1 – *Continued from previous page*

Cell #	Use	I_{sc} (A)	V at I_{sc} (V)	P_{max}(W)	V at P_{max} (V)	I at P_{max} (A)
BV23	2	2.590	0.234	1.294	0.538	2.407
BV24	2	2.560	0.053	1.330	0.552	2.412
BV25	1	2.623	0.044	1.335	0.555	2.406
BV26	2	2.557	0.041	1.328	0.543	2.446
BV27	1	2.599	0.041	1.275	0.533	2.393
BV28	1	2.636	0.041	1.351	0.546	2.472
BV29	1	2.629	0.046	1.330	0.545	2.441
BV30	1	2.619	0.065	1.354	0.558	2.425
BV31	1	2.632	0.046	1.336	0.543	2.46
BV32	1	2.607	0.044	1.319	0.541	2.437
BV33	1	2.606	0.046	1.321	0.548	2.411
BV34	1	2.590	0.417	1.312	0.540	2.431
BV35	1	2.633	0.041	1.324	0.548	2.416
BV36	1	2.654	0.425	1.349	0.548	2.461
BV37	1	2.633	0.043	1.318	0.548	2.404
BV38	2	2.594	0.058	1.354	0.548	2.470
BV39	2	2.588	0.087	1.313	0.543	2.417
BV40	1	2.614	0.044	1.374	0.558	2.460
BV41	1	2.572	0.048	1.321	0.553	2.387
BV42	1	2.595	0.046	1.347	0.560	2.405
BV43	2	2.571	0.050	1.329	0.555	2.394
BV44	2	2.541	0.053	1.327	0.565	2.347
BV45	1	2.614	0.044	1.353	0.567	2.386
BV46	1	2.601	0.056	1.299	0.536	2.424
BV47	2	2.578	0.041	1.334	0.553	2.411
BV48	2	2.578	0.048	1.302	0.541	2.405
BV49	2	2.565	0.063	1.303	0.529	2.461
BV50	2	2.575	0.109	1.352	0.567	2.386
BV51	2	2.565	0.082	1.264	0.529	2.389
BV52	2	2.552	0.089	1.323	0.553	2.392
BV53	2	2.561	0.046	1.336	0.553	2.416
BV54	N	2.549	0.038	1.325	0.558	2.373
BV55	2	2.559	0.043	1.313	0.552	2.381
BV56	1	2.614	0.111	1.325	0.560	2.367

Continued on next page

Table A.1 – *Continued from previous page*

Cell #	Use	I_{sc} (A)	V at I_{sc} (V)	P_{max}(W)	V at P_{max} (V)	I at P_{max} (A)
BV57	2	2.552	0.063	1.315	0.570	2.306
BV58	2	2.572	0.079	1.321	0.553	2.387
BV59	1	2.556	0.043	1.315	0.546	2.407
BV60	1	2.585	0.046	1.310	0.562	2.332
BV61	1	2.552	0.048	1.310	0.548	2.400
BV62	1	2.547	0.043	1.310	0.552	2.380
BV63	1	2.554	0.044	1.260	0.540	2.340
BV64	1	2.553	0.067	1.270	0.528	2.406
BV65	1	2.550	0.041	1.301	0.562	2.316
BV66	1	2.547	0.109	1.310	0.545	2.405
BV67	1	2.570	0.237	1.342	0.563	2.382
BV68	1	2.595	0.041	1.341	0.552	2.432
BV69	1	2.614	0.062	1.353	0.558	2.423
BV70	1	2.618	0.041	1.340	0.558	2.400
BV71	1	2.622	0.178	1.346	0.560	2.403
BV72	1	2.629	0.062	1.354	0.548	2.470
BV73	1	2.651	0.056	1.278	0.531	2.408
BV74	1	2.629	0.056	1.309	0.548	2.388
BV75	1	2.551	0.046	1.342	0.567	2.367
BV76	1	2.536	0.043	1.327	0.555	2.391
BV77	1	2.542	0.038	1.308	0.557	2.349
BV78	2	2.504	0.104	1.296	0.563	2.301
BV79	N	2.502	0.046	1.304	0.557	2.343
BV80	1	2.657	0.055	1.406	0.570	2.465
BV81	2	2.593	0.063	1.360	0.569	2.393
BV82	1	2.641	0.075	1.387	0.563	2.462
BV83	1	2.508	0.039	1.290	0.550	2.345
BV84	1	2.509	0.050	1.288	0.555	2.320
BV85	1	2.485	0.041	1.259	0.557	2.262
BV86	1	2.491	0.041	1.314	0.567	2.318
BV87	1	2.495	0.155	1.323	0.572	2.313
BV88	1	2.475	0.067	1.285	0.553	2.322
BV89	1	2.480	0.039	1.290	0.567	2.276
BV90	1	2.489	0.039	1.246	0.546	2.280

Continued on next page

Table A.1 – *Continued from previous page*

Cell #	Use	I_{sc} (A)	V at I_{sc} (V)	P_{max}(W)	V at P_{max} (V)	I at P_{max} (A)
BV91	1	2.488	0.082	1.315	0.558	2.355
BV92	2	2.490	0.048	1.299	0.560	2.319
BV93	1	2.494	0.379	1.302	0.558	2.332
BV94	1	2.483	0.046	1.306	0.562	2.325
BV95	1	2.474	0.038	1.278	0.555	2.303
BV96	1	2.473	0.043	1.268	0.557	2.278
BV97	1	2.501	0.036	1.262	0.538	2.346
BV98	N	2.483	0.067	1.297	0.565	2.296
BV99	2	2.490	0.063	1.278	0.562	2.273
BV100	1	2.484	0.055	1.273	0.551	2.308
BV101	2	2.513	0.051	1.290	0.552	2.339
BV102	2	2.509	0.038	1.217	0.533	2.284
BV103	1	2.474	0.039	1.271	0.543	2.340
BV104	1	3.128	0.091	1.580	0.548	2.883
BV105	1	3.182	0.056	1.588	0.545	2.916
BV106	1	3.102	0.072	1.524	0.538	2.834
BV107	1	3.183	0.077	1.578	0.538	2.930
BV108	1	3.151	0.053	1.595	0.545	2.930
BV109	1	3.133	0.060	1.593	0.552	2.890
BV110	1	3.162	0.070	1.561	0.543	2.95
BV111	1	3.109	0.051	1.564	0.553	2.826
BV112	1	3.157	0.068	1.523	0.519	2.934
BV113	1	3.154	0.115	1.550	0.534	2.900
BV114	1	3.083	0.050	1.574	0.563	2.790
BV115	1	3.089	0.046	1.605	0.577	2.780
BV116	1	3.045	0.062	1.597	0.563	2.834
BV117	1	3.113	0.051	1.587	0.553	2.870
BV118	1	3.104	0.092	1.543	0.534	2.887
BV119	1	3.064	0.109	1.595	0.557	2.866
BV120	2	3.103	0.207	1.542	0.546	2.823
BV121	2	3.110	0.055	1.609	0.560	2.872
BV122	2	3.092	0.074	1.572	0.557	2.825
BV123	1	3.033	0.130	1.506	0.548	2.749
BV124	1	3.104	0.051	1.595	0.550	2.901

Continued on next page

Table A.1 – *Continued from previous page*

Cell #	Use	I_{sc} (A)	V at I_{sc} (V)	P_{max}(W)	V at P_{max} (V)	I at P_{max} (A)
BV125	1	3.063	0.048	1.577	0.560	2.816
BV126	N	3.014	0.048	1.534	0.552	2.782
BV127	1	3.086	0.072	1.533	0.553	2.771
BV128	1	3.063	0.053	1.572	0.563	2.789
BV129	1	3.077	0.046	1.556	0.550	2.829
BV130	1	3.029	0.046	1.579	0.555	2.845
BV131	1	3.067	0.258	1.572	0.550	2.859
BV132	2	3.163	0.056	1.517	0.528	2.875
BV133	2	3.149	0.063	1.531	0.533	2.874
BV134	2	3.097	0.072	1.474	0.517	2.850
BV135	2	3.033	0.046	1.543	0.560	2.755
BV136	2	3.080	0.051	1.541	0.534	2.883
BV137	2	3.045	0.077	1.553	0.552	2.816
BV138	2	3.061	0.048	1.522	0.543	2.811
BV139	2	3.114	0.077	1.513	0.533	2.840
BV140	2	3.037	0.051	1.525	0.557	2.740
BV141	2	3.097	0.103	1.558	0.541	2.878
BV142	2	3.170	0.106	1.569	0.534	2.936
BV143	1	3.073	0.046	1.552	0.553	2.805
BV144	1	3.076	0.080	1.567	0.545	2.878
BV145	2	3.014	0.150	1.494	0.553	2.701
BV146	1	3.094	0.058	1.478	0.519	2.848
BV147	1	3.103	0.053	1.572	0.545	2.885
BV148	1	3.085	0.094	1.582	0.558	2.834
BV149	1	3.111	0.243	1.514	0.524	2.889
BV150	1	3.153	0.075	1.517	0.526	2.883
BV151	1	3.113	0.065	1.497	0.534	2.802
BV152	1	3.102	0.058	1.606	0.545	2.947
BV153	1	3.140	0.094	1.526	0.522	2.920
BV154	2	3.077	0.053	1.542	0.545	2.831
BV155	2	3.139	0.116	1.477	0.519	2.846
BV156	2	3.129	0.050	1.661	0.562	2.956
BV157	2	3.070	0.101	1.574	0.565	2.785
BV158	2	3.101	0.048	1.602	0.557	2.880

Continued on next page

Table A.1 – *Continued from previous page*

Cell #	Use	I_{sc} (A)	V at I_{sc} (V)	P_{max}(W)	V at P_{max} (V)	I at P_{max} (A)
BV159	2	3.068	0.044	1.561	0.543	2.870
BV160	2	3.116	0.063	1.553	0.551	2.816
BV161	2	3.054	0.060	1.572	0.558	2.816
BV162	2	3.060	0.065	1.586	0.550	2.885
BV163	2	3.120	0.077	1.540	0.553	2.784
BV164	2	3.070	0.042	1.549	0.567	2.732
BV165	2	3.040	0.042	1.530	0.536	2.863
BV166	2	3.100	0.124	1.542	0.542	2.840
BV167	2	3.020	0.070	1.536	0.556	2.759
BV168	2	3.100	0.053	1.524	0.546	2.790
BV169	2	3.090	0.065	1.489	0.537	2.768
BV170	2	3.116	0.070	1.532	0.534	2.840
BV171	2	3.071	0.143	1.546	0.555	2.785
BV172	2	3.119	0.132	1.581	0.557	2.840
BV173	2	3.145	0.190	1.543	0.538	2.869
BV174	2	3.127	0.046	1.539	0.524	2.937
*BV175	2	3.142	0.073	1.582	0.553	2.600
BV176	2	3.161	0.239	1.557	0.538	2.895
BV177	2	3.142	0.060	1.617	0.558	2.896
BV178	2	3.107	0.060	1.576	0.553	2.849
BV179	2	3.107	0.058	1.622	0.567	2.861
BV180	2	3.154	0.058	1.623	0.550	2.951
BV181	2	3.201	0.075	1.602	0.540	2.969
BV182	2	3.141	0.072	1.606	0.548	2.931
BV183	2	3.074	0.096	1.556	0.548	2.840
BV184	2	3.110	0.058	1.576	0.555	2.840
BV185	2	3.132	0.051	1.579	0.546	2.890
BV186	2	3.106	0.155	1.540	0.543	2.836
BV187	N	3.083	0.055	1.469	0.528	2.784
BV188	N	3.090	0.072	1.462	0.517	2.827
BV189	2	3.116	0.060	1.539	0.531	2.899
BV190	2	3.131	0.055	1.471	0.517	2.842
BV191	2	3.096	0.231	1.544	0.543	2.843
BV192	N	3.065	0.060	1.541	0.545	2.829

Continued on next page

Table A.1 – *Continued from previous page*

Cell #	Use	I_{sc} (A)	V at I_{sc} (V)	P_{max}(W)	V at P_{max} (V)	I at P_{max} (A)
BV193	N	3.085	0.091	1.571	0.541	2.902
BV194	N	3.071	0.097	1.529	0.531	2.879
BV195	2	3.096	0.055	1.571	0.543	2.893
BV196	2	3.123	0.050	1.581	0.545	2.903
BV197	2	3.078	0.050	1.564	0.545	2.871
BV198	2	3.091	0.070	1.573	0.562	2.799
BV199	2	3.106	0.082	1.563	0.541	2.887
BV200	N	3.072	0.048	1.506	0.538	2.801
BV201	N	3.081	0.044	1.567	0.558	2.806
BV202	N	3.067	0.065	1.551	0.538	2.884
BV203	2	3.084	0.050	1.552	0.541	2.868
BV204	2	3.092	0.091	1.592	0.565	2.817
BV205	2	3.113	0.056	1.600	0.560	2.857
BV206	2	3.099	0.051	1.577	0.546	2.887
BV207	2	3.129	0.065	1.591	0.543	2.930
BV208	2	3.100	0.068	1.599	0.560	2.854
BV209	2	3.109	0.113	1.566	0.555	2.823
BV210	2	3.138	0.048	1.552	0.553	2.806
*BV211	2	3.136	0.048	1.356	0.482	2.817
BV212	2	3.099	0.103	1.633	0.567	2.880
BV213	2	3.112	0.173	1.631	0.574	2.844
BV214	2	3.125	0.073	1.618	0.560	2.889
BV215	2	3.126	0.253	1.582	0.552	2.869
BV216	2	3.139	0.055	1.610	0.560	2.875
BV217	2	3.160	0.118	1.591	0.563	2.824
BV218	2	3.142	0.108	1.643	0.581	2.830
BV219	2	3.153	0.048	1.605	0.565	2.839
BV220	1	3.168	0.068	1.602	0.542	2.950
BV221	1	3.166	0.051	1.600	0.552	2.902
BV222	1	3.107	0.136	1.545	0.555	2.785
BV223	1	3.162	0.133	1.656	0.573	2.886
BV224	1	3.113	0.051	1.598	0.556	2.870
BV225	1	3.076	0.059	1.525	0.537	2.835
BV226	1	3.091	0.066	1.525	0.532	2.863

Continued on next page

Table A.1 – *Continued from previous page*

Cell #	Use	I_{sc} (A)	V at I_{sc} (V)	P_{max}(W)	V at P_{max} (V)	I at P_{max} (A)
BV227	1	3.102	0.046	1.489	0.513	2.898
BV228	1	3.091	0.075	1.601	0.551	2.903
BV229	1	3.098	0.046	1.491	0.529	2.817
BV230	1	3.094	0.063	1.501	0.529	2.836
BV231	1	3.139	0.095	1.533	0.532	2.878
BV232	1	3.086	0.046	1.505	0.541	2.780
BV233	2	3.094	0.136	1.560	0.548	2.847
BV234	1	3.134	0.055	1.541	0.531	2.901
*BV235	1	3.142	0.061	1.309	0.479	2.730
BV236	1	3.076	0.063	1.527	0.546	2.795
BV237	1	3.098	0.064	1.558	0.556	2.799
BV238	1	3.083	0.119	1.542	0.541	2.850
BV239	1	3.103	0.165	1.563	0.551	2.835
BV240	1	3.135	0.054	1.554	0.536	2.898
BV241	1	3.094	0.066	1.577	0.553	2.851
BV242	1	3.085	0.071	1.573	0.548	2.870
BV243	N	2.993	0.142	1.520	0.547	2.791
BV244	1	3.054	0.048	1.516	0.541	2.801
BV245	1	3.063	0.046	1.521	0.536	2.837
BV246	2	3.039	0.050	1.520	0.545	2.790
BV247	1	3.077	0.106	1.539	0.552	2.791
BV248	2	3.039	0.070	1.543	0.553	2.788
BV249	1	3.070	0.063	1.531	0.557	2.750
BV250	1	3.060	0.050	1.513	0.552	2.743
BV251	1	3.165	0.056	1.530	0.533	2.873
BV252	2	3.030	0.062	1.556	0.555	2.804
BV253	2	3.037	0.056	1.560	0.557	2.803
BV254	1	3.043	0.048	1.500	0.529	2.835
BV255	N	3.026	0.046	1.554	0.560	2.776
BV256	1	3.072	0.102	1.568	0.546	2.870
BV257	1	3.076	0.046	1.523	0.537	2.833
BV258	2	3.047	0.046	1.536	0.558	2.752
BV259	N	3.071	0.047	1.499	0.533	2.806
BV260	1	3.071	0.056	1.518	0.533	2.841

Continued on next page

Table A.1 – *Continued from previous page*

Cell #	Use	I_{sc} (A)	V at I_{sc} (V)	P_{max}(W)	V at P_{max} (V)	I at P_{max} (A)
BV261	1	3.091	0.077	1.502	0.537	2.793
*BV262	N	2.591	0.445	1.396	0.583	2.391
BV263	2	3.014	0.047	1.564	0.565	2.767
BV264	1	3.110	0.066	1.542	0.539	2.859
BV265	2	3.021	0.060	1.563	0.571	2.732
BV266	N	3.036	0.056	1.417	0.525	2.695
BV267	2	3.026	0.090	1.538	0.542	2.832
BV268	N	2.986	0.050	1.532	0.546	2.804
BV269	2	3.048	0.058	1.535	0.558	2.749
*BV270	N	3.022	0.056	1.533	0.656	1.712
BV271	2	3.043	0.058	1.528	0.541	2.823
BV272	1	3.129	0.066	1.509	0.527	2.860
BV273	2	3.019	0.059	1.531	0.554	2.760
BV274	2	3.016	0.071	1.494	0.548	2.720
BV275	1	3.054	0.061	1.575	0.554	2.838
BV276	2	3.037	0.105	1.543	0.556	2.772
BV277	2	3.029	0.053	1.485	0.529	2.807
BV278	2	3.019	0.075	1.551	0.558	2.770
BV279	2	3.011	0.056	1.533	0.555	2.762
BV280	2	3.047	0.101	1.515	0.553	2.739
BV281	2	3.310	0.080	1.535	0.529	2.919
BV282	2	3.060	0.065	1.578	0.553	2.852
BV283	2	3.068	0.046	1.540	0.545	2.828
BV284	2	3.040	0.046	1.535	0.569	2.700
BV285	2	3.099	0.048	1.548	0.541	2.859
BV286	2	3.086	0.118	1.570	0.562	2.796
BV287	2	3.037	0.050	1.564	0.558	2.801
BV288	2	3.034	0.051	1.564	0.548	2.854

* Cracked Cell

Appendix B

Encapsulation Checklist

B.1 Preparation For Testing the Cells Individually

1. Put gloves on.

2. Decide which module layout you will be building.

3. Check the cells selecting those without cracks.

4. Place one or two pieces of white matching size/shape paper/protector of a flat surface and place the cell upside down (blue color facing down).

5. Make sure to have soldering iron with a flat tip, turn it on and set its temperature to 650° F.

6. Solder a piece of copper ribbon to the middle bond pad (white spot found at the ends of each cell) following the steps below:

    - Carefully heat the middle bond pad (white spot) with the soldering iron.
    - Use the soldering iron to heat both sides of the copper ribbon end to be attached.
    - Place the ribbon on the middle bond pad of the cell.

- Using tweezers keep the ribbon in place while heating it with the soldering iron (add solder if desired/needed).
- Once the solder is melted, keep holding the ribbon in place with the tweezer for a few seconds to let it cool off and have it soldered to the cell.

B.2 Testing Individual Cells

7. Measure/test the short circuit current and open-circuit voltage of the cell:
   - Measurements taken outside on a sunny day are expected to be approximately 6A (or even higher) and 0.6V from each cell.
   - Inside expected measurements in the lightbox is approximately 4-5A and 0.5-0.6V.
8. Record the measurements results.
9. After each cell has been tested and produced the expected outputs remove the copper ribbons of each cell as follows:
   - With the soldering iron set to 650° F and using the solder iron flat tip, heat the connection while with your other hand gently pull the copper ribbon, so it detaches from the cell. Once the ribbon comes off, take the hot solder tip-off.

10. As you are taking off the copper ribbons, place them on the mold with a piece of white paper protectors (to avoid scratches) under each cell.

B.3 Interconnecting the Cells Into Modules

1. Cautiously place spacers in the mold to have a uniform separation between cells and prevent tweaked modules.

2. Carefully check polarities for every cell and make sure to place them in series (every + must be connected to a -).

3. Place double-sided Kapton tape between the three bond pads of each cell to solder the middle connectors leaving free just the bond pads spots to solder the connectors.

4. Place interconnector tab sticking it on the exposed Kapton tape.

5. After the interconnector tab is fixed, now you can solder them using the soldering iron with the flat tip and adding solder little by little as needed/about a drop or two (be careful of not spilling solder outside of the bond pad which creates short circuits), you will NOT need much solder.

6. Once the cells have been interconnected, carefully take the mold dividers out (if you pull them out carelessly you might crack the cells).

7. After the middle connectors are soldered, move the soldered module in the middle of the mold (do not remove the white paper protectors from

underneath of the cells.

8. If needed, carefully tape the module to the mold with blue masking tape, so it does not move around.

9. Check how the module will be connected to the next (refer to the electrical wiring diagrams provided in Appendix B) to determine which side will be wired to the diode and which side will be wired to the next module depending on the layout you have chosen.

10. Determine how the end wire will be solder in a way that will allow this module to connect correctly to the next one.

11. Place double-sided Kapton tape (or double-sided insulator tape) underneath of the end wire/ribbon at the opposite side of the diode placement.

12. Solder the end wire/ribbon at the end/corner of the module that will connect locally within the module.

13. Now its time to solder the diode and place the wires/ribbons that will connect to the next module and will protrude the encapsulation.

14. Take the diode, check its polarity and solder a small piece of tinned copper ribbon at each end of the diode according to polarity placement that will allow you to connect it as shown in the individual electrical module diagram.

15. Place double-sided Kapton tape underneath of the wires that will connect the diode to the module (to avoid short circuits).

16. Now solder the diode to the module as the corresponding electrical wiring diagram shows.

17. Place double-sided Kapton tape underneath of the wires between the back of the cell and the wires that will be used to connect the next module.

18. Then solder the wires that will connect to the next module (most of them should be placed at the corners of the module).

19. On the wires protruding from the module, place a 5mm piece of double-sided Kapton tape at each side of the ribbon at the end closer to the cell (to have clean access to the wire when soldering/connecting the module to the next.

20. It is time to test the module as a whole before being encapsulated to ensure there are not bad connections and everything is soldered properly (measure and record the results for short circuit and open circuit of each module).

    - For outside testing expect up to 6A or higher for short circuit current (Isc) and approximately 0.6V times the number of cells in the module for the open circuit (Voc).

- For lightbox testing expect up to 5A for Isc and up to 0.5V times the number of cells for the Voc per module.

21. With the module as it is with the cells facing down (blue side down, wiring side facing you as you had them while soldering them) Place two pieces of double-sided Kapton tape of 120 mm length centered in each cell.

22. Leave the module there until you prepare and put the materials ready to put the stack together.

B.4 Preparing Tools and Materials

1. Use a frame suitable for the module size you will be laminating.

2. Cut a piece of vacuum bag with two inches of excess for the frame you will be using.

3. Cut two pieces of Teflon fabric with about two inches of excess larger than the module you will be encapsulating.

4. Cut a piece of Teflon film **treated on one side** approximately one inch larger than the module (or 3 mm larger than the EVA piece around the perimeter).

5. Cut a piece of Teflon film **treated on both sides** approximately one inch larger than the module (or 3 mm larger than the EVA piece around the perimeter).

6. Cut a piece of EVA with approximately two millimeters larger than the module around its perimeter.

7. Using double-sided scotch tape, tape the vacuum bag to the frame leaving it as tense and without wrinkles as possible.

8. Wipe the aluminum plate (on top of the three griddles) with denaturalized alcohol paper towel; after the plate is clean, now give a last wipe with isopropyl alcohol and organic wipes.

9. According to the size of the frame, determine where you will be putting the yellow sealant "tacky" tape on the aluminum plate and place two pieces of it around the perimeter of the plate.

B.5 Putting the Stack Together

1. Remove the release liner from the Kapton tape pieces on the back of the cells in the module previously prepared.

2. Check that the piece of Teflon film treated on both sides is clean (if dusted clean it with alcohol and organic wipes).

3. Carefully center and stick the clean piece of Teflon film (**treated on both sides**) on the module with Kapton tape and leave it there.

4. Inside of the enclosed area by the yellow sealant tape place a piece of the previously cut Teflon fabric.

5. Then, place the module centered on top of the Teflon fabric with the Teflon film treated on both sides and sticked to it facing down (blue color facing up/you).

6. Next, center the EVA piece on top of the module (blue side).

7. After, clean (with alcohol and organic wipes) the piece of Teflon film treated on one side.

8. Try to make a small line with a black sharpie marker to check which is the treated side (treated side will allow you to write on it/make a line).

9. With the treated side facing down (to the module) center the Teflon film on top of the EVA in the stack.

10. Now take the second piece of the Teflon fabric and centered it on the Teflon film (stack).

11. Put the base of the thru-bag vacuum connector in a spot where it doesnt disturb the module.

12. Take the frame (with the vacuum bag stuck to it) and place it on the stack in a way that it is easier to press down, so the vacuum bag sticks to the yellow sealant tape.

13. Press down hard the vacuum bag around the perimeter until there are no air leaks (to check for leaks you can make a hole in the middle of the

thru-bag vacuum connector, insert the hose into it, and secure it; then, turn on and off the vacuum until you hear no air leakages).

14. If you hear air leaks, with the vacuum on fix them pressing down the bag, so it sticks to the yellow sealant tape until you close the leak.

15. When there are no more air leaks, keeping the vacuum on cut the vacuum bag as close as you can to the frame (as far as you can from the yellow sealant tape) take the frame away carefully without creating air leaks by pulling it hard away.

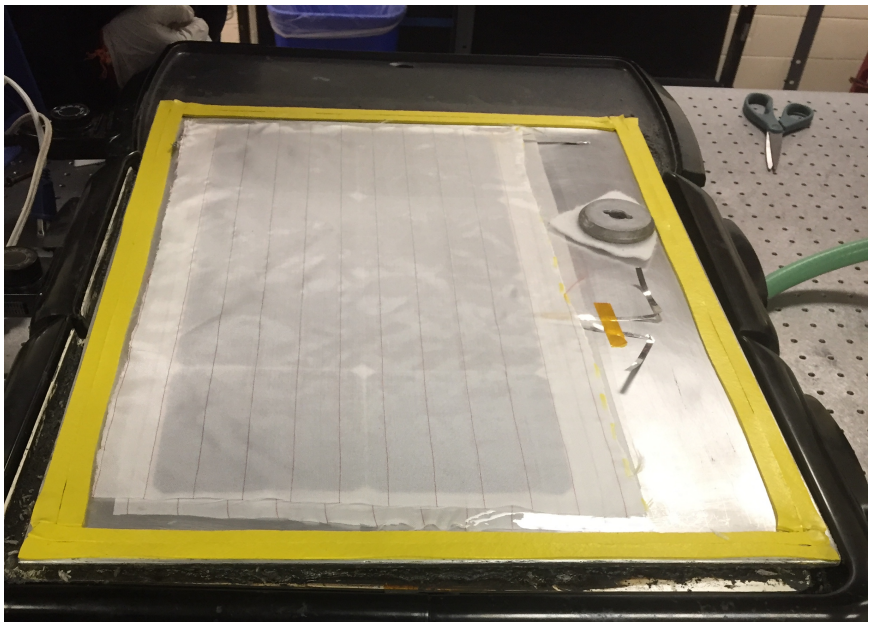

Figure B.1: **Completed stack ready to be laminated.**

B.6 Curing Time

1. Set the griddles temperature to 375°F and turn them on.

2. Turn on the filter extractors (at least three of them).

3. Check their temperature constantly using the infrared camera as soon as it reaches 280°F put a timer for 7 minutes.

4. After the timer is done turn the griddles off.

5. Turn on the fans to help bring down the temperature faster.

6. Once the temperature decreases to 100°F, turn off the fans and the vacuum.

7. Carefully disassemble the stack by cutting the vacuum bag around the module and removing the module before anything else.

B.7 After Lamination

1. After the module has been removed, the yellow sealant tape along with everything else can be removed and the aluminum plate cleaned.

2. Clean the aluminum plate with denaturalized alcohol and regular paper towels from any yellow sealant tape residuals.

3. Carefully trim the material excess from the module leaving a perimeter of 1-1.5mm around it.

4. Test the short circuit and open circuit of each module (it is normal to have a slight 2%-4% decrease on current although not always happens).

- For outside testing expect 6A or higher for Isc and approximately 0.6V times the number of cells in the module for Voc.
- For lightbox testing expect 4-5A or higher for Isc and up to 0.5V times the number of cells in the module for Voc.

Appendix C

Array Modules Electrical Layout

This Appendix shows every type of electrical layout found in BeVolt's array. Although some of then seem to be the same there is always a small difference that allows the correct connection when placing them in the shape of the car.

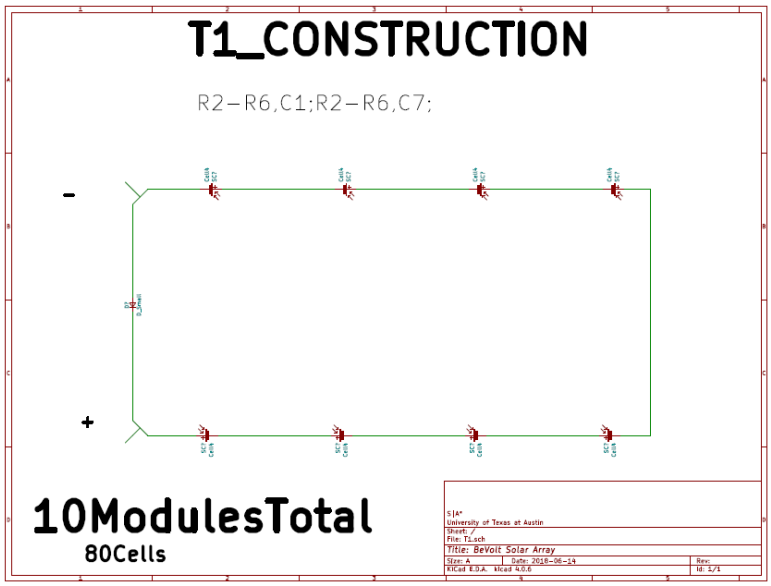

Figure C.1: **Type #1 Electrical Connection.**

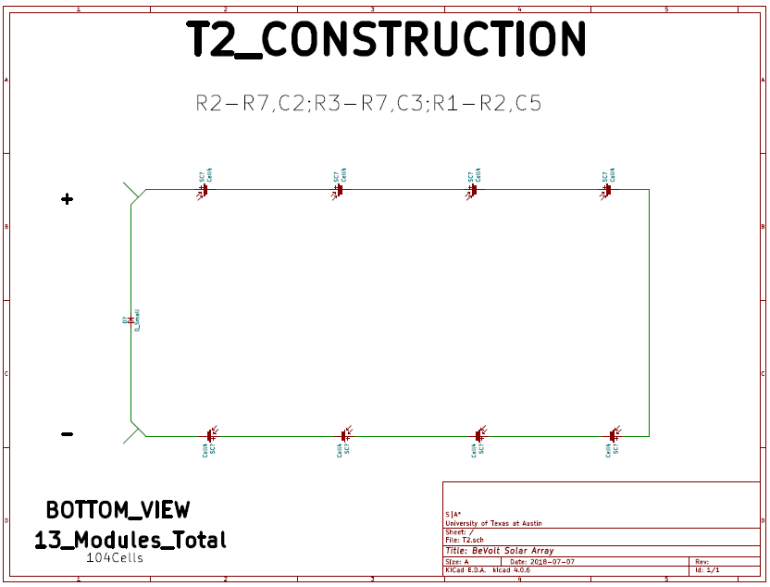

Figure C.2: **Type #2 Electrical Connection.**

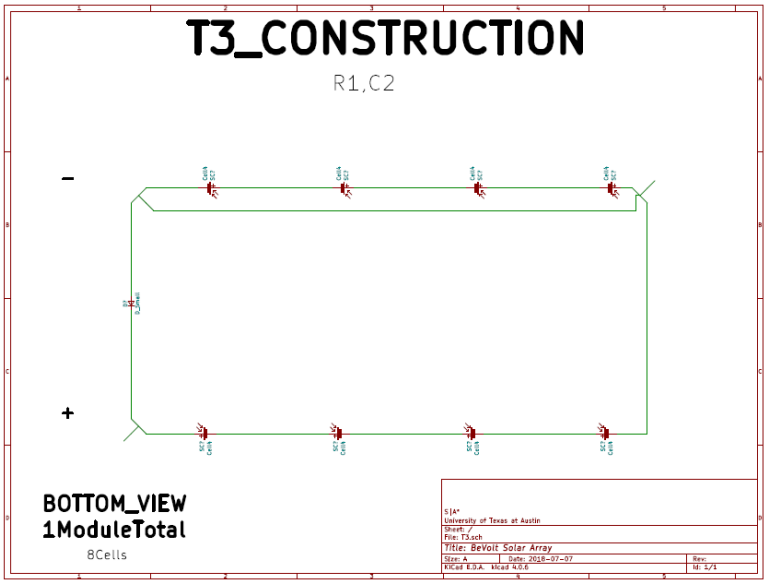

Figure C.3: **Type #3 Electrical Connection.**

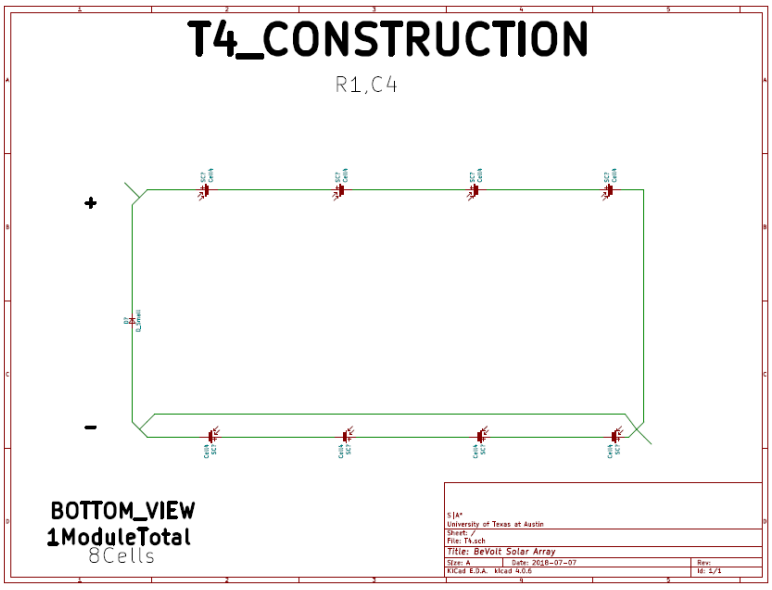

Figure C.4: **Type #4 Electrical Connection.**

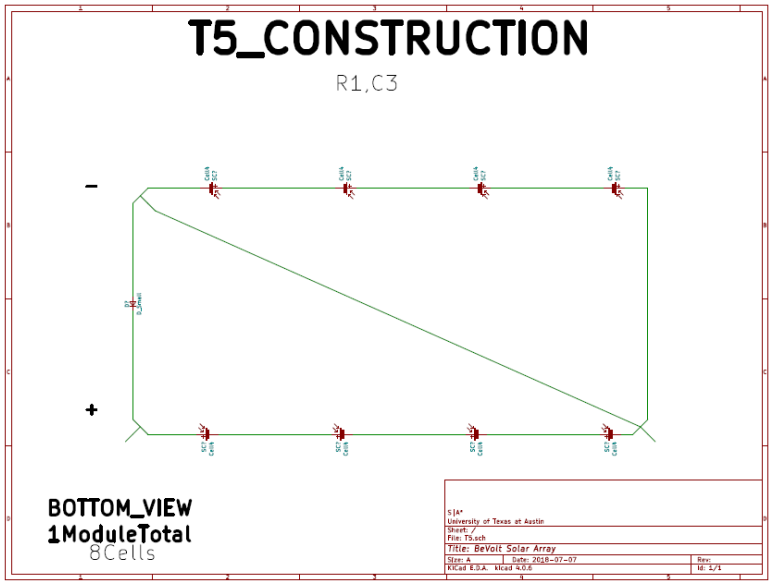

Figure C.5: **Type #5 Electrical Connection.**

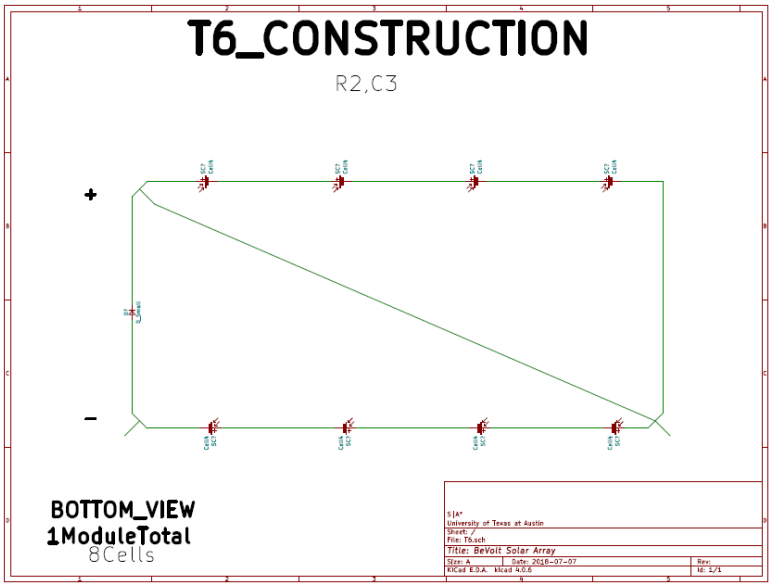

Figure C.6: **Type #6 Electrical Connection.**

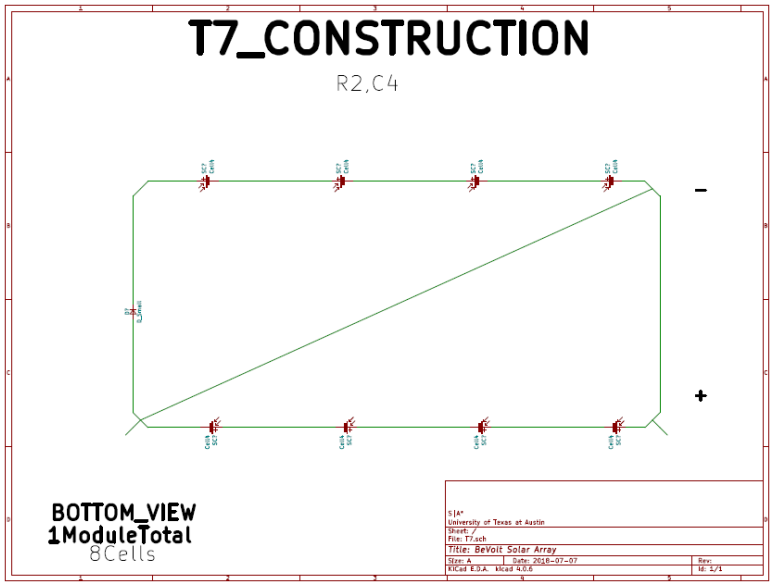

Figure C.7: **Type #7 Electrical Connection.**

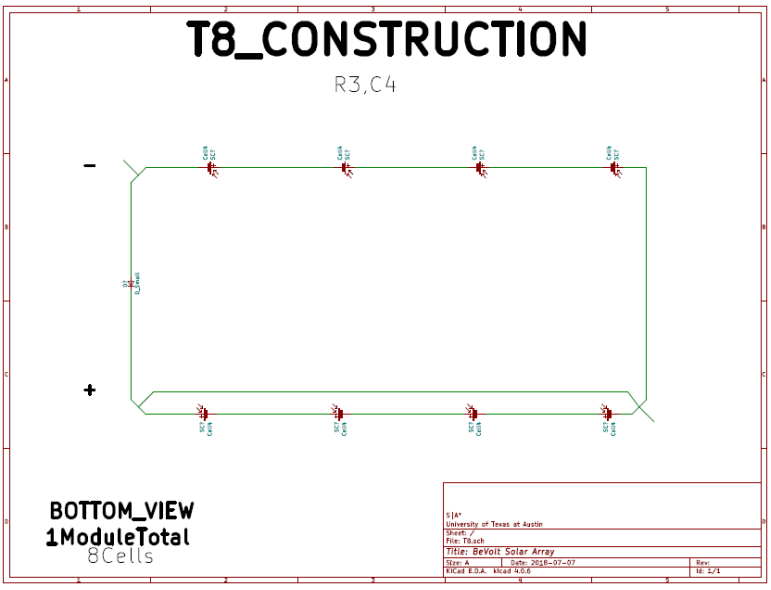

Figure C.8: **Type #8 Electrical Connection.**

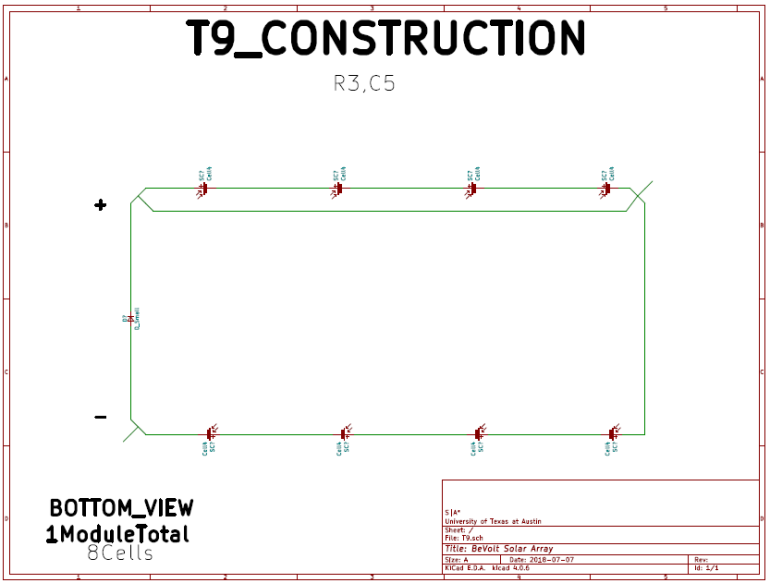

Figure C.9: **Type #9 Electrical Connection.**

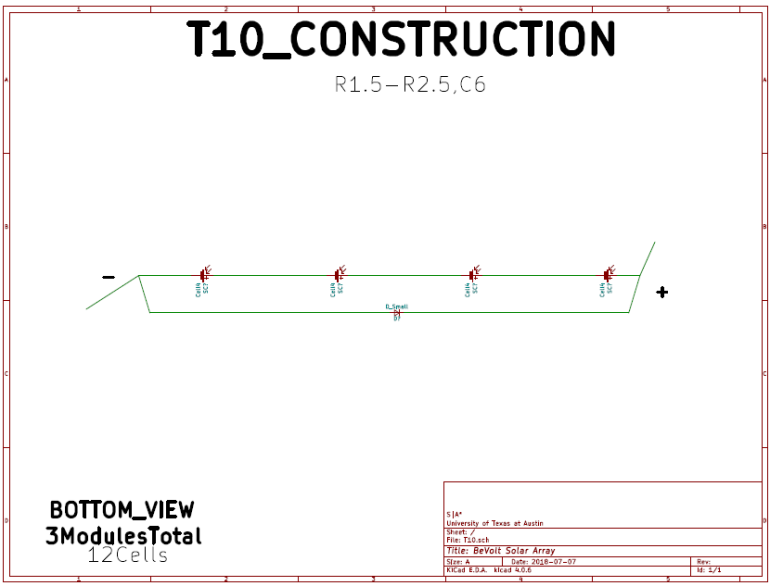

Figure C.10: **Type #10 Electrical Connection.**

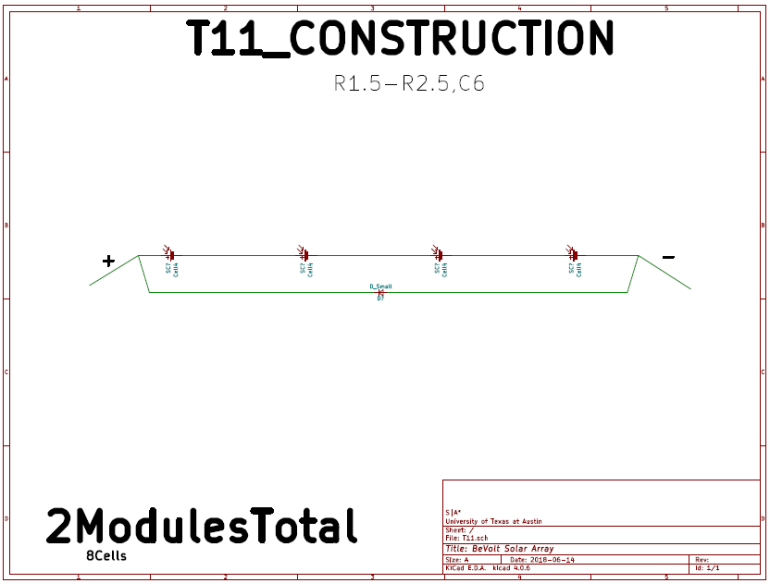

Figure C.11: **Type #11 Electrical Connection.**

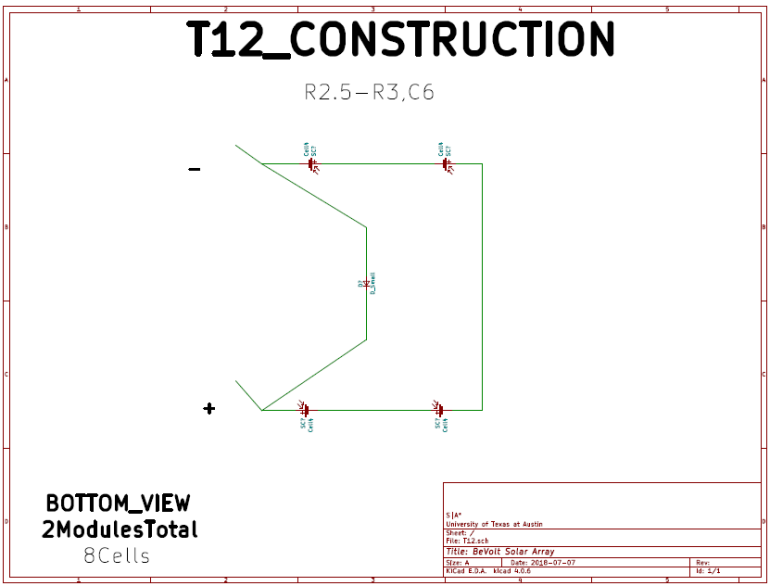

Figure C.12: **Type #12 Electrical Connection.**

Appendix D

Data Sheets

This appendix is devoted to the data sheets for the different components used in the design and manufacturing of the array described in this thesis. Data sheets are the documents to review when we want to know the rating specified by the manufacturers to ensure the proper performance of the component.

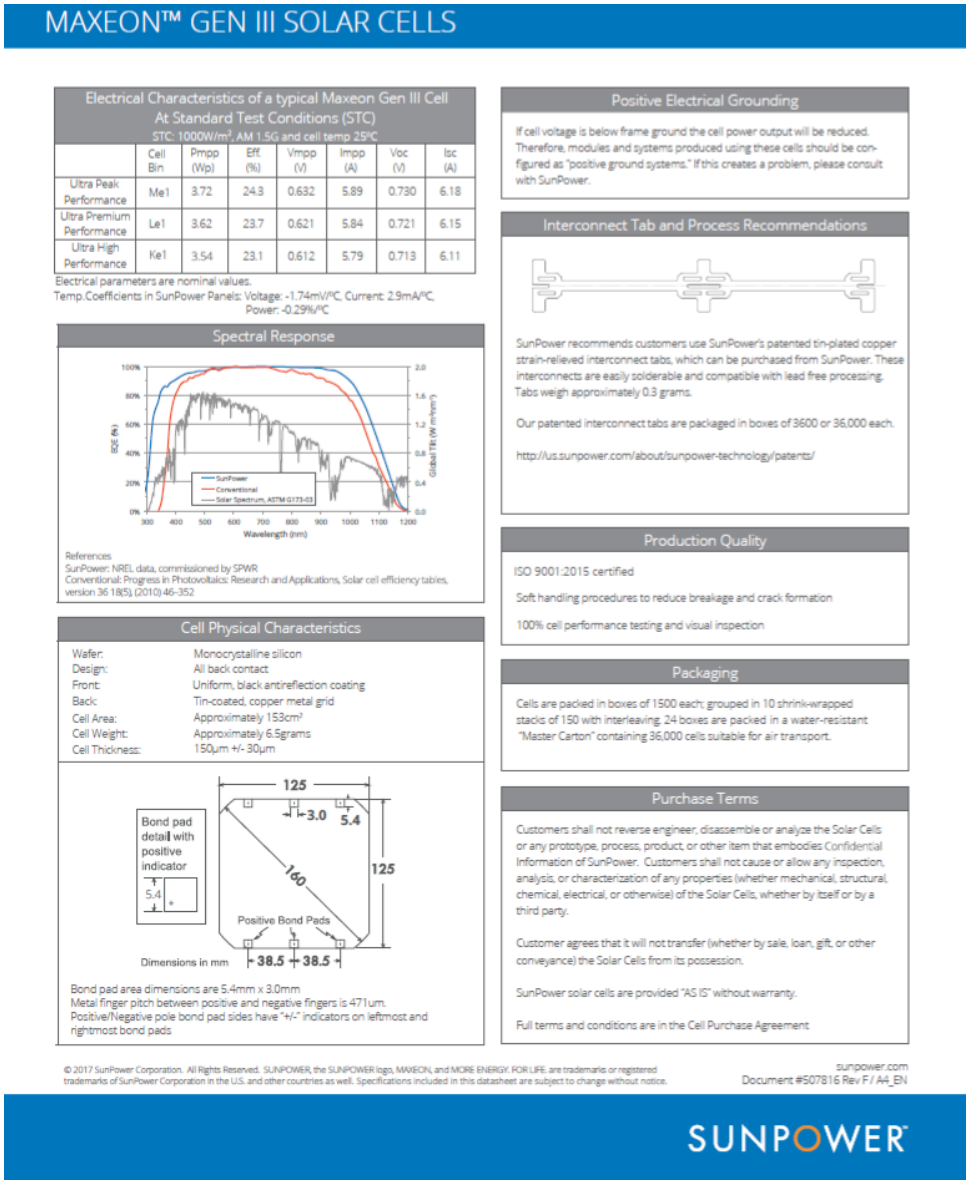

Figure D.1: **Maxeon Gen III Solar cell datasheet.**

International
IOR Rectifier

PD - 97322

IRFP4368PbF

HEXFET® Power MOSFET

Applications
- High Efficiency Synchronous Rectification in SMPS
- Uninterruptible Power Supply
- High Speed Power Switching
- Hard Switched and High Frequency Circuits

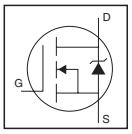

V_{DSS}	75V
$R_{DS(on)}$ typ.	1.46mΩ
max.	1.85mΩ
$I_{D\ (Silicon\ Limited)}$	350A①
$I_{D\ (Package\ Limited)}$	195A

Benefits
- Improved Gate, Avalanche and Dynamic dv/dt Ruggedness
- Fully Characterized Capacitance and Avalanche SOA
- Enhanced body diode dV/dt and dI/dt Capability

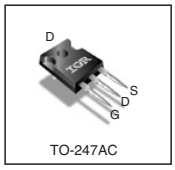

TO-247AC

G	D	S
Gate	Drain	Source

Absolute Maximum Ratings

Symbol	Parameter	Max.	Units
I_D @ T_C = 25°C	Continuous Drain Current, VGS @ 10V (Silicon Limited)	350①	A
I_D @ T_C = 100°C	Continuous Drain Current, V_{GS} @ 10V (Silicon Limited)	250①	
I_D @ T_C = 25°C	Continuous Drain Current, V_{GS} @ 10V (Wire Bond Limited)	195	
I_{DM}	Pulsed Drain Current ②	1280	
P_D @T_C = 25°C	Maximum Power Dissipation	520	W
	Linear Derating Factor	3.4	W/°C
V_{GS}	Gate-to-Source Voltage	± 20	V
dv/dt	Peak Diode Recovery ④	13	V/ns
T_J	Operating Junction and	-55 to + 175	°C
T_{STG}	Storage Temperature Range		
	Soldering Temperature, for 10 seconds	300	
	(1.6mm from case)		
	Mounting torque, 6-32 or M3 screw	10lb·in (1.1N·m)	

Avalanche Characteristics

$E_{AS\ (Thermally\ limited)}$	Single Pulse Avalanche Energy ③	430	mJ
I_{AR}	Avalanche Current ②	See Fig. 14, 15, 22a, 22b	A
E_{AR}	Repetitive Avalanche Energy ⑤		mJ

Thermal Resistance

Symbol	Parameter	Typ.	Max.	Units
$R_{\theta JC}$	Junction-to-Case ⑨	—	0.29	°C/W
$R_{\theta CS}$	Case-to-Sink, Flat Greased Surface	0.24	—	
$R_{\theta JA}$	Junction-to-Ambient ⑧⑨	—	40	

Figure D.2: **MOSFET datasheet.**

34769-OP

50W Grow LED Module

REQUIRES ~ 600in² OF HEATSINKING
Designed to be hardwired into a fixture

High-power 50W LED White Grow Light module with constant power regulation, over Temperature and Voltage protection.
Sealed to IP65
Power: 110VAC
Color Temperature: 6000-6500K
Lumens: 2500min.
L: 3-1/16" **W:** 1-3/4" **T:** 1/4" **WT:** .05

NOTE: AC Line Connections are Solder Pads. Recommend that Leads be Attached Before Mounting to Heatsink

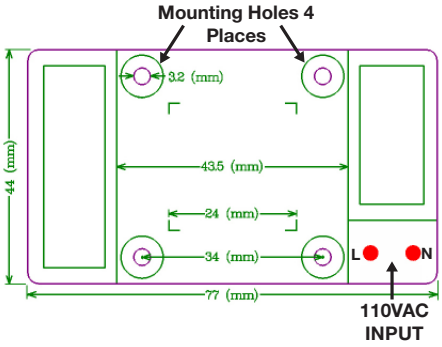

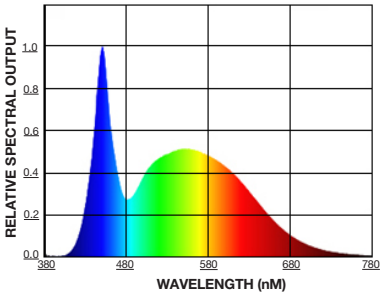

MARLIN P. JONES & ASSOC., INC.
P.O. Box 530400 Lake Park, Fl 33403
800-652-6733 FAX 561-844-8764
WWW.MPJA.COM

Figure D.3: **50W Grow LED module.**

Littelfuse
Expertise Applied | Answers Delivered

Schottky Barrier Rectifier

DST10100S-A, 10A, 100V, TO-277B, Single

DST10100S-A

HF RoHS e3

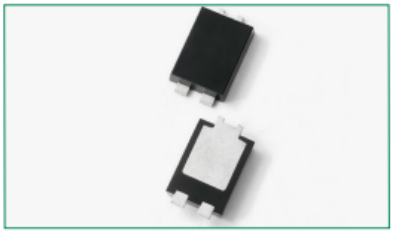

Description

Littelfuse DST series Ultra Low V_F Schottky Barrier Rectifier is designed to meet the general requirements of Automotive applications by providing high temperature, low leakage and lower V_F products.

It is suitable for high frequency switching mode power supply, free-wheeling diodes and polarity protection diodes.

Pin out

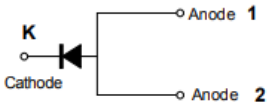

Features

- High reliability application and AEC-Q101 qualified.
- Ultra low forward voltage drop
- High frequency operation
- MSL: Level 1 - unlimited
- High junction temperature capability
- Trench MOS Schottky technology
- Single die in TO-277B Package
- Pb-free E3 means 2nd level interconnect is Pb-free and the terminal finish material is tin(Sn) (IPC/ JEDEC J-STD-609A.01)

Applications

- Switching mode power supply
- DC/DC converters
- Free-Wheeling diodes
- Polarity Protection Diodes

Maximum Ratings

Parameters	Symbol	Test Conditions	Max	Unit
Peak Inverse Voltage	V_{RRM}	-	100	V
Single Peak Reverse Voltage	V_{RSM}	-	105	V
Average Forward Current*	$I_{F(AV)}$	50% duty cycle @T_L =125°C rectangular wave form	10	A
Peak One Cycle Non-Repetitive Surge	I_{FSM}	8.3 ms, half Sine pulse	150	A

* Mounted on 30 mm x 30 mm pad areas aluminum PCB

Electrical Characteristics

Parameters	Symbol	Test Conditions	Max	Unit
Forward Voltage Drop *	V_{F1}	@2A, Pulse, T_J = -40 °C	0.60	V
	V_{F2}	@5A, Pulse, T_J = -40 °C	0.65	
	V_{F3}	@10A, Pulse, T_J = -40 °C	0.70	
	V_{F4}	@2A, Pulse, T_J = 25 °C	0.50	
	V_{F5}	@5A, Pulse, T_J = 25 °C	0.60	
	V_{F6}	@10A, Pulse, T_J = 25 °C	0.70	
	V_{F7}	@2A, Pulse, T_J = 125 °C	0.40	
	V_{F8}	@5A, Pulse, T_J = 125 °C	0.55	
	V_{F9}	@10A, Pulse, T_J = 125 °C	0.65	
Reverse Current *	I_{R1}	@V_R = rated V_R T_J = 25 °C	0.25	mA
	I_{R2}	@V_R = rated V_R T_J = 125 °C	36	

* Pulse Width < 300µs, Duty Cycle <2%

Figure D.4: **Schottky barrier rectifier.**

Littelfuse
Expertise Applied | Answers Delivered

Leaded RTDs
Thin Film Platinum RTD Sensors

PPG Series Thin Film Platinum RTDs

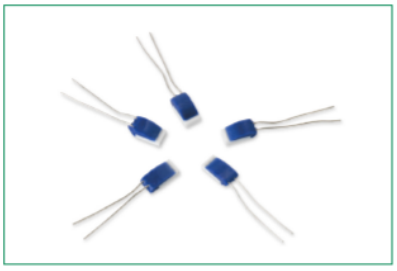

Dimensions

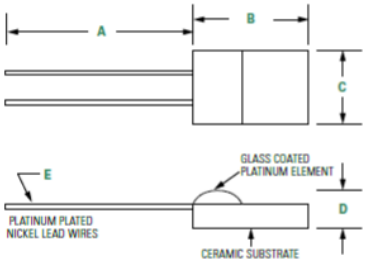

Dimensions shown in inches.

A	B	C	D	E
0.200" Min	See Specs Table	See Specs Table	0.049 Nom	32 AWG (0.008")

Description

Littelfuse thin film platinum RTDs (Pt-RTD) consist of a passivated thin film platinum element deposited on a ceramic substrate. Thin film Pt-RTDs provide cost advantages when compared to wirewound platinum resistance temperature detectors.

Features

- Glass coated platinum element
- Virtually linear relationship between temperature and resistance
- Capable of withstanding temperatures ranging from -50°C to +500°C. Higher temperature ratings are available by special order
- Excellent stability even at high temperatures
- High accuracy: Resistance and temperature deviation can be controlled to within ±0.06% and ±0.15°C, a tolerance that corresponds to Class "A" of IEC 751 or ½ DIN of DIN 43760
- High Reliability: Capable of withstanding extreme environmental conditions
- Available in various configurations for specific applications

Part Numbering System

PPG 50 1 A 1

- PPG — Series
- 50 — Resistance @ 0°C Base Value
- 1 — Multiplier, Power of 10. Ex: 501 = 50 Ω x 10^1 = 500 Ω
- A — Resistance Tolerance Class (IEC) 60751: A = Class A, B = Class B, C = Class C
- 1 — No Significance

Note: Not all combinations of Part Number codes are available. Contact Littelfuse for details.

Figure D.5: **Thin film platinum RTD sensor.**

Appendix E

Sub-array Testing Text File Output

```
Get Epoch time at https://www.epochconverter.com
Example 6/15/19 12:00:00 is 1560600000
Enter Epoch time (seconds since Jan. 1, 1970) : 1570279785

Array Temperature 1 = 47.2 deg C   Array Temperature 2 = 47.7 deg C
MPPT In Vol = 21.7V Out Vol = 111.9V Input Cur = 0.2A In Pwr = 3.59W
Sat Oct  5 12:49:47 2019

Array Temperature 1 = 47.2 deg C   Array Temperature 2 = 47.8 deg C
MPPT In Vol = 21.7V Out Vol = 111.9V Input Cur = 0.2A In Pwr = 3.59W
Sat Oct  5 12:49:48 2019

Array Temperature 1 = 47.2 deg C   Array Temperature 2 = 47.8 deg C
MPPT In Vol = 21.7V Out Vol = 112.1V Input Cur = 0.2A In Pwr = 3.40W
Sat Oct  5 12:49:49 2019

Array Temperature 1 = 47.1 deg C   Array Temperature 2 = 47.8 deg C
MPPT In Vol = 21.7V Out Vol = 112.1V Input Cur = 0.2A In Pwr = 3.59W
Sat Oct  5 12:49:49 2019

Array Temperature 1 = 47.0 deg C   Array Temperature 2 = 47.7 deg C
MPPT In Vol = 21.7V Out Vol = 112.1V Input Cur = 0.2A In Pwr = 3.59W
Sat Oct  5 12:49:50 2019

Array Temperature 1 = 47.1 deg C   Array Temperature 2 = 47.6 deg C
MPPT In Vol = 21.8V Out Vol = 112.1V Input Cur = 0.2A In Pwr = 3.43W
Sat Oct  5 12:49:51 2019

Array Temperature 1 = 47.1 deg C   Array Temperature 2 = 47.6 deg C
MPPT In Vol = 21.7V Out Vol = 112.1V Input Cur = 0.2A In Pwr = 3.59W
Sat Oct  5 12:49:52 2019

Array Temperature 1 = 47.3 deg C   Array Temperature 2 = 47.7 deg C
MPPT In Vol = 26.0V Out Vol = 111.9V Input Cur = 0.2A In Pwr = 4.09W
Sat Oct  5 12:49:53 2019

Array Temperature 1 = 47.0 deg C   Array Temperature 2 = 47.6 deg C
MPPT In Vol = 26.2V Out Vol = 112.1V Input Cur = 0.2A In Pwr = 4.11W
Sat Oct  5 12:49:54 2019

Array Temperature 1 = 47.1 deg C   Array Temperature 2 = 47.6 deg C
MPPT In Vol = 49.7V Out Vol = 112.1V Input Cur = 0.1A In Pwr = 6.93W
Sat Oct  5 12:49:54 2019

Array Temperature 1 = 47.1 deg C   Array Temperature 2 = 47.6 deg C
MPPT In Vol = 64.3V Out Vol = 111.9V Input Cur = 0.1A In Pwr = 3.36W
Sat Oct  5 12:49:55 2019
```

Figure E.1: **An example of the output text file data for Sub-array one.**

Get Epoch time at https://www.epochconverter.com
Example 6/15/19 12:00:00 is 1560600000
Enter Epoch time (seconds since Jan. 1, 1970) : 1568482115

Array Temperature 1 = 45.3 deg C Array Temperature 2 = 45.2 deg C
MPPT In Vol = 44.2V Out Vol = 117.1V Input Cur = 0.0A In Pwr = 0.39W
Sat Sep 14 17:28:37 2019

Array Temperature 1 = 45.2 deg C Array Temperature 2 = 45.2 deg C
MPPT In Vol = 56.1V Out Vol = 117.1V Input Cur = 0.0A In Pwr = 0.00W
Sat Sep 14 17:28:38 2019

Array Temperature 1 = 45.4 deg C Array Temperature 2 = 45.1 deg C
MPPT In Vol = 56.1V Out Vol = 117.1V Input Cur = 0.0A In Pwr = 0.00W
Sat Sep 14 17:28:39 2019

Array Temperature 1 = 45.4 deg C Array Temperature 2 = 44.9 deg C
MPPT In Vol = 50.9V Out Vol = 117.1V Input Cur = 0.0A In Pwr = 0.00W
Sat Sep 14 17:28:39 2019

Array Temperature 1 = 45.2 deg C Array Temperature 2 = 45.0 deg C
MPPT In Vol = 43.8V Out Vol = 117.5V Input Cur = 0.0A In Pwr = 0.76W
Sat Sep 14 17:28:40 2019

Array Temperature 1 = 45.4 deg C Array Temperature 2 = 44.9 deg C
MPPT In Vol = 56.9V Out Vol = 117.5V Input Cur = 0.0A In Pwr = 0.00W
Sat Sep 14 17:28:41 2019

Array Temperature 1 = 45.2 deg C Array Temperature 2 = 45.0 deg C
MPPT In Vol = 34.6V Out Vol = 117.3V Input Cur = 0.0A In Pwr = 0.91W
Sat Sep 14 17:28:42 2019

Array Temperature 1 = 45.2 deg C Array Temperature 2 = 44.9 deg C
MPPT In Vol = 56.9V Out Vol = 117.3V Input Cur = 0.0A In Pwr = 0.00W
Sat Sep 14 17:28:43 2019

Array Temperature 1 = 45.2 deg C Array Temperature 2 = 44.9 deg C
MPPT In Vol = 56.9V Out Vol = 117.1V Input Cur = 0.0A In Pwr = 0.00W
Sat Sep 14 17:28:44 2019

Array Temperature 1 = 45.0 deg C Array Temperature 2 = 45.2 deg C
MPPT In Vol = 56.9V Out Vol = 117.3V Input Cur = 0.0A In Pwr = 0.50W
Sat Sep 14 17:28:44 2019

Array Temperature 1 = 45.3 deg C Array Temperature 2 = 44.9 deg C
MPPT In Vol = 57.2V Out Vol = 117.5V Input Cur = 0.0A In Pwr = 0.50W
Sat Sep 14 17:28:45 2019

Figure E.2: **An example of the output text file data for Sub-array two.**

Appendix F

Fabrication Parts List and Costs

Table F.1: **List of materials and tools used to manufacture BeVolt's array with their respective prices.**

Material/Tool	**Qty**	**Price p.u.**	**Total Price**	**Comments**
Cells	450	$ 6.77	$ 3,046.50	
Kapton Tape (1" width)	10	$ 48.10	$ 481.00	
Kapton Tape (1/2" width)	15	$ 33.43	$ 501.45	
EVA	1	$ 100.00	$ 100.00	Shipping cost
Teflon (Single Sided)	31	$ 8.79	$ 272.52	
Teflon (Double Sided)	31	$ 8.79	$ 272.52	
Cell's Interconnectors	450	$ 0.00	$ 0.00	Donated
Tinned Copper Ribbon (roll)	2	$ 0.00	$ 0.00	Donated
Gloves (boxes)	15	$ 15.82	$ 237.30	
Vacuum System	1	$ -	$ -	Lab Supplies
Vacuum Bag (roll)	1	$ 300	$ 300.00	
Yellow Sealant Tape	20	$ 9.00	$ 180.00	
Teflon Fabric (roll)	1	$ 300	$ 300.00	
Breather Fabric (roll)	1	$ -	$ -	Lab Supplies
Griddles	3	$ 25.00	$ 75.00	
Aluminum Plate 1	1	$ -	$ -	Lab Supplies
Thermal IR Camera 1	1	$ 200.00	$ 200.00	
Thermal Paste (bucket)	1	$ -	$ -	
Vacuum System	1	$ -	$ -	Lab Supplies
Soldering Mold	1	$ 30.00	$ 30.00	
Fans	2	$ -	$ -	Lab Supplies
Grand Total			$ 5,996.29	

Index

Bibliography

[1] NREL. Best research-cell efficiency chart. https://www.nrel.gov/pv/cell-efficiency.htm, Dec 2019. Accessed on 2020-01-23.

[2] Mike Brown. Toyota's new solar car boasts a staggering range, defying solar car critics. https://www.inverse.com/article/57449-toyota-solar-car/amp, Jul 2019. Accessed on 2019-07-19.

[3] ASC. American solar challenge. https://www.americansolarchallenge.org/, March 2000. Accessed on 2020-03-20.

[4] SunCat Solar. Suncat solar. https://www.facebook.com/pg/SunCatSolar/about/?ref=page_internal, March 2017. Accessed on 2020-03-20.

[5] Innovators Educational Fundation. American solar challenge 20202 regulations. https://www.americansolarchallenge.org/ASC/wp-content/uploads/2020/01/ASC2020-Regs-EXTERNAL-RELEASE-C.pdf, Jan 2020. Accessed on 2020-04-24.

[6] Bausch & Lomb Inc. Acu-rite ii digital measuring system. https://www.acu-rite.com/pdf/manuals/obsolete/ACURITEIImanual.pdf, 1981. Accessed on 2020-04-30.

[7] ATER. Thermo neslab rte-110 temperature bath/circulator. https://www.atecorp.com/products/thermo-fisher-scientific/rte-110. Accessed on 2020-04-20.

[8] Newport Corporation. Introduction to solar radiation. https://www.newport.com/t/introduction-to-solar-radiation, 2020. Accessed on 2020-04-30.

[9] Christiana Honsberg and Stuart Bowden. Mismatch for cells connected in series. https://www.pveducation.org/pvcdrom/modules-and-arrays/mismatch-for-cells-connected-in-series, 2019. Accessed on 2019-12-20.

[10] Aniket. How much does an average solar panel weigh? https://ecotality.com/solar-panel-weights/, Aug 2019. Accessed on 2019-10-25.

[11] Hong Yang, He Wang, Dingyue Cao, Dangmin Sun, and Xiaobao Ju. Analysis of power loss for crystalline silicon solar module during the course of encapsulation. *International Journal of Photoenergy*, 2015:1–5, 2015.

[12] M. J. Bertin et al. *Pisot and Salem Numbers*. user Verlag, Berlin, 1992.

[13] Jacob Douglas. Teslas musk says solar panels on cars make little sense, but thats not stopping toyota, hyundai. https://www.cnbc.com/2019/09/28/teslas-musk-rejects-solar-on-cars-its-not-stopping-toyota-hyundai.html, Sept 2019. Accessed on 2019-12-19.

Vita

Silvia Arzate-Gomez was born in Michoacan, Mexico. After completing her work in the Austin Community College, in 2011, she entered the Unversity of Texas at Austin. She received the degree of Bachelor of Science in Electrical Engineering from the University of Texas at Austin in May 2016. In September 2017 she entered the Graduate School in the University of Texas at Austin.

Permanent address: 12828 Buenos Aires Pkwy
Del Valle, Texas 78617

This thesis was typeset with LaTeX[†] by the author.

[†]LaTeX is a document preparation system developed by Leslie Lamport as a special version of Donald Knuth's TeX Program.